




5-2023

Comparative Analysis on Low Cost Continuous Carbon Fiber Polypropylene Composite Using Compression Molding and Automated Tape Placement

Benjamin U. Schwartz
bschwar6@vols.utk.edu

Follow this and additional works at: https://trace.tennessee.edu/utk_gradthes

 Part of the [Manufacturing Commons](#), [Polymer and Organic Materials Commons](#), and the [Structural Materials Commons](#)

Recommended Citation

Schwartz, Benjamin U., "Comparative Analysis on Low Cost Continuous Carbon Fiber Polypropylene Composite Using Compression Molding and Automated Tape Placement." Master's Thesis, University of Tennessee, 2023.

https://trace.tennessee.edu/utk_gradthes/9256

This Thesis is brought to you for free and open access by the Graduate School at TRACE: Tennessee Research and Creative Exchange. It has been accepted for inclusion in Masters Theses by an authorized administrator of TRACE: Tennessee Research and Creative Exchange. For more information, please contact trace@utk.edu.

To the Graduate Council:

I am submitting herewith a thesis written by Benjamin U. Schwartz entitled "Comparative Analysis on Low Cost Continuous Carbon Fiber Polypropylene Composite Using Compression Molding and Automated Tape Placement." I have examined the final electronic copy of this thesis for form and content and recommend that it be accepted in partial fulfillment of the requirements for the degree of Master of Science, with a major in Mechanical Engineering.

Uday Vaidya, Major Professor

We have read this thesis and recommend its acceptance:

Merlin Theodore, Chad Duty

Accepted for the Council:

Dixie L. Thompson

Vice Provost and Dean of the Graduate School

(Original signatures are on file with official student records.)

**Low-Cost Continuous Carbon Fiber Thermoplastic Composites Tape - Compression
Molding and Automated Tape Placement**

**A Thesis Presented for the
Master of Science
Degree
The University of Tennessee, Knoxville**

**Benjamin Schwartz
May 2023**

Copyright © 2023 by Benjamin Schwartz
All rights reserved.

DEDICATION

I dedicate this work to the family and friends (*_*)

ACKNOWLEDGEMENTS

Thank you to Dr. Uday Vaidya for all your guidance and leadership but most of all thank you for providing me this opportunity to learn and grow under your mentorship. Thank you to Saurabh Pethe for your exceptional mentorship during my undergraduate and graduate programs. A special thank you to Joel Rodeghiero, Nicholas Crowder, Tyler Sundstrom, Mckade Patrick, Tonia Helmboldt, Anne Gosnell, John Klepsig and Mason Rucinski for being exceptional researchers. This work could not have been completed without you! Thank you to Cole Frenz and Jaydeep Kolape for the continued support and advisement with polishing and microscopy. Last but certainly not least thank you to all the graduate students and staff for all your counsel, insight and unwavering support during my time as an undergraduate and graduate student at the Fibers and Composites Manufacturing Facility.

ABSTRACT

Carbon fiber reinforced plastics (CFRP) are widely used throughout the aerospace industry where a weight reduction remains the highest priority with less emphasis on cost. Textile grade carbon fiber (TCF) and other low-cost carbon fiber (LCCF) alternatives have recently emerged for use in the automotive market where emissions regulations have pushed automotive manufacturers and research institutions to look for cost effective light weight materials. Fiber reinforced thermoplastics provide an effective solution that align with automotive design including low cost, high processing rates, high impact toughness, unlimited shelf life, and recyclability.

TCF and Zoltek_PX35 fibers are two LCCF aimed at the automotive, wind energy and commercial markets that are helping to push the cost of CF down to approximately \$5 per lb. In combination with a hot melt thermoplastic pultrusion impregnation technique, an intermediate low-cost composite tape can be produced that is shown to have good mechanical performance when consolidated through hot compression molding (CM). Automation is critical to the required rapid part production and process control within the automotive industry. Research was conducted into the manufacturing process parameters of LCCF composite tapes through in-situ consolidation with an automated tape placement (ATP) or automated fiber placement (AFP) robotic system. This research focuses on the manufacturing of low-cost continuous polypropylene composites and explores the mechanical and morphological properties associated with compression molding and automated tape placement.

TABLE OF CONTENTS

CHAPTER 1: INTRODUCTION	1
CHAPTER 2: BACKGROUND STUDY AND LITERATURE REVIEW	3
2.1 INTEGRATION OF LOW-COST CARBON FIBER	3
2.2 CARBON FIBER REINFORCED PLASTICS (CFRP)	4
2.3 CONTINUOUS INTERMEDIATE MATERIALS	7
2.3.1 Pultrusion	7
2.3.2 Process Line Development and Overview	11
2.3.3 Continued Process Line Development	14
2.4 AUTOMATED TAPE PLACEMENT (ATP)	19
2.5 SUMMARY AND RESEARCH GAPS	23
2.6 RELEVANT LITERATURE	23
2.6.1 Low Velocity Impact	23
2.6.2 Effect of fiber shape on Mechanical Performance	25
2.6.3 Thermoplastic Pultrusion	26
2.6.4 Automated Tape Placement	26
CHAPTER 3: MATERIALS AND METHODS	29
3.1 TEXTILE GRADE CARBON FIBER	29
3.2 ZOLTEK PX35	29
3.3 POLYPROPYLENE EXXONMOBIL™ PP3155 POLYPROPYLENE HOMOPOLYMER	29
3.4 AUTOMATED TAPE PLACEMENT ROBOTIC SYSTEM	29
3.5 CF-POLYPROPYLENE TAPE PRODUCTION	33
3.6 COMPOSITES PLATE(S) PREPARATION	33
3.7 DETERMINING PROCESS PARAMETERS	34
3.8 TENSILE TESTS (ASTM D3039)	35
3.9 FLEXURAL TEST ASTM 790	38
3.10 DROP TOWER TEST EQUIPMENT AND TESTING (ASTM D7136)	39
3.11 THERMAL ANALYSIS	41
CHAPTER 4: RESULTS AND DISCUSSION	42
4.1 THERMAL ANALYSIS	42

4.2	ATP PROCESSING PARAMETERS STUDY	42
4.2.1	Examination of Void Content in Process Parameters Study.....	42
4.2.2	Effect of Process Parameters on In Plane Waviness.....	42
4.2.3	Relationship of ATP Processed Width and Thickness	44
4.2.4	Process Parameters Conclusion	46
4.3	ILSS RESULTS	46
4.3.1	Effect of Fiber Shape on ILSS Properties CM.....	46
4.3.2	ATP vs CM Processed Materials	49
4.3.3	Effect of microstructure on ILSS strength of ATP laminates.....	50
4.4	TENSILE RESULTS	53
4.4.1	LCCF CM Samples and Theoretical Values.....	53
4.4.2	CM vs ATP Tensile Strength and modulus	57
4.5	FLEXURAL RESULTS	58
4.5.1	CM and ATP Processed Flexural Results.....	58
4.5.2	Force response curves CM vs. ATP.....	61
4.5.3	Failure modes of Flexural Samples.....	61
4.6	LVIDROP TOWER RESULTS	63
4.6.1	LVI Failure Modes.....	63
4.6.2	ZT-PP vs TCF-PP Results	63
4.6.3	Peak Force vs Impact Energy	65
4.6.4	Laminate Structures Effect on Failure Modes	65
4.6.5	Volumetric Damage Trends.....	68
	CHAPTER 5: CONCLUSIONS	71
	BIBLIOGRAPHY.....	73
	APPENDIX.....	82
	VITA	96

LIST OF TABLES

Table 1: Cost vs mechanical properties of common engineering materials	5
Table 2: Textile Grade Carbon Fiber (From CFTF) ^{3,4,31}	30
Table 3: Zoltek PX35 Fiber ³⁰	30
Table 4: ExxonMobil™ PP3155 Polypropylene Homopolymer ⁷⁸	30
Table 5: List of processing parameters used for an ATP HGT system.	36
Table 6: Average fiber weight and fiber volume percentages for all material plates produced. Overall average fiber weight (FWF) was 35.86% and average fiber volume (FVF) was 24.48%.	43
Table 7: Impact results from TCF-PP and ZT-PP compression molded tape.....	66
Table 8: Mechanical Characterization Data for all Mechanical Tests	92
Table 9: Low Velocity Impact Data.....	93
Table 10: Volumetric Damage Data	94

LIST OF FIGURES

Figure 1: Schematic of traditional pultrusion process where resin is sent through a resin bath and is then cured through a heated die system. This process produces continuous CFRP products with constant cross-section in large scale composite manufacturing.	8
Figure 2: Thermoplastic pultrusion process breakdown. Thermoplastic pultrusion is broken up into two main categories: Reactive and Non-Reactive pultrusion.....	10
Figure 3 : Thermoplastic tape impregnation process. This system was designed for the impregnation of wide tow (+350K) textile grade carbon fiber (TCF).....	13
Figure 4: Optimized pin configuration of the heated pin die system. Dual pin configurations were set to +45, -45, +45, -45 respectively. Fiber was weaved through the pin system as shown. This pin configuration and weave pattern was found to optimally impregnate the CF tow. 15	
Figure 5: Images of Thermoplastic impregnation line electrical system. (A) Front view of electrical box. (B) View of the open electrical box. (DC – Top Section) (AC – Bottom Section) (PID wires on open door). (C) Distribution box on the base of the tape line. (D) Quick connects on the side of the main electrical box where wires can be easily removed. 17	
Figure 6: New Pin Die System. (a) View of Pin die system mounted onto the tape impregnation (b) Front side view showing heater and thermocouple wires inserted into rotating pins. Pins can be turned and locked into places at intervals of 22.5° covering a 180° operational window. (c). Top view (d) Back side view	17
Figure 7: Tape Slitting system. (A) large view of tape slitting. (B & C) close up of AM manufactured spacers and pinch rollers. This system was designed to allow for the ease of taking on and off the line by the removal of two bolts. Five blades are attached to continuously slit 4 one half inch tapes to be placed on an automated tape placement system.	18
Figure 8: 7 axis robotic arm and HGT thermoplastic Automated Tape Placement head. Robotic system works in tandem with the mandrel to place and consolidate thermoplastic tape.....	20
Figure 9 : Illustration of a hot gas torch (HGT) automated tape placement (ATP) head configuration.	20

Figure 10: Curved compaction rollers for matching mandrel curvature. These compaction rollers can easily be swapped out during the hot gas torch (HGT) in-situ consolidation process to match the mandrel curvature.....	22
Figure 11: Inter-diffusion of polymer chains between laminates during autohesion ⁶⁵	24
Figure 12: Kawasaki Robot arm specifications. (a) Shows the robotic arm axis system with all degrees of freedom and (b) shows the make and model of the robotic system used in this study along with relevant information about the robot.....	31
Figure 13: 18 Foot Robotic Spindle for mandrel rotation for large part manufacturing. ATP robotic arm for precise placement of CFRP tape.....	31
Figure 14: Photo of robotic arm and spindle working in tandem on a rotating off axis cylinder. This figure represents how the robotic system can move in complex motions to conform to complex mold geometries.....	32
Figure 15: Image enhancement for void analysis on two layers of in-situ consolidated CF-PP Tape produced on and Automated Tape Placement (ATP) system. SEM stitched images were enhanced by increasing exposure, contrast, and tint to allow the program to more easily discern the sample boundary. Image processing program outlines edges of tape to exclude voids outside of the tape region.....	37
Figure 16: Low Velocity Impact (LVI) Test setup. Sample is placed and clamped down to insure no movement of the plate. This set up is then placed into a climate-controlled chamber where a steel weighted head strikes the center of the plate.....	40
Figure 17: 2D visualization of volumetric damage approximation used for LVI samples.....	40
Figure 18: Fiber waviness and increased width between fast and slow speed processing. Straight and consistent edges can be observed with faster processing speeds (4 in/s – 140lb. – 450° C). inconsistent laydown width can be observed due to matrix squeeze can be observed in low processing speeds (2 in/s – 140lb. – 450 °C).....	45
Figure 19: (A) shows the trend of two layers of ATP processed tape and how an increase in thickness was quantifiable correlated to a decrease in width. (B) shows the average thickness and width of ATP processed materials with respect to laydown speed.....	47
Figure 20: ILSS Properties of ZT-PP and TCF-PP plates produced with compression molding (CM) and an Automated Tape Placement (ATP) process. An average ILSS strength of ZT-PP and TCF-PP CM samples was found to be 17.9 MPa and 14.1 MPa respectively. ZT-PP	

and TCF-PP ATP samples were found to have an ILSS strength of 7.1 MPa & 5.7 MPa respectively. 47

Figure 21: SEM Images of Zoltek PX35 fiber vs Textile Grade Carbon Fiber. Zoltek fiber exhibits a kidney bean shape while TCF fibers are circular in nature. This Shape could be attributed to the higher tensile strength of ZT-PP over TCF-PP. This kidney been shape may allow for better interfacial bond between the fiber and matrix allowing the fibers to carry a higher tensile load. 48

Figure 22: A1 & A2 Show laminate structure of ZT-PP compression molded (CM) sample. B1 & B2 show ZT-PP processed using ATP methods of manufacturing. A large crack can be observed along the top laminate due to incomplete autohesion of the laminates during in-situ consolidation. 51

Figure 23: CM vs ATP processed laminates where voids are present. (A) shows TCF-PP CM samples with voids mostly present within polymer rich regions likely due to trapped air bubbles within the sample. (B) Shows TCF-PP ATP processed material where voids were mostly present in fiber rich regions or at ply boundaries..... 52

Figure 24: (A) ZT-PP Compression Molded. Laminates structures are not visible due to complete diffusion of the laminate’s plies. (B) ZT-PP ATP processed materials show signs of little fiber dispersion between laminate plies. 52

Figure 25: SEM image unpolished tape with fully impregnated top surface and dry region on the bottom surface. This was due to the polymer injection sight on the top surface of the fiber bed..... 54

Figure 26: Tensile strength and modulus of unidirectional ZT-PP composite tape shown with unidirectional TCF-PP composite tape. 55

Figure 27: Representative Force vs displacement curves for tested tensile samples. (A) Representative curves for ZT-PP CM and ATP processed tensile samples. (B) Representative curves for TCF-PP CM and ATP processed tensile samples. 56

Figure 28: Failure points and failure modes of ATP processed TCF-PP and ZT-PP tensile samples. (A) shows lateral failure (B) Shows edge delamination the primary failure mode of ZT-PP ATP samples. 59

Figure 29: Fiber waviness found within TCF-PP ATP samples. Surface of samples were found to have unconsolidated regions. 59

Figure 30: Flexural strength and modulus comparison chart of unidirectional ZT-PP and TCF-PP composite tape processed using compression molding and automated tape placement. 60

Figure 31: Representative force vs displacement curves for tested flexural samples. (A) Representative curves for ZT-PP CM and ATP processed flexural samples. (B) Representative curves for TCF-PP CM and ATP processed flexural samples. 62

Figure 32: Flexural samples and failure modes: (A) ZT-PP CM sample showed signs of compression buckling, (B) TCF-PP CM showed signs of compression buckling and delamination on the bottom of the laminate, (C) ZT-PP ATP sample showed signs of delamination inside the laminate due to interlaminar delamination and (D) TCF-PP ATP sample showed signs of interlaminar delamination. 64

Figure 33: Force vs time graphs of LVI samples. (A) ZT-PP force vs time. All strikes represent plastic deformation. (B) TCF-PP Unidirectional Force vs. Time Plastic deformation. (C) ZT-PP 0/90 cross ply samples where 30J and 40J are elastic and 50-80 are plastic deformation. (D) TCF-PP 0/90 cross ply plastic deformation. 67

Figure 34: LVI Peak force vs drop energy. A parametric relationship between peak force and drop energy can be observed which was correlated the transition from delamination mode failure to fiber mode failure. 69

Figure 35: Initiation of LVI damage within a 0/90/0 composite structure. Failure occurs within the matrix region and load is take up by the preceding ply ⁹⁷ 69

Figure 36: Volumetric damage vs. impact energy trends. TCF -PP Samples show a linear trend between calculated volumetric damage and impact energy while ZT-PP samples did not. . 70

Figure 37: Images of Thermoplastic impregnation line electrical system. (A) Front view of electrical box. (B) View of the open electrical box. (DC – Top Section) (AC – Bottom Section) (PID wires on open door). (C) Distribution box on the base of the tape line. (D) Quick connects on the side of the main electrical box where wires can be easily removed. 83

Figure 38: Temperatures vs. Time graphs of the old and new pin die system. Temperature grades for the old pin dies system (A) varied between as much as 200°C during a 15-minute period while the new pin die system (B) remains constant with in around 5° degrees. 85

Figure 39: Old 5 in Pin Die system with thermocouples located at the end of the heaters. Due to the placement of the heaters large thermal spikes and a high thermal gradient could be observed within the system. 85

Figure 40: New Pin Die System. (a) View of Pin die system mounted onto the tape impregnation
 (b) Front side view showing heater and thermocouple wires inserted into rotating pins. Pins
 can be turned and locked into places at intervals of 22.5° covering a 180° operational
 window. (c). Top view (d) Back side view 86

Figure 41: Tape Slitting system. (A) large view of tape slitting. (B & C) close up of AM
 manufactured spacers and pinch rollers. This system was designed to allow for the ease of
 taking on and off the line by the removal of two bolts. Five blades are attached to
 continuously slit 4 one half inch tapes to be placed on an automated tape placement system.
 88

Figure 42: LFT Die CAD model and Thermal model 90

Figure 43: Rod die cad and thermal model 90

Figure 44: Extruder speed vs Weight of PP (Grams/min) 91

Figure 45: Low velocity impact samples after testing. (A) ZT-PP 0/90 samples from 30J - 80J,
 (B) ZT-PP Unidirectional Samples from 10J - 30J, (C) TCF-PP 0/90 samples from 20J –
 50J and (D) TCF-PP Unidirectional samples from 10J - 25J 95

KEY WORDS AND ACRONYMS

- Automated Tape Placement (ATP) – A robotic system that automates the placement of composite tape
- Aspect ratio – ratio between the fiber length and fiber diameter $\rightarrow \frac{l}{d}$
- Autohesion – Diffusion and crosslinking of the polymer between two laminates
- Axis – a straight line about which a body or geometric figure rotates about
- Band – One strip of placed tape from the point tape is placed and cut
- Composite – Produced from two or more constituent materials that work together as a single material
- Composite Tape – A thin and wide strip of fiber reinforced material with all fibers aligned in a uni-directional orientation.
- Fiber Tow – A continuous bundle of fibers
- Nip point – Point at which the newly placed tape meets the substrate directly underneath the compaction roller.
- Ply – One complete layer of placed taped
- Pultrusion – Process of producing continuous composites with a constant cross-section
- Scrap Rate – Amount of material that goes to waist during the manufacturing process
- Tape placement head – An attachment onto the end of the robotic arm where the tape is fed, heated, placed and compacted
- Textile Grade Carbon Fiber (TCF) – Produced at CFTF by use of a textile grade PAN precursor
- Tote – The weighted striker of a low velocity impact (LVI) drop tower setup.
- Wet out – the degree to which reinforcement fibers are covered by the polymer matrix
- CF – Carbon Fiber
- CFRP – Carbon Fiber Reinforced Polymer
- CFTF – Carbon Fiber Technology Facility located at ORNL
- D-LFT – Direct Long Fiber Thermoplastic
- HGT – Hot Gas Torch
- LFT – Long Fiber Thermoplastic
- ORNL – Oak Ridge National Laboratory

- PAN – Polyacrylonitrile, a common precursor used to make Carbon Fiber
- PP – Polypropylene
- TCF – Textile Grade Carbon Fiber
- TCF-PP – Textile Grade Carbon Fiber with a Polypropylene Matrix
- T_g – Glass Transition Temperature
- T_m – Melting Temperature
- ZT-PP – Zoltek_PX35 Carbon Fiber with a Polypropylene Matrix

Chapter 1: Introduction

New emission regulations imposed by the federal government in May 2022 require the industry-wide fuel efficiency average to be approximately 49 miles per gallon for passenger cars and light trucks by model year 2026¹. To meet these demands, the incorporation of cost-effective carbon fiber reinforced polymer (CFRP) composites into body panels and structural members of vehicles is crucial. Carbon fiber (CF) is a highly desired material and has only been growing in popularity for top end automotive, aerospace and renewable energy markets due to its desirable tensile strength, stiffness, and modulus. These properties make CF ideal for applications where weight is a priority. Despite its numerous advantages, CF has been unable to penetrate the bulk of the automotive market due to the high cost associated with raw materials (Polyacrylonitrile or PAN), energy consumption during production and labor-intensive manufacturing²⁻⁶. Composites derived from PAN based precursors are the industry lead accounting for more than 90% of the carbon fiber market today. The cost associated with PAN based CF, often termed aerospace grade CF, is highly dependent on the price of oil with 40 to 60 percent of CF's total cost being derived from the precursor^{4,5}. The cost of PAN based CF was reported to be approximately \$30 per/lb. while the automotive industry would require the cost to be less than half this to be marketable⁷. To make this transition economical, two main challenges must be overcome, which include the reduction in cost of CF and more efficient manufacturing methods. To reduce the cost of CF, several types of precursors have been investigated including lignin, cellulose, pitch and textile grade PAN as a cheaper option to aerospace grade PAN^{3,4,7-13}. Each of these precursors provides their own unique solution to replacing aerospace grade CF although textile grade PAN provides the most readily available solution for CF in the automotive market. The second aspect is to provide an economical solution to continuous thermoplastic CF processing. Thermoplastics provide benefits that complement the automotive industry's needs including low cost, high processing rates, high impact toughness, unlimited shelf life, and recyclability^{6,14-18}. This has been shown by manufacturing continuous CF Tape on a hot melt thermoplastic impregnation line and the exploration of automated tape placement (ATP) with commodity polymers.

Traditional manufacturing of continuous CFRP composites are often highly labor and time intensive processes making continuous composites uneconomical for any industry other than aerospace or high end commercial markets. In addition, depending on the complexity of the preform, traditional manufacturing of CFRP's lead to a scrap rate of around 25 to 30 %. When considering the high cost of material, the high wastage hinders economic part production. Moreover, the orthotropic mechanical properties of traditional woven fabric limit the load specific design process resulting in over dimensioned parts limiting the light weighting potential for composite parts^{19,20}. Unidirectional tapes can be oriented in a specific load barring directions to maximize mechanical performance. For these reasons, automated fiber placement (AFP) or automated tape placement (ATP) provides a unique solution for the potential economic feasibility of CFRP's in the automotive market. This research focuses on CF manufactured from a textile grade precursor and processed on a hot melt impregnation line. The two main objectives of this thesis are to (a) develop and explore mechanical and morphological properties of two types of low cost CF tapes produced by thermoplastic hot melt impregnation; and (b) to compare mechanical properties of the low cost tape with two manufacturing methods; compression molding and automated tape placement.

Chapter 2: Background Study and Literature Review

2.1 Integration of Low-Cost Carbon Fiber

Composites derived from Polyacrylonitrile (PAN) based precursors account for 90% of the carbon fiber market today because of its high strength and modulus. The PAN based precursor accounts for the largest majority of the cost of CF^{4,5,7} with around 51% being precursor cost, 18% utilities, 12% depreciation, 10% labor and 9% represented by other fixed costs⁷. This PAN based petroleum chemical feedstock embodies the largest barrier for CF to enter the automotive and wind energy markets, hence the introduction of Textile Grade PAN (TG-PAN). Textile acrylic fibers come from the textile industry where they are manufactured for commodity and clothing applications. The TG-PAN precursor contains 85% acrylonitrile and 10-15% co-monomers where aerospace grade PAN contains 95% acrylonitrile and 5% co-monomers^{4,13,21}. Upon carbonization, the larger co-monomers reduce the carbonization yield and in turn reduce the mechanical properties of the TG-PAN CF^{4,21}. TG-PAN also exhibits half the molecular weight of aerospace grade PAN (TG-PAN 100,000 g/mol & CF-PAN 200,000 g/mol). This lower molecular weight contributes to a lower viscosity creating processing challenges during the spinning process⁴. Despite these many production challenges and the reduction of mechanical properties compared to aerospace grade CF, the significant cost reduction of the CF precursor provides TG-PAN CF the opportunity to emerge as a relevant material for the automotive, wind energy and sports industries.

To further the cost savings, this textile grade carbon fiber (TCF) that has been developed at Oak Ridge National Laboratory (ORNL) at the Carbon Fiber Technology Facility (CFTF) has increased production rates by increasing tow size. Aerospace grade CF is often produced in tow sizes of 3K to 12K (3000 to 12000 filaments). These low production rates partially attribute to the high material cost. To overcome this production issue, the TCF material has been produced with a tow size ranging from 300K to 600K filaments²². Due to this combination of precursor and material throughput, the potential cost for this TCF is estimated to be between 5-10 \$/lb⁵.

Similarly, to TCF, Zoltek's product development process was driven by the push to reduce the cost of CF to a target price of 5\$/lb while the design philosophy heavily differed. Zoltek PX_35

CF is intended to be used as a commercial product for non-aerospace applications. This product was produced to fill the demand for low density lightweight materials in the automotive, wind energy and sports market while providing cost stability in a relatively volatile market. For this study Zoltek PX_35 product was chosen as a direct comparison to TCF. Zoltek used a wet spinning technique combining a traditional PAN precursor with a high concentration of lignin that was shown to have good results with up to 40% lignin²³. Lignin as a precursor to carbon fiber has been heavily explored as an alternative CF precursor due to its low cost and availability from the paper industry¹¹. Table 1 shows a cost comparison and relevant properties of engineering materials.

2.2 Carbon Fiber Reinforced Plastics (CFRP)

Carbon fiber reinforced plastics (CFRP's) saw its emergence in the 1960s with commercially available CF due to its high tensile strength and significant light weighting potential³². These materials, mainly used in aerospace applications, primarily used thermoset resin systems like epoxies due to their high strength, innately low viscosity and manufacturability. Despite this, these materials came with a high cost due to labor intensive layups and energy intensive autoclave cycles^{18,33-35}. In recent decades, more cost-effective resin systems have been explored in the advanced materials industry which primarily include thermoplastic resin systems. Thermoplastics provide a multitude of advantages including high impact resistance, chemical and solvent resistance, infinite shelf life, recyclability, and out of autoclave manufacturing^{33,36,37}. Due to some of these advantages extreme cost savings can be explored.

Plastics were first explored in the mid 19th century but did not become wide spread until after World War II³⁸. With this rapid expansion of plastics, specifically thermoplastics, manufacturing techniques became highly efficient. Many well established thermoplastic manufacturing techniques including vacuum molding, extrusion, injection molding and compression molding can be directly applied to thermoplastic composites. Commodity polymers like polypropylene (PP) and polyethylene (PE) provide suitable choices for CFRP's in the automotive market due to their low cost and market availability¹⁶. These polymer matrices (PP and PE) are already used in numerous industrial applications including automotive manufacturing, electronics, and

Table 1: Cost vs mechanical properties of common engineering materials

Cost Comparison vs. Mechanical properties of Common Engineering Material			
	Price/lb	Density	Modulus
Steal 1010	\$0.71 /lb ²⁴	7.87 g/cc ²⁵	200 GPa ²⁵
Aluminum 2024	\$2.79/ lb ²⁴	2.78 g/cc ²⁶	73.1 GPa ²⁶
S-Glass Fiber	\$5 / lb ²⁷	2.53 g/cc ²⁸	89 GPa ²⁸
Aerospace CF	\$30 / lb ²⁷	1.8 g/cc ²⁹	300-400 GPa ²⁹
Zoltek PX_35	\$ 5-10 /lb ²³	1.81 g/cc ³⁰	242 GPa ³⁰
TCF	\$ 5-10 / lb ⁵	1.76 g/cc ^{3,4,31}	275 GPa ^{3,4,31}

packaging applications^{15,16}. These previously mentioned manufacturing techniques can provide high quality complex parts with short cycle time and little to no post processing^{14,17}.

Much of the work in discontinuous thermoplastic reinforced fibers has been done with short and long fiber thermoplastics. One of the methods for processing these discontinuous CFRP's is twin screw compounding. This manufacturing method is an effective method of manufacturing short fiber composite pellets which has been shown to produce good results. This process has been shown to have a significant effect on tensile and modulus properties of thermoplastics. Yeole, showed a 26% increase in tensile strength and 162% increase in Young's modulus in TCF reinforced polypropylene composites when compared to neat polymer³. Long fiber thermoplastics (LFT's) maintain higher strength and modulus properties than short fiber due to higher aspect ratios. A large interest has been shown toward LFT concentrates which contain 60% to 75% fiber offering a compromise between the high investment cost of direct LFT and the comparatively high material cost of pre-compounded pellets. LFT concentrates can be mixed with neat polymer pellets to achieve the desired fiber weight or fiber volume fraction allowing for mechanical properties to be designed for their application. Automotive applications for LFT's include automobile seats, instrument panel retainers, front end modules and door modules¹⁷.

Over the last two decades, the automotive industry has been pursuing a variety of technological developments and design strategies to meet increasingly stringent automobile performance requirements in the areas of fuel economy and emissions⁶. To help meet these requirements, continuous CFRP's are required as they maintain the highest aspect ratios and allow for the greatest potential yield.

In the automotive industry, good impact properties including energy absorption and strain to failure are required to withstand the extreme forces of an automobile accident. Carbon fiber has a poor interaction with majority of the polymers due to its nonpolar surface and extremely crystallized graphitic basal planes with inert structures¹⁶. Because of this, the strength of interfacial bonding between polymer matrix and CF is low; hence, composites with good interfacial mechanical performance are difficult to fabricate¹⁶. Pore interfacial bonding between the fiber and matrix has been shown to have a positive effect on the impact properties of the

composite. This allows some slipping of the fiber within the matrix allowing the material to absorb more energy during the impact³⁹. Due to this, commodity polymers like PP provide a balance between good mechanical properties while providing high impact toughness.

2.3 Continuous Intermediate Materials

2.3.1 Pultrusion

Pultrusion systems are one of the cheapest and most widely used methods of producing high quality continuous CFRP's in the advanced materials industry today. The process consists of pulling a resin infused fiber bundle through a die system. Through this process, continuous parts can be produced with a constant cross-section^{18,40,41}. This process is widely used in the industry due to its high processing speeds, high efficiency and low production cost^{18,34,35,41}. Figure 1 outlines the general pultrusion process.

The pultrusion market is dominated by thermoset pultrusion while thermoplastic pultrusion remains a relatively new area of study. Thermoplastics are often more difficult to process due to higher working viscosities (average thermoset viscosity 0.03–1 Pa·s^{18,42}, as opposed to 500–5000 Pa·s for thermoplastics^{18,43}). Due to this issue, high quality thermoplastic pultrusion remains a relatively expensive process due to the low production and constituent material availability. Amongst thermoplastic pultrusion manufactures, two main branches of thermoplastic pultrusion exists: reactive and non-reactive. Reactive thermoplastic pultrusion (RIM Pultrusion) is a process where the thermoplastic is polymerized by a catalyst causing a chemical reaction while simultaneously impregnating the fiber tow^{18,44}. This thesis will focus on non-reactive thermoplastic pultrusion. Non-reactive thermoplastic pultrusion relies on a thermal process of bringing the polymer up to its melting temperature (T_m) and impregnating the reinforcement fibers with the matrix. Several types of non-reactive thermoplastic impregnation processes exist including powder impregnation, comingled filaments and hot melt impregnation^{18,43,44}. Comingled filaments are produced by intermingling thermoplastic and reinforcement fibers where the fibers are intertwined in the winding phase. The comingled polymer and reinforcement fibers are then heated to form the composite matrix. Powder impregnation is a method of impregnating a reinforcement fiber with a powdered polymer. In this method, reinforcing fibers

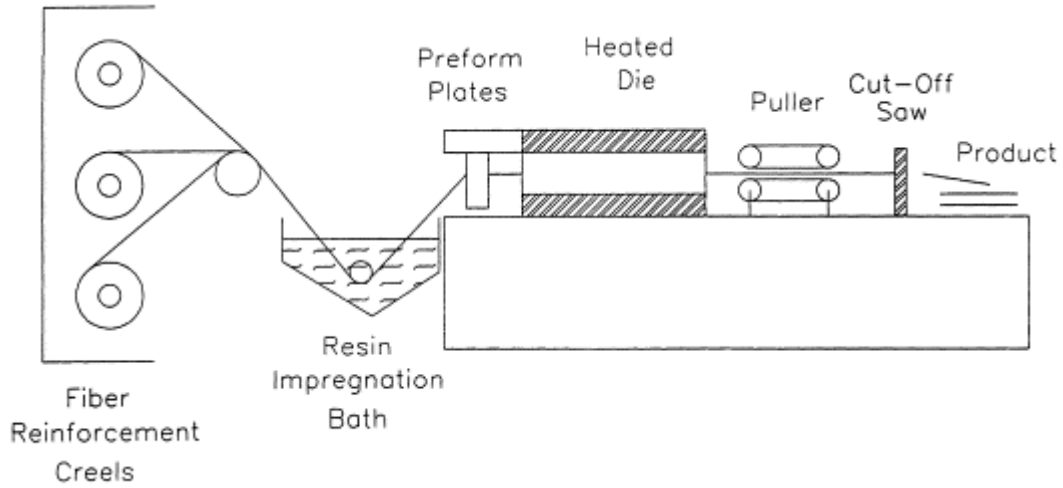


Figure 1: Schematic of traditional pultrusion process where resin is sent through a resin bath and is then cured through a heated die system. This process produces continuous CFRP products with constant cross-section in large scale composite manufacturing.

pass through a chamber with the powdered polymer. This polymer is then picked up by the fiber and fed into the heated chamber where the thermoplastic polymer is melted and joined with reinforcement fibers under heat and pressure¹⁸. Hot melt impregnation is a process where thermoplastic pellets are fed through an extruder and are directly shot into a heated die system where the reinforcement fiber is impregnated with the resin system. A breakdown of these pultrusion processes can be found in Figure 2. This method of impregnation was used in this thesis.

Hot melt impregnation is a process the reinforcement fibers are pulled directly through a melted polymer bath or where thermoplastic polymer is extruded directly onto the reinforcing fibers^{18,45,46}. Melt impregnation methods that use a molten polymer bath work similar to a thermoset pultrusion system where reinforcement fiber is submerged within a molten bath of polymer⁴⁷. Squeegee rollers are often used control fiber content within the composite. This method of thermoplastic pultrusion is an effective method of impregnation although degradation of the polymer is likely due to the polymers increased time under high temperature⁴⁸. Hot melt impregnation methods that use an extruder generally inject molten polymer directly into the die system. This method of impregnation provides good process control, high processing speeds and low production costs⁴⁶.

The hot melt impregnation process provides numerous processing challenges due to the high viscosity of thermoplastic polymers. If not processed properly, the matrix will not fully impregnate the fiber tow creating fiber rich and resin rich regions affecting the part quality and performance. Despite processing challenges hot-melt impregnation provides the cheapest solution for thermoplastic impregnation due to the readily available pelletized polymer that is used throughout the plastics industry.

Pultrusion processing lines generally use a closed die system which induces increasing pressure along the length of the die. The applied heat and pressure inside the die helps to create an even fiber distribution, increase consolidation and reduce void formation in the composite part⁴¹. The thermoplastic impregnation line used in this study differs from traditional pultrusion mainly in the type and application of the die system. An open die system was used for this study which

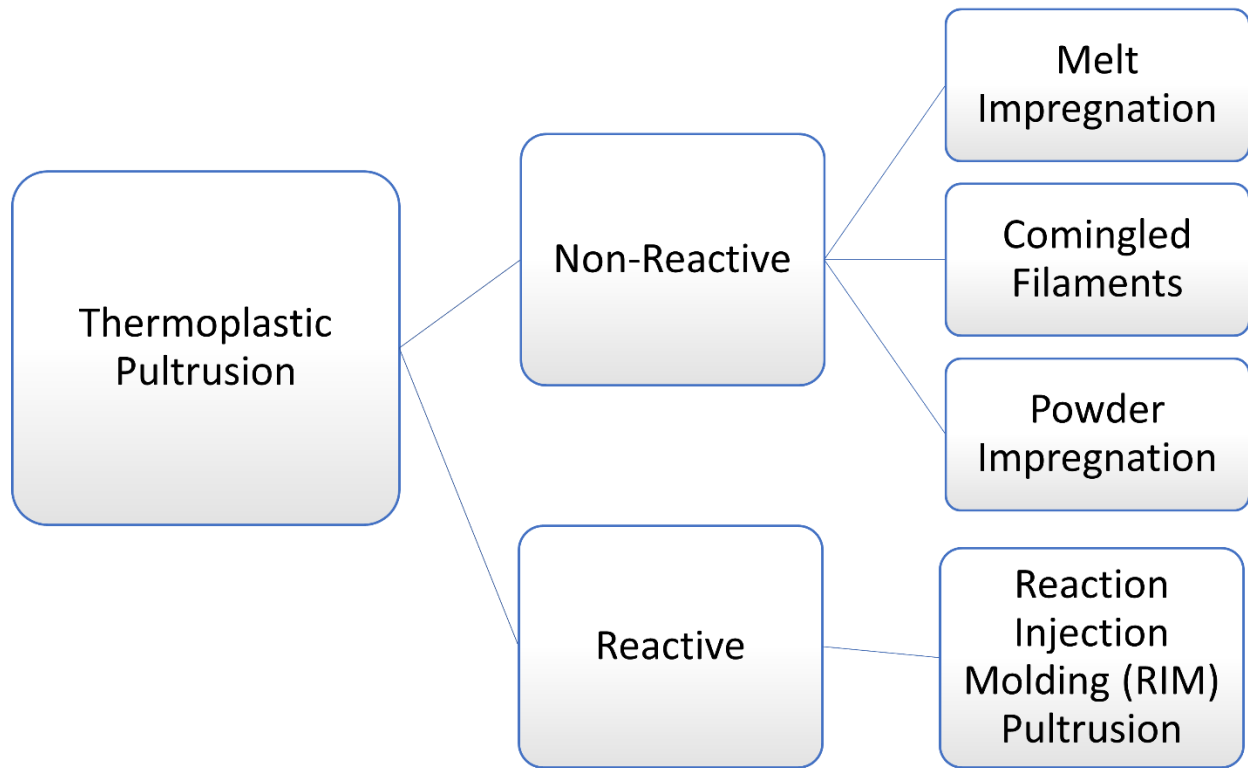


Figure 2: Thermoplastic pultrusion process breakdown. Thermoplastic pultrusion is broken up into two main categories: Reactive and Non-Reactive pultrusion.

consisted of two stage die system. Firstly, a sheet of polymer is extruded onto the fiber. Secondly, a heated pin system pushed polymer through the fiber by inducing tension and spreading resulting in full fiber wet-out. This process produces an intermediate material known as composite tape which can be used in several well established manufacturing methods including compression molding, injection molding and automated tape placement.

2.3.2 Process Line Development and Overview

This study is focused around the application, parameters, and mechanical properties of low cost CF tape produced on a lab scale thermoplastic impregnation line. There were two main considerations when it comes to the production control and quality of thermoplastic tape; fiber weight (or volume) percentage and fiber wet out⁴⁹. With each of these considerations there are several variables that affect the outcome. For fiber weight percentage line speed and extruder speed are the main considerations. Equation 1 shows the relationship between line speed and polymer flowrate. These parameters affect the amount of polymer that is placed on fiber tow over a certain time interval, which directly relates to the CFRP fiber weight as a percentage of the overall composite⁵⁰. This percentage of fiber content or fiber weight fraction (FWF) has a direct correlation to the outcome of the mechanical properties where higher fiber content generally increases mechanical properties of the composite. This is true up until the critical fiber volume fraction (FVF) where beyond which mechanical properties are degraded due to insufficient spacing between individual fibers within the matrix⁵¹. For fiber wet out pin angle, fiber path and spreading have the largest effect on the production quality of tape. This is explained in more detail when discussing Darcy's law (Equation 2 & Equation 3).

$$\text{Equation 1} \quad FWF = \frac{\text{Fiber Density} * \text{Pultrusion Line Speed}}{(\text{Fiber Density} * \text{Pultrusion Line Speed}) + (\text{Polymer Density} * \text{Polymer Flowrate})}$$

Larock and Hahn⁴⁵ note several design flaws with closed die thermoplastic pultrusion systems which include: (a) fibers may become pinched between the two halves of the die system when assembling causing fiber breakage and (b) molten polymer may stick to the die walls hindering or blocking passage of the composite through the closed die. For both situations a complete shut down and restringing of the line must be performed. Development of this impregnation line was done in consideration of the previous development challenges by focusing mainly on an open die

process compared to a traditional closed die system^{18,46}. This, in theory, was developed to increase break angle and tension inside the die for optimal fiber wet-out while simultaneously streamlining the thermoplastic impregnation process⁵².

This thermoplastic impregnation system consists of 5 modules. (a) The fiber initially comes off a creel where the fiber is pre-tensioned and (b) is then passed across a heated pin. This heated pin partially degrades and softens the sizing allowing the fiber to spread. (c) The fiber is then sent over an adjustable roller where the curvature of the roller can be changed to increase or decrease the amount of spreading. The optimal tow spread width for this system was 4 inches. (d) The tow was then passed across a final heated pin where the fiber is heated up to match the temperature of the polymer. (e) A coat hanger die is attached to a modified Dyze Design™ single screw extruder. The coat hanger die is designed to spread the polymer into a flat sheet to match the width of the fiber tow. (f) The fiber and polymer are then sent through a series of heated pins where induced tension and spreading on the fiber which forced polymer through the fiber medium. (g) The composite tape was passed underneath an air knife attached to a vortex tube where approximately 0°C compressed air, flash cools the composite. (h) The composite is pulled with a pinch puller system which maintains the constant line speed for the system. (i) A load cell and clutch then work in tandem to take up the composite tape maintaining even tension insuring a neat roll of tape. Figure 3 shows a visual representation of this hot melt thermoplastic impregnation system.

Equation 2

$$q = -\frac{k}{\mu} \Delta P$$

Equation 3

$$s = \sqrt{\frac{2 * k * \Delta P * t}{\mu}}$$

q = instantaneous flow rate

k = permeability constant

μ = dynamic viscosity of the fluid

Δp = pressure drop

s = impregnation depth

t = time of impregnation

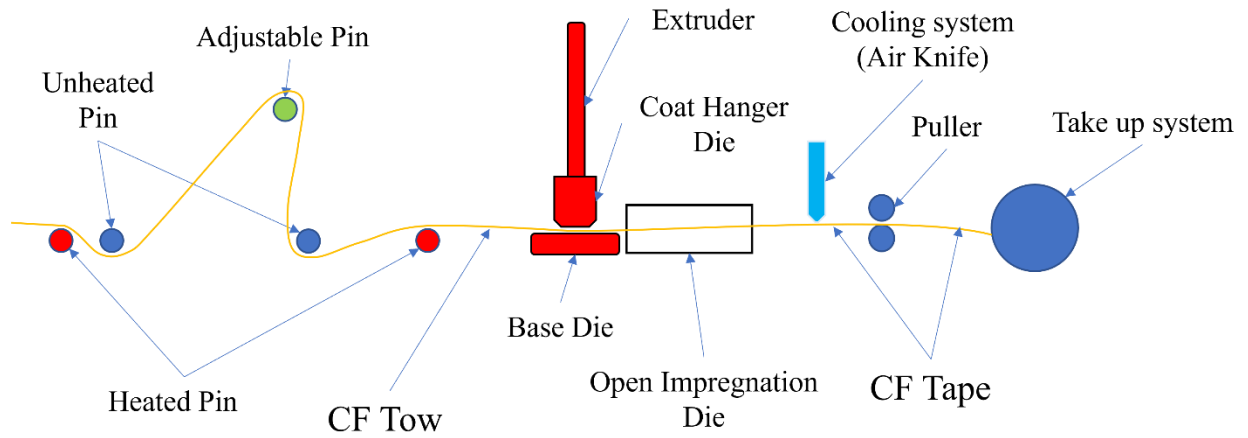


Figure 3 : Thermoplastic tape impregnation process. This system was designed for the impregnation of wide tow (+350K) textile grade carbon fiber (TCF).

These die systems are modeled using Darcy's law represented in Equation 2⁵². Darcy's law describes how a viscous fluid passes through a porous media where q represents the instantaneous flow rate of the polymer through the fiber matrix, k represents the permeability constant of the reinforcement fibers, μ is the viscosity of the fluid and Δp describes the pressure drop through the fiber media^{53,54}. Darcy's law is a well-established model for calculating the resin flow through a fiber matrix in composite manufacturing⁵⁵. Darcy's law can then be integrated over time to solve for impregnation depth (Equation 3) where s is the impregnation depth⁴⁹.

Pethe⁵² studied the effects of pin configuration and fiber wrap on the impregnation quality of a 363K TCF tow impregnated with a PP matrix. Four pin configurations were studied where fiber breakage within the heated pins and impregnation quality was analyzed. Understanding Darcy's law is critical to the methodology implemented in this study⁴⁹. An optimized system would have a high permeability constant and pressure drop across the fiber medium while simultaneously induce a low dynamic viscosity of the polymer. This was found to be achieved by increasing tension within the line inducing shear thinning of the polymer while simultaneously increasing pressure drop through the thickness of the fiber. The permeability constant could also be increased by increasing tension within the line due to induced spreading of fiber during impregnation. The other consideration for this study was fiber breakage while the fiber and polymer pass through the heated pin system. In the first part of the study an extreme wrap angle of all 8 pin was found to induce a high enough tension to break the fiber tow. Through the several iterations the optimized pin configuration and fiber wrap was settled on where the pin configuration was set to +45, -45, +45, -45. The fiber wrap was set to pass over the first dual pin set while only passing over a single pin on the other three dual pin setup. A visual representation of the optimized pin configuration can be found in Figure 4.

2.3.3 Continued Process Line Development

Development of the thermoplastic tape impregnation line continued with an (a) upgraded electrical system, (b) pin die system for optimal temperature control and (c) an in-line tape slitting system. (d) Further development continues with the development of a LFT, and rod die system. A detailed overview of each system can be found in the appendix.

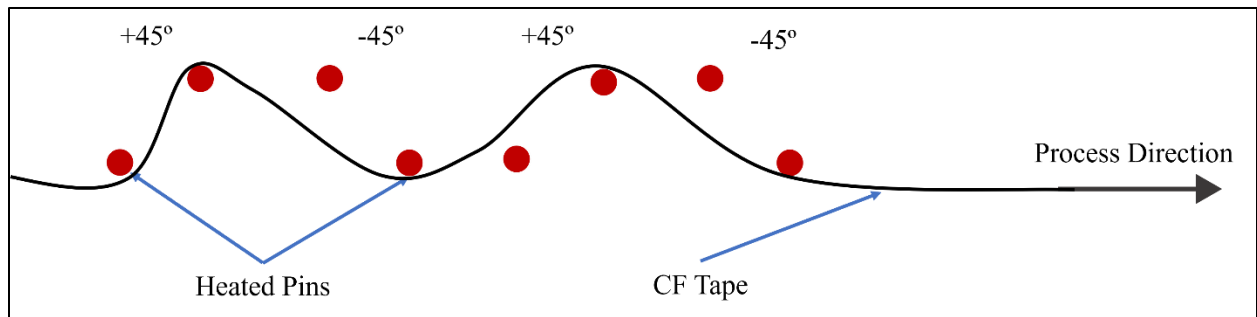


Figure 4: Optimized pin configuration of the heated pin die system. Duel pin configurations were set to +45, -45, +45, -45 respectively. Fiber was weaved through the pin system as shown. This pin configuration and weave pattern was found to optimally impregnate the CF tow.

Electrical System

The upgraded electrical system was developed to have higher process control and improve the user interface (Figure 5). This electrical system was designed in collaboration with Stephen Sherriff (Staff Engineer), Saurabh Pete (MS Student), Nicholas Crowder (UG), Joel Rodeghiero (UG) and Mason Rucinski (UG). The electrical system features 3 phase, 240 Volt, 100-amp power supply that supplies power to 20 heaters and three motor drivers. The motor driver and display system was controlled by an Arduino mega while PID controllers with K-Type thermocouples were used for heater control. Power supply and control was organized in the main power supply box. A secondary distribution box was set as a stable platform on the tape line to distribute power to the respective systems. Detachable outlets were integrated on to both the main power supply box and distribution box to carry electrical power and control between the systems. Two emergency stop systems were integrated onto the impregnation line with one on each end of the system that was connected to an arc suppressing contactor for immediate shut off of the impregnation system.

Upgraded Pin Impregnation Die

A new pin impregnation die was developed to increase temperature control over the impregnation pins (Figure 6). Large fluctuations in temperature was observed within the old pin impregnation system and was correlated to the placement of thermocouples located at the at the end of the insertion heaters. The new pin die was developed to minimized temperature fluctuations by using custom heaters with thermocouples located within the center of the heater. Also, the pin impregnation system was also scaled up with thicker pin walls to act as a heat sink preventing thermal spikes. (This pin impregnation system was not used in this study)

In-Line Tape Slitting System

A tape slitting system was developed to slit the impregnated tapes down to the ½ inch required for use on the automated tape placement system (Figure 7). The design philosophy for this tape slitting system was to have multiple rotating blades spaced at precise intervals where the tape could be pulled along under tension and be cut into long strips. This simplistic design incorporated three parts: Rotary blades, Spacers, and a pinch roller as seen in

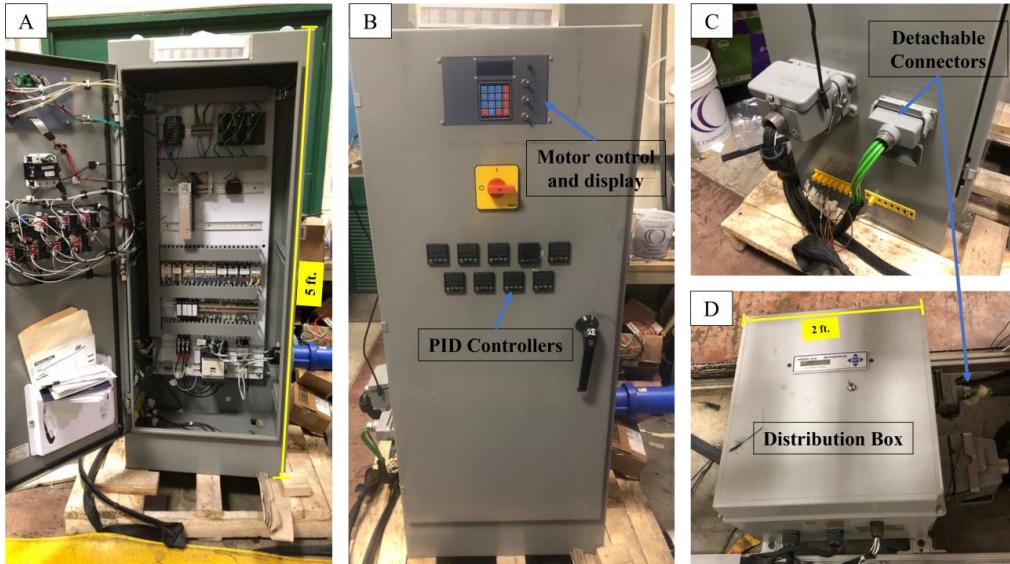


Figure 5: Images of Thermoplastic impregnation line electrical system. (A) Front view of electrical box. (B) View of the open electrical box. (DC – Top Section) (AC – Bottom Section) (PID wires on open door). (C) Distribution box on the base of the tape line. (D) Quick connects on the side of the main electrical box where wires can be easily removed.

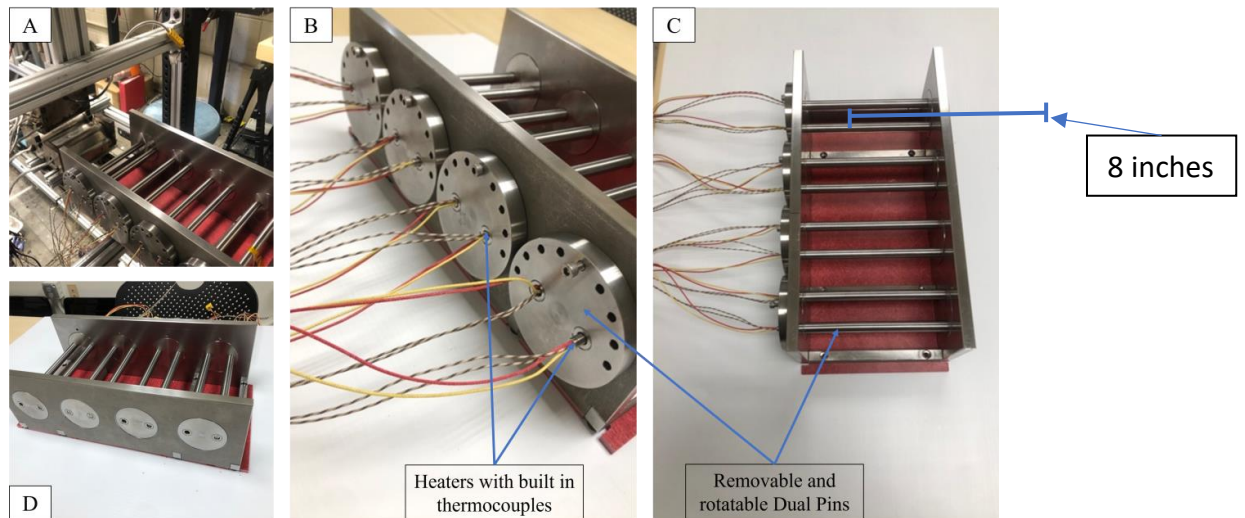


Figure 6: New Pin Die System. (a) View of Pin die system mounted onto the tape impregnation (b) Front side view showing heater and thermocouple wires inserted into rotating pins. Pins can be turned and locked into places at intervals of 22.5° covering a 180° operational window. (c). Top view (d) Back side view

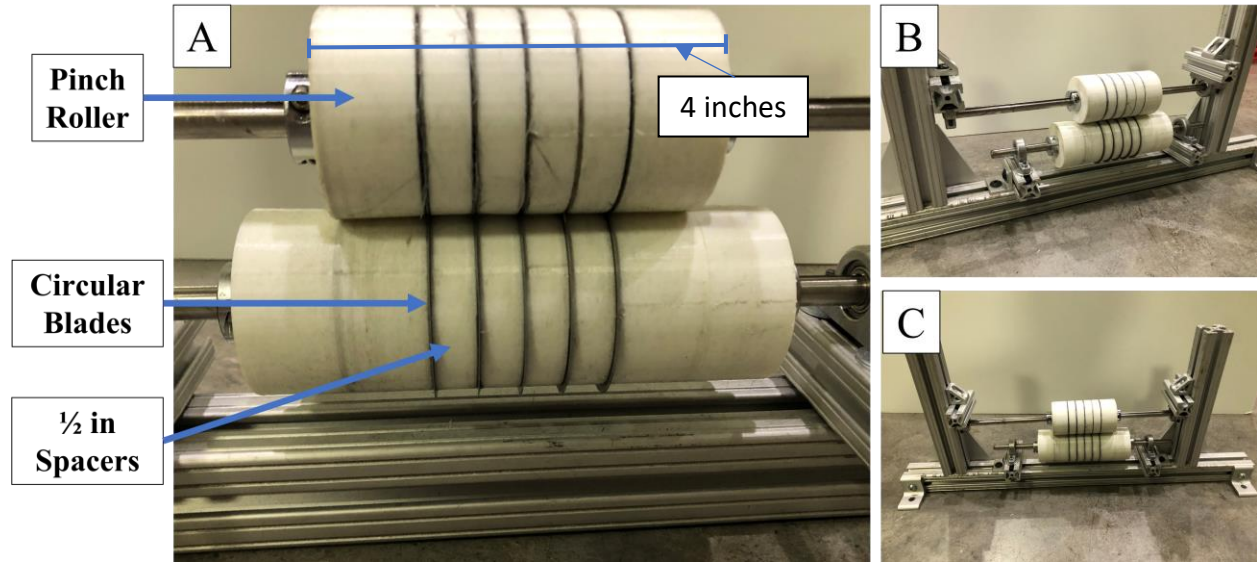


Figure 7: Tape Slitting system. (A) large view of tape slitting. (B & C) close up of AM manufactured spacers and pinch rollers. This system was designed to allow for the ease of taking on and off the line by the removal of two bolts. Five blades are attached to continuously slit 4 one half inch tapes to be placed on an automated tape placement system.

Figure 7. The spacers and pinch roller utilized polymer additive manufacturing (AM) of Thermoplastic Polyurethanes (TPU) which was chosen due to its natural flexibility allowing the pinch system to deform as the slitting system rotates.

LFT and Rod Die System

An open die concept was developed to produce long fiber thermoplastic (LFT) pellets and rods in-line with the hot melt impregnation system (This system is currently under development). LFT pellets and composite rods traditionally use a closed die design as a part of a pultrusion system. These closed die pultrusion systems were initially developed for thermoset resin systems and were modified when thermoplastic pultrusion systems started to be developed. Often fiber breakage within a die system can mean a shutdown of a production line costing extensive time, money, and resources. A complete rethink of how pultrusion systems form shapes is needed for thermoplastic manufacturing especially for the production of ultra-wide tow CF. This system was conceptualized to use the tension within the pultrusion system as a means of rod consolidation. This system would have a flaw where highly tolerance parts would be unable to be produced although for production of intermediate materials like LFT through this consolidation process could stream line the production process.

2.4 Automated Tape Placement (ATP)

The automated tape placement (ATP) or automated fiber placement (AFP) process (Figure 8) takes advantage of a multi-axis robotic arm with a head that does the primary function of placing pre-impregnated composite tape⁵⁶. The tape is placed on a creel where it is fed through a series of guide slots^{33,36,57,58}. These guide slots hold the tape in place to insure the accurate placement of the tape. The tape is then passed through the heating element which provides the required processing temperature for the material^{33,36,56,57}. The fiber is then fed into the nip point or the place where the tape meets the substrate^{36,57}. A compaction roller is then passed over the new ply providing downward pressure adhering it to the substrate. When placement is finished, a pneumatic knife cuts the tape to prepare for the next band or ply⁵⁶. Both thermoplastic and/or thermoset ATP use this method of placement although temperature and post processing requirements differ⁵⁷. A visual representation of this process is shown in Figure 9.

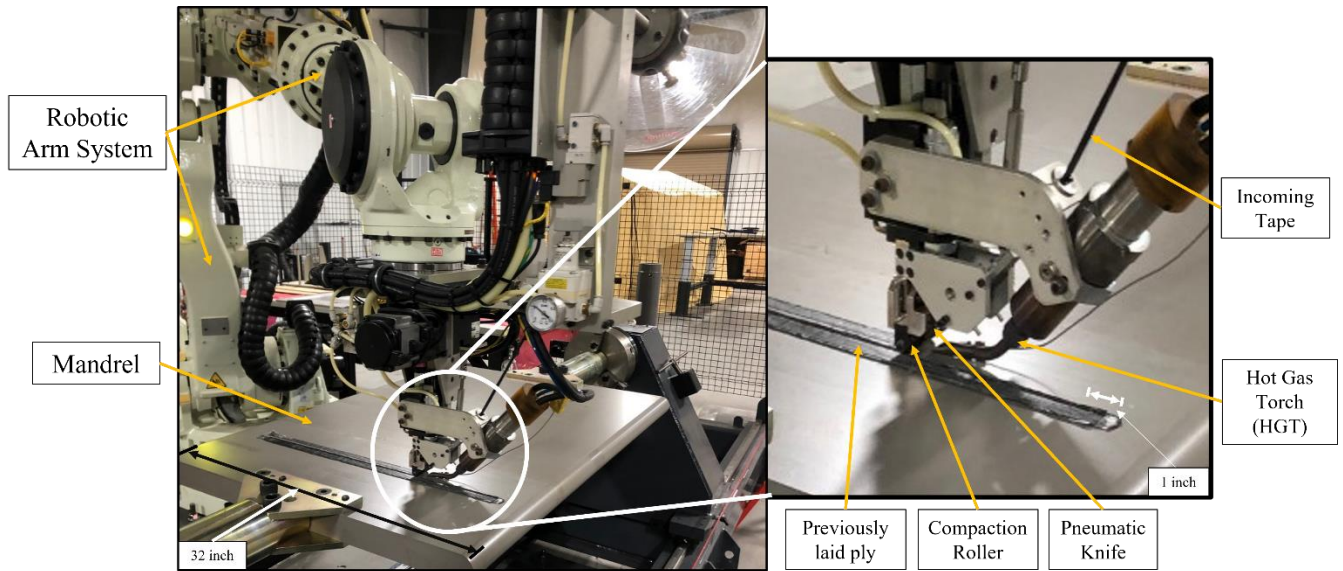


Figure 8: 7 axis robotic arm and HGT thermoplastic Automated Tape Placement head. Robotic system works in tandem with the mandrel to place and consolidate thermoplastic tape.

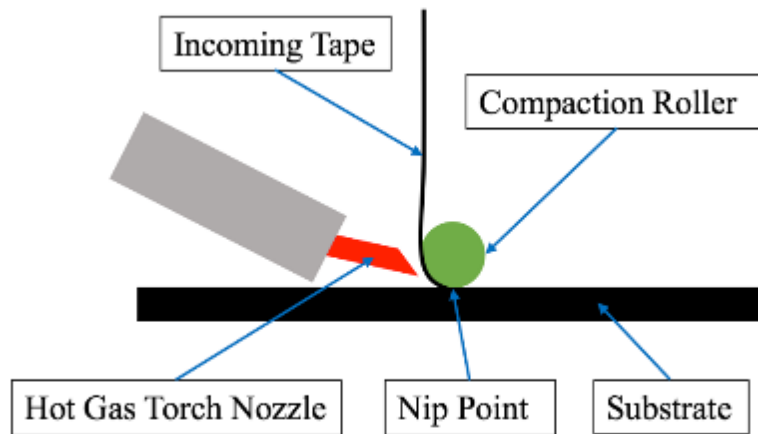


Figure 9 : Illustration of a hot gas torch (HGT) automated tape placement (ATP) head configuration.

For thermoplastic ATP processes several different types of heating elements have been investigated for in-situ tape placement. These methods include infrared (IR) heating³³, ultrasonic consolidation^{33,59}, laser assisted heating^{33,36,60} and hot gas torch^{33,57,61}. Each of these methods of heating provides a unique and effective solution for adhering layers of tape together. This study will focus primarily on the method of hot gas torch (HGT) heating. HGT uses convective heating of an inert gas (nitrogen) that is directed toward the tape at the point just before compaction^{33,62}. The hot gas rapidly heats the thermoplastic composite tape providing consistent convective heating to melt the polymer above melting temperature (T_m). A thermocouple measures the temperature of the gas at the point where the gas leaves the HGT nozzle. This provides accurate feedback for the temperature control system.

Much of the research relating to in-situ consolidation of thermoplastic been focused primarily on the use of laser assisted heating methods due to generally higher deposition rates due to higher energy density and better process control⁶³. Because of this, laser systems are often viewed as elite, but HGT systems do provide some advantage over laser heating. Laser systems are designed to be transparent to the polymer matrix and directly heat the CF. Due to this laser systems are strictly used for CF in-situ consolidation where HGT systems would be required for glass fiber (GF) composites. Secondly, laser systems pose an extreme health and safety risk needing large safety wall systems to protect operators. Additionally, laser systems require precise directional control of the beam to be aimed at the nip point where HGT systems require less directional optimization⁶⁴.

The compaction rollers play an important role in the consolidation and adhesion between newly added layers and the substrate. The most common types of materials used are steel, brass and silicone³³. Generally, rigid rollers like steel are used for HGT ATP due to steels high temperature resistance. Rigid rollers have one main problem which is that the roller does not conform to the curvature of the mold. With complex mold geometries, this can lead to a reduction of intimate contact between the new ply and the substrate, intern reducing the bond strength between laminates. To solve this issue, rollers with curvatures (Figure 10) that match the mold geometry can be attached to increase the contact surface between the roller, tape and laminate ultimately contributing to the degree of autohesion between the two laminates.

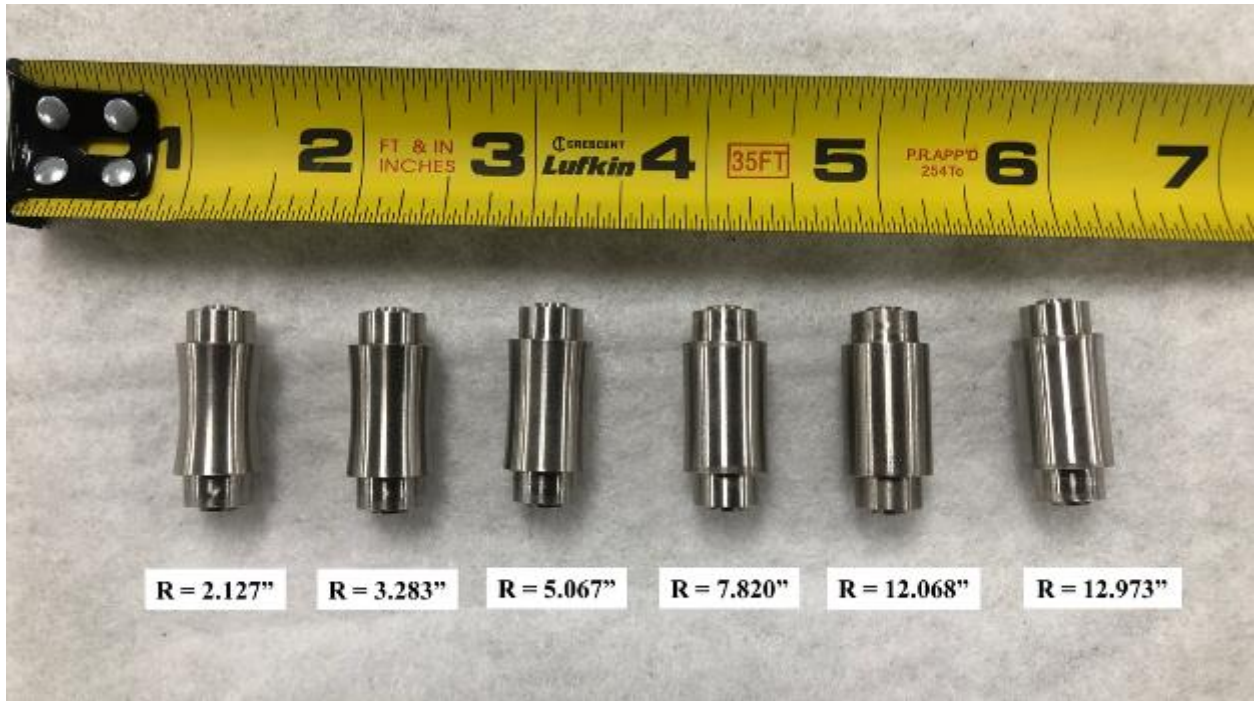


Figure 10: Curved compaction rollers for matching mandrel curvature. These compaction rollers can easily be swapped out during the hot gas torch (HGT) in-situ consolidation process to match the mandrel curvature.

Autohesion is defined by the inter-diffusion of polymer chains between added laminates⁶⁵. A visual representation of this process can be found in Figure 11. Diffusion of the polymer between the added layer and the composite substrate increases with time under pressure. Thusly, increasing intimate contact between the compaction roller is critical to the reduction of void formation ultimately increasing bond strength between laminates^{33,57}.

2.5 Summary and Research Gaps

This thesis is intended to analyze mechanical and morphological properties of the available low cost continuous CF for applications in the automotive industry. To the best of the author's knowledge, no research is available on the process parameters and properties of low cost CF applied to an ATP or AFP system. Also, no research is available on the LVI impact properties of continuous TCF and Zoltek_PX35 fiber. This research is intended to fill in the gap between discontinuous CFRP's mainly being explored in the automotive industry and continuous CFRP's widely accepted in the aerospace industry. To do this, a low-cost polypropylene has been paired with low-cost CF and been impregnated on a lab scale hot melt pultrusion impregnation line to produce an intermediate CFRP tape. This tape was then used to produce composite plates using compression molding and ATP manufacturing to analyze their mechanical and morphological characteristics.

2.6 Relevant Literature

2.6.1 Low Velocity Impact

Understanding impact properties and failure modes of CFRP laminates is critical to uphold the high degree of safety required in the automotive industry. Accurately capturing force and displacement measurements can help to better understand the failure mechanisms of the composite structures⁶⁶.

Nogueira et al.⁶⁷ performed impact analysis on plain weave CF-PP-PE plates to analyze fracture mechanics and impact strength of composite structures related to tensile strength. Woven CF

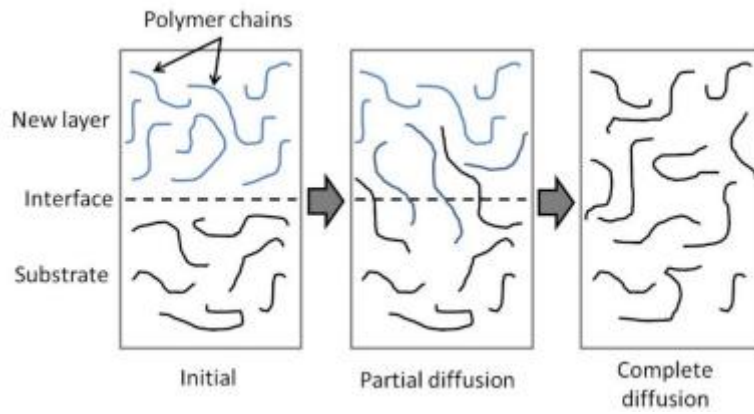


Figure 11: Inter-diffusion of polymer chains between laminates during autohesion ⁶⁵.

laminates were stacked with films of PP, PP-PE, interfacial compatibilizer - AM1 and an elastomeric modifier – AM2 which was processed using hot compression molding. Samples were produced by varying the matrix components to analyze how these polymers affect the tensile and impact properties. Conclusions from this research showed CF-PP/PE-AM1 samples exhibited the highest tensile strength due to strong interfacial bonding between the fiber and matrix. Inversely, the strong interfacial bonding negatively affected the impact properties of this material as little delamination was observed during failure. Following this same logic, CF-PP/PE-AM2 was observed to exhibit the lowest tensile strength and highest impact strength due to reduced fiber matrix interfacial bonding allowing delamination of the composite and increasing impact strength.

2.6.2 Effect of fiber shape on Mechanical Performance

Fiber shape has been shown to have a profound effect on the mechanical performance and failure of composite materials due to the fiber matrix interface mechanics⁶⁸. Thermoplastic composites structures often exhibit fiber pull out implying poor fiber matrix interface⁶⁹. An increase strength of the fiber matrix interface through mechanical or chemical bonding can increase the overall performance of the composite material⁷⁰. The two fibers used in this study showed differing fiber shapes and is critical to understanding the differences in mechanical performance of the materials.

Xu et al.^{71,72} conducted a comprehensive study on the effect of CF with kidney structures vs. circular structures to determine how the surface characteristics affect the fiber matrix interface and mechanical performance of CFRP's. It was revealed that kidney shaped CF's were found to have significantly better inter-laminar shear properties and overall better mechanical performance when compared to circular shaped fibers. This increase in mechanical performance was attributed to the increased surface area to volume resulting in a higher load transfer between the fiber and matrix at the interface. It was also presented that due to kidney fibers higher specific surface area and pore volume, these fibers showed increased impregnation performance when compared to circular fibers.

2.6.3 Thermoplastic Pultrusion

Pultrusion systems are one of the cheapest and most widely used method for producing high quality continuous composites with a constant cross section^{18,40,41}. This process is widely used in the industry due to its high processing speeds, high efficiency and low production cost^{18,34,35,41}.

Novi et al.⁷³ studied the effects of three thermoplastic impregnation methods on the mechanical and morphological properties of CF-PP and GF-PP pultruded bars. The three impregnation methods in question were melt impregnated tapes, co-mingled fibers and powder impregnation. Rule of mixtures was used to calculate theoretical values to be compared against mechanical results. This study found that co-mingled fibers exhibited slightly better mechanical properties as compared to pultruded tapes and powder impregnation. Through scanning electron microscopy (SEM) pre-consolidated tapes exhibited the highest quality impregnation while powder impregnation was found to have large voids within fiber rich regions indicating a low quality of impregnation. Co-mingled fibers also showed a high degree of impregnation with small voids located around individual fibers. These voids were likely due the inconsistent dispersion of PP and reinforcement fibers during the pultrusion process. This literature found good agreement between theoretical values and experimental values using the rule of mixtures.

Hartness et al.⁴⁶ developed a novel hot melt thermoplastic impregnation technique which can produce fully impregnated continuous composites with high operating speeds. This method of manufacturing continuous thermoplastic composites (DRIFT™ - Direct Reinforcement Fabrication Technology) was developed to increases availability and production speeds of high-quality, low-cost thermoplastic composites.

2.6.4 Automated Tape Placement

Automated tape placement (ATP) has become the golden standard for the automation of continuous composite layups. Much of the research and investigation into ATP has been focused on high performance aerospace polymers like PEEK, PEAK, and PPS^{56,74}. As ATP processing of thermoplastics becomes more available and better understood this manufacturing process can help to reduce time and labor-intensive nature of composite manufacturing.

Tierney et al.⁷⁵ created a static model for predicting the heat transfer through thickness and the development of bond strength at the ply interface with the use of a HGT ATP system. This was done to simulate the effect of processing parameters on the process of autohesion of an in-situ consolidation process. The properties that affect the bonding and adhesion between the tape and laminate are temperature, and pressure. A static model has been created using these factors to simulate the effect of the processing parameters. It is noted that two main factors attribute to the development of autohesion process: (a) The development of intimate contact between the two laminates and (b) the degree of polymer chain diffusion across the contact surface. In this study, it was found that bond strength between laminates varied through thickness due to processing history and heat sink effects. The center of the laminate was found to have the highest degree of bond strength due to the heat sink effect where repeated compaction cycles could have maximum impact.

A study by **Tafreshi et al.**⁶⁴ involving the heat transfer of through a flat laminate with the use of an HGT ATP process was done using the standard heat transfer equation for orthotropic materials. In this study, an energy balance approach was taken to formulate a 2D heat transfer problem considering the composite substrate and aluminum mandrel subjected to a moving heat source. This model found that through thickness temperature decreases where after five layers of CF-PEAK material the polymer temperature was below its T_g .

Liu X. et al.⁷⁶ on the isothermal crystallization of glass fiber filled polypropylene tape on a HGT setup. This study focused on the effect of substrate temperature on the isothermal crystallization during an ATP process and its effect on the bond strength, matrix squeeze (waviness), warpage, and mechanical properties. It is noted that high temperature and pressure are needed to reduce porosity within the laminates and activate the autohesion process. However, these same parameters coupled with fast cooling rates can attribute to the matrix squeeze resulting in a waviness pattern at the edges of the band during the placement process. This study concluded that an increase in mandrel temperature between 132 °C and 138 °C had a significant effect on the mechanical and morphological properties of ATP processed materials. Results showed an increased isothermal crystallinity, reduction in over all waviness, improved fiber

distribution throughout the laminate cross section, lowered lateral warpage and in increase in ILSS and flexural properties.

Chanteli et al.⁷⁷ studied the effects of repass compression cycles and its effects on interlaminar shear strength and surface roughness within a CF/PEEK laser assisted ATP processed material. Several passing treatments were explored in this study including single, double, perpendicular, and tool side repassing and was compared with a baseline composite processed in an autoclave. Between all four repass methods all samples no significant increase in ILSS strength was found. For this study ATP processed materials were found to have an approximate 60% reduction in ILSS strength and an approximate 40% reduction in open hole compression strength as compared to autoclave processed materials.

Chapter 3: Materials and Methods

3.1 Textile Grade Carbon Fiber

The corresponding textile grade carbon fiber obtained from the Carbon Fiber Technology Facility (CFTF) from Oak Ridge National Laboratory (ORNL) contains approximately 70 wt% of TG-PAN and has a tensile strength of 2.2 GPa, a tensile modulus of 210 GPa and a 1% elongation to failure. Table 2 displays the relevant fiber properties for textile grade carbon fiber (TCF).

3.2 Zoltek *PX*₃₅

Zoltek (a Toray group) has provided a cost equivalent fiber to TCF to be directed toward the automotive industry known as Zoltek_PX35. The tensile strength and modulus of were reported to be 4.12 GPa and 242 GPa respectively³⁰. Table 3 displays the relevant fiber properties for Zoltek_PX35 fiber.

3.3 Polypropylene ExxonMobil™ PP3155 Polypropylene Homopolymer

The polypropylene polymer used for this study was a homopolymer resin designed for spun bond nonwovens. The resin is particularly suited for melt spinning of uniform, high quality fabrics. This polymer has a reported density of 0.900 g/cm³ and a melt mass-flow rate (MFR) (230°C/2.16kg) of 36g/10min tested using ASTM standards D792 and D1238 respectively⁷⁸. Tensile Strength and modulus of ExxonMobil PP3155 were published to be 23.71 MPa and 1.25 GPa respectively.

3.4 Automated Tape Placement Robotic System

The ATP placement heads were designed and manufactured by Automated Dynamics. The Robotic arm that the heads attach to is a Kawasaki ZX-130L 6 axis robot as shown in Figure 12, Figure 13 and Figure 14. In total this robotic system has 9 axis. Axis 1-6 represents the 6 axis of the Kawasaki robot. The 7th axis rotates the tape feed motor. The 8th axis is a spindle system for mandrel rotation. The 9th axis is a phantom axis created by the design team as an encoder to ensure all other axis are synced working off the same clock. This robotic system is

Table 2: Textile Grade Carbon Fiber (From CFTF)^{3,4,31}

Textile Grade Carbon Fiber		
	SI	US
Tensile Strength	3000 Mpa	335 ksi
Tensile Modulus	275 GPa	40 msi
Density	1.76 g/cc	0.0636 lb/in ³
Fiber Diameter	7-10 μm	0.00027-0.00039 in

Table 3: Zoltek PX₃₅ Fiber³⁰

Zoltek PX₃₅ Fiber		
	SI	US
Tensile Strength	4137 MPa	600 ksi
Tensile Modulus	242 GPa	35 msi
Electrical Resistivity	0.00155 ohm-cm	0.00061 ohm-in
Density	1.81 g/cc	0.065 lb/in ³
Fiber Diameter	7.2 μm	0.283 mils
Carbon Content	95%	95%
Yield	267 m/kg	397 ft/lb

Table 4: ExxonMobil™ PP3155 Polypropylene Homopolymer⁷⁸

ExxonMobil™ PP3155 Polypropylene Homopolymer		
	SI	US
Melt Mass Flow Rate	36 g/10min	0.022 lb/10 min
Density	0.900 g/cc	0.0325 lb/in ³
Tensile Strength	23.71 MPa	3.44 ksi
Tensile Modulus	1.25 GPa	0.181 msi

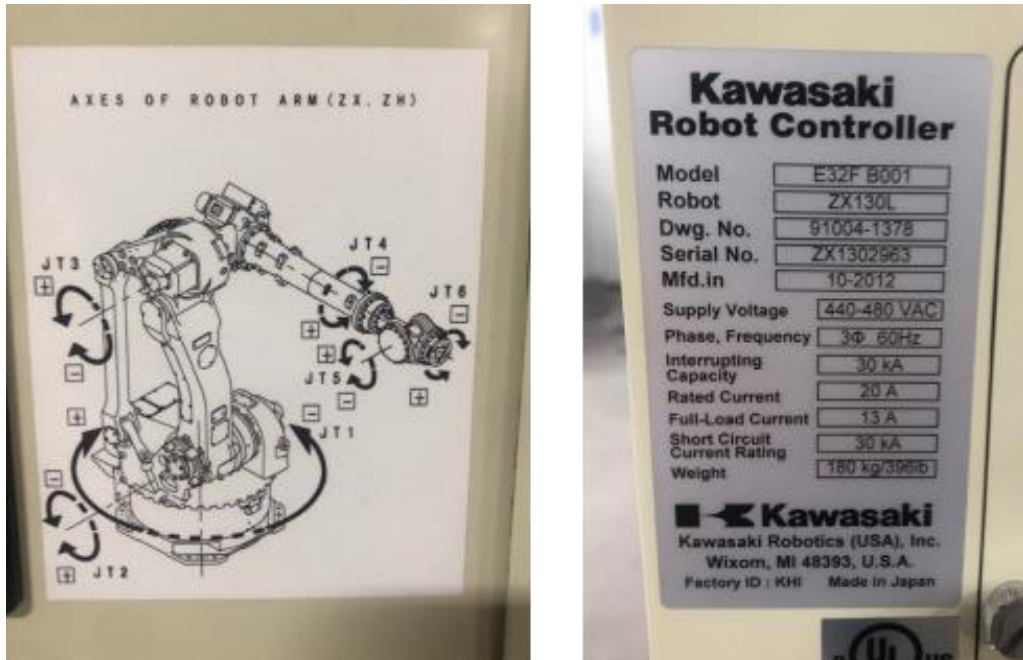


Figure 12: Kawasaki Robot arm specifications. (a) Shows the robotic arm axis system with all degrees of freedom and (b) shows the make and model of the robotic system used in this study along with relevant information about the robot.

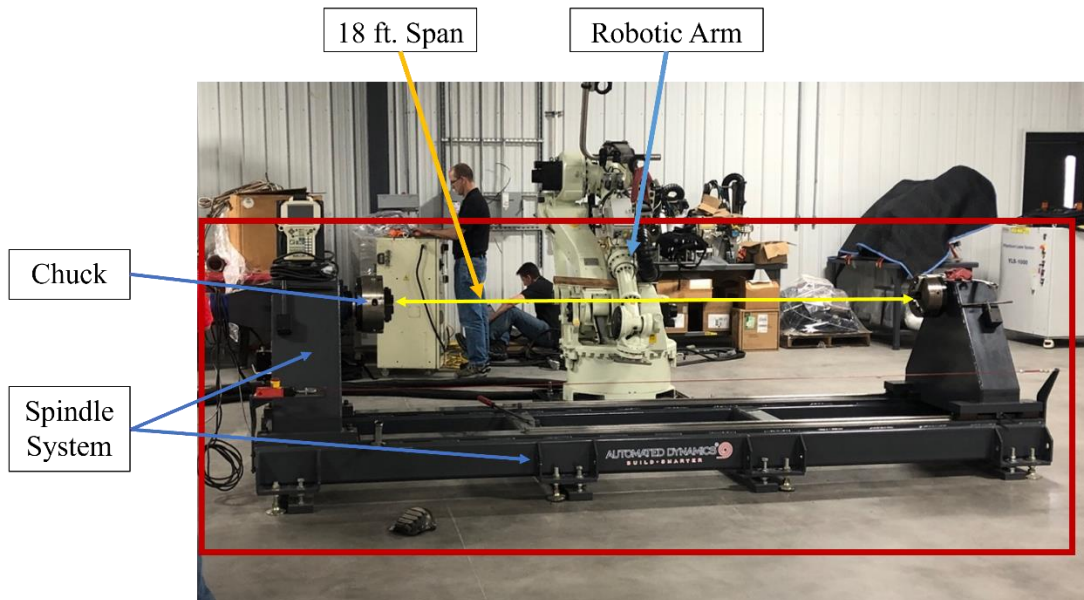


Figure 13: 18 Foot Robotic Spindle for mandrel rotation for large part manufacturing. ATP robotic arm for precise placement of CFRP tape.

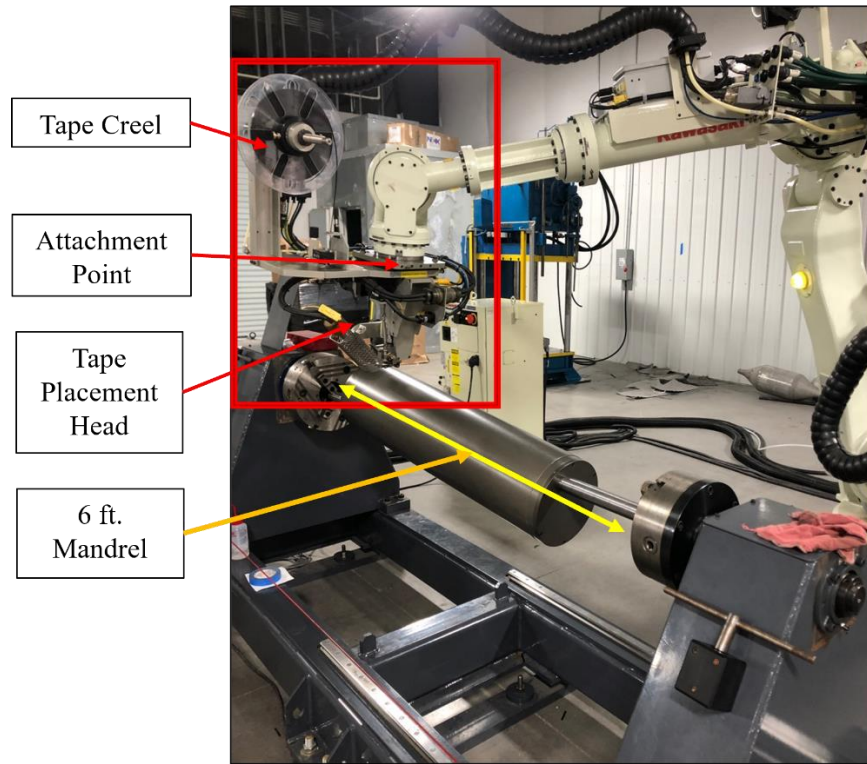


Figure 14: Photo of robotic arm and spindle working in tandem on a rotating off axis cylinder. This figure represents how the robotic system can move in complex motions to conform to complex mold geometries.

controlled by a control system designed by Automated Dynamics that has been integrated with a Solid Works plugin for complex mandrels. Programs are designed by the user based on desired ply angle and number of layers.

3.5 CF-Polypropylene Tape Production

All thermoplastic tape made in this study was produced on a hot melt thermoplastic impregnation line. This impregnation line was developed for wide tow CF (+350K) specifically for the use of TCF developed at the Carbon Fiber Technology Facility (CFTF), Oak Ridge National Laboratory (ORNL).

A preliminary study was conducted on a Dyze's Design™ extruder to determine polymer flow rate vs. motor speed. Results from this study showed a linear relationship between motor speed and PP flow rate. A similar study was conducted on the line speed vs motor speed to determine production line speed vs stepper motor speed. These two preliminary studies were used to determine processing parameters (line speed and extruder speed) of the impregnation system to produce composite tape at a desired fiber weight fraction (FWF).

Zoltek_PX35 and TCF was impregnated with ExxonMobil™ PP3155 Polypropylene homopolymer to produce composite tape (ZT-PP & TCF-PP respectively). ZT-PP and TCF-PP tape was produced with extrusion temperature for polypropylene of 215°C and impregnation pin temperatures were set to 220°C. The intension for this study was to produce tape at a FWF of approximately 35%. To produce ZT-PP tape, two 50K tows were set up and run at a line speed of 1.22 meters per minute with a polymer flow rate of 19 grams per minute. For TCF-PP tape production a 363K tow of TCF was set up and run at a line speed of 1 meter per minute with a polymer flow rate of 24 grams per minute.

3.6 Composites Plate(s) Preparation

The Carver (Model# - 3895.4NE1000) (Serial # - 130181) press has a maximum compression force of 30 tons which utilizes cartridge heaters with a water and air coolant system. Carver press was used to produce all 6x6 inch plates. Flexural samples were produced with 77 grams of tape and was used to make a 0.118 inch (3mm) thick plate. The tape was then placed into the mold

with the desired fiber orientation and put into the Carver Press. The mold was then heated up to 175°C under 1.5 tons (83.33lb/in²). When the mold reached its desired temperature, the pressure was bumped up to 2 tons (111.11 lb/in²). The sample was carefully watched for flow of polymer out of the mold. As soon as flow was observed on the edges of the mold both air and water cooling was started. Once cooled, the mold and plate were then taken out of the press and the mold was disassembled

The Wabash press (Model # - DA150H-36-BOX) (Serial # - 190324) has a maximum compression force of 150 tons with oil heated platens and a water coolant system. The Wabash Press was used to produce all 12x12 plates because this mold was too large to fit in the Carver press. TCF-PP plate was made using layers of TCF-PP tape orientated in a Unidirectional fashion and placed into a 12 by 12 in mold. Platen temperature set to 175°C and 6 tons (83.3 lb/in²) of force was applied. When the mold temperature reached 175°C 8-tons (111lb/in²) of force was applied to the mold with a dwell time of 10 min. The mold was watched carefully for polymer flow and was set to cool at the end of the dwell time. Once cooled, the mold and plate were then taken out of the press and the mold was disassembled.

Drop tower sample layups used approximately 320 grams of tape which was even and oppositely laid up with 22 laminates and pressed in a 12x12 aluminum mold. Plate processing used the compression molding process under the same processing conditions as all other samples prepared. These samples were pressed to a thickness of 0.2 in (5 mm) and cut using a tile saw to 4 by 6 inch rectangles as described in low velocity impact (LVI) test ASTM standard D7136⁷⁹.

3.7 Determining Process Parameters

Little research has been done on low strength polymers like PP on an ATP system as most research in this field has been done on high grade polymers like PEAK, PEAK, PEEK and PPS. Due to the unavailability of processing parameters for HGT ATP process on PP matrix composites a process optimization study was conducted. To determine best processing parameters for PP matrix composites three main parameters determine quality of autohesion between laminates: (a) processing speeds, (b) temperature and (c) compaction pressure⁶². The heat transfer equation given to describe the ATP process is shown in Equation 4.

Equation 4

$$K_x \frac{\delta^2 T}{\delta x^2} + K_y \frac{\delta^2 T}{\delta y^2} + K_z \frac{\delta^2 T}{\delta z^2} + \rho U = \rho C_p \frac{\delta T}{\delta t}$$

Equation 5

$$q'' = h_{HGT} * \Delta T$$

For Equation 4, ρ represents the mass density of the material ($\frac{kg}{m^3}$), C_p is the specific heat ($\frac{J}{kg \cdot ^\circ C}$),

T is the temperature and K_x, K_y, K_z are the thermal conductivities in the x, y, z orientations.

Equation 5 shows the heat transfer (q'') where the process was governed by the convective heat transfer coefficient (h_{HGT}) and the temperature difference (ΔT) between the HGT heated fluid and the composite surface⁶⁴.

This study was performed with Zoltek PX35 fiber impregnated with a PP matrix on a hot melt impregnation line. This material was then slit down to one half inch rolls and was set up to run on an ATP system with the use of HGT. The three main processing conditions used in this study was temperature, pressure and laydown speed. Temperature processing conditions were set to 752°, 797°, and 842° Fahrenheit (400°C, 425°C and 450°C respectively). Pressure processing conditions were set to 100, 120, 140, and 160 lbs force. Laydown speeds were varied between 2, 3 and 4 inches per second. In total, an array of 36 samples were produced by laying down two plies of composite tape on top of each other (Table 5). A section of each sample was chosen and was mounted using Buehler EpoxiCure™ 2 resin and hardener. Each sample was then ground and polished to a surface finish of 1 μm . Microscopy images were then taken of the entire cross-section where the images were stitched together. Stitched images were then modified to enhance the contrast between mounting resin, PP composite matrix and voids. Each cross-section of tape was then analyzed to determine the void percentage of the sample. Figure 15 shows the progression of image enhancement and image processing to determine void content.

3.8 Tensile Tests (ASTM D3039)

Test coupons were cut by method of CNC water jet cutting. Samples were cut to 10in by 0.5, prepared and tested in accordance with ASTM Standard D3039⁸⁰. Tabs were cut and beveled to 90 degrees to help prevent stress concentrations during loading. The tabs were then glued onto the ends of the sample. Sample thickness and width was then measured in three places along

Table 5: List of processing parameters used for an ATP HGT system.

	Pressure (lb)	Speed (in/s)	Temperature (°C)
SET 1	100	2	400
			425
			450
SET 2	100	3	400
			425
			450
SET 3	100	4	400
			425
			450
SET 4	120	2	400
			425
			450
SET 5	120	3	400
			425
			450
SET 6	120	4	400
			425
			450
SET 7	140	2	400
			425
			450
SET 8	140	3	400
			425
			450
SET 9	140	4	400
			425
			450
SET 10	160	2	400
			425
			450
SET 11	160	3	400
			425
			450
SET 12	160	4	400
			425
			450

SEM image taken of sample cross section

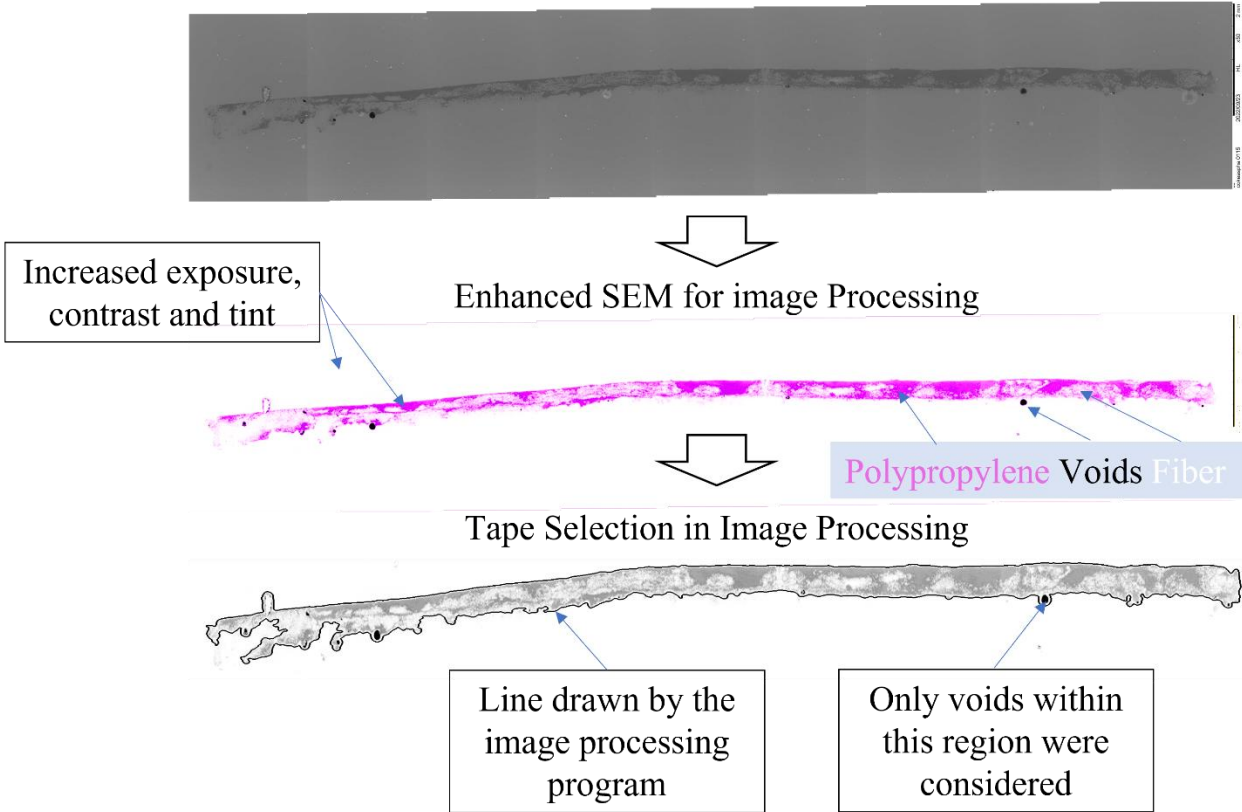


Figure 15: Image enhancement for void analysis on two layers of in-situ consolidated CF-PP Tape produced on and Automated Tape Placement (ATP) system. SEM stitched images were enhanced by increasing exposure, contrast, and tint to allow the program to more easily discern the sample boundary. Image processing program outlines edges of tape to exclude voids outside of the tape region.

length of the sample and an average thickness and width was calculated. For this data set 13 samples were tested on a 50 KN Test Resources frame (product # 313Q, Test Resources, Minnesota, USA).

$$\text{Equation 6} \quad \text{Tensile Strength} = F^{tu} = \frac{P^{max}}{A}$$

$$\text{Equation 7} \quad \text{Tensile Strain} = \sigma_i = \frac{P_i}{A}$$

$$\text{Equation 8} \quad \text{Tensile Strain} = \epsilon_i = \frac{\delta_i}{L_g}$$

F^{tu} = Ultimate tensile strength (MPa)

P^{max} = maximum force before failure (MPa)

σ_i = tensile stress at i^{th} data point (MPa)

P_i = force at i^{th} data point (N)

A = average cross – sectional area (mm^2)

ϵ_i = tensile strain at i^{th} point ($\mu\epsilon$)

δ_i = extensometer displacement at i^{th} data point (mm)

L_g = extensometer gage length (mm)

3.9 Flexural Test ASTM 790

Eighteen flexural samples were cut by method of CNC water jet cutting. These samples were then tested according to the ASTM Standard D790 under ambient room temperature conditions⁸¹.

Rate of Cross head motion

$$\text{Equation 9} \quad R = \frac{zL^2}{6d}$$

$$\text{Equation 10} \quad \text{Midspan deflection} = D = \frac{rL^2}{6d}$$

Flexural Stress

$$\text{Equation 11} \quad \sigma_f = \frac{3PL}{2bd^2}$$

Flexural Strain

Equation 12

$$\varepsilon_f = \frac{6Dd}{L^2}$$

Modulus of Elasticity

Equation 13

$$E_f = \frac{L^3m}{4bd^3}$$

3.10 Drop tower test equipment and testing (ASTM D7136)

LVI tests were performed on an Instron CEAST 9340 that has a maximum velocity of 4.65 m/s with max energy being 405 J. A minimum of 5 samples were prepared for Unidirectional ZT-PP, 0/90 ZT-PP, Unidirectional TCF-PP, and 0/90 TCF-PP. Samples were placed into the LVI equipment and clamped into place (Figure 16). Samples were tested by incrementally increasing the applied impact energy. This was done to determine the maximum impact energy the samples could experience before complete failure. Unidirectional samples were tested by incrementally increasing force by 5 N while cross-ply samples were tested by incrementally increasing force by 10 N. This was done to show the full range of impact properties for each layup pattern.

For analysis of the samples, A Matlab script was written to approximate volumetric damage for each LVI sample. In this preliminary study, some assumptions were made for the calculation of volumetric damage. Firstly, damage was assumed to be consistent through thickness of the sample between the top and bottom superficial damage and secondly, damage was assumed to take on bending deformation that intern takes on a truncated cone or trapezoidal prism shape⁸². A 2D representation of this volumetric analysis is shown in Figure 17. Superficial damage was visually inspected and outlined on the top and bottom of each sample. An image of the top and bottom surface was taken and input into MATLAB script were the image was cropped to exclude the area outside of the sample. Sample dimensions were known (4x6 in.) and were used to calculate pixel size for scale. Color threshold values were adjusted to reduce noise in the image. Area within the outlined damage region was calculated and scaled via known pixel dimensions.

To calculate volumetric damage, the calculated top and bottom damaged surface areas were used. Upon visual inspection, unidirectional samples represented a trapezoidal prism shape due

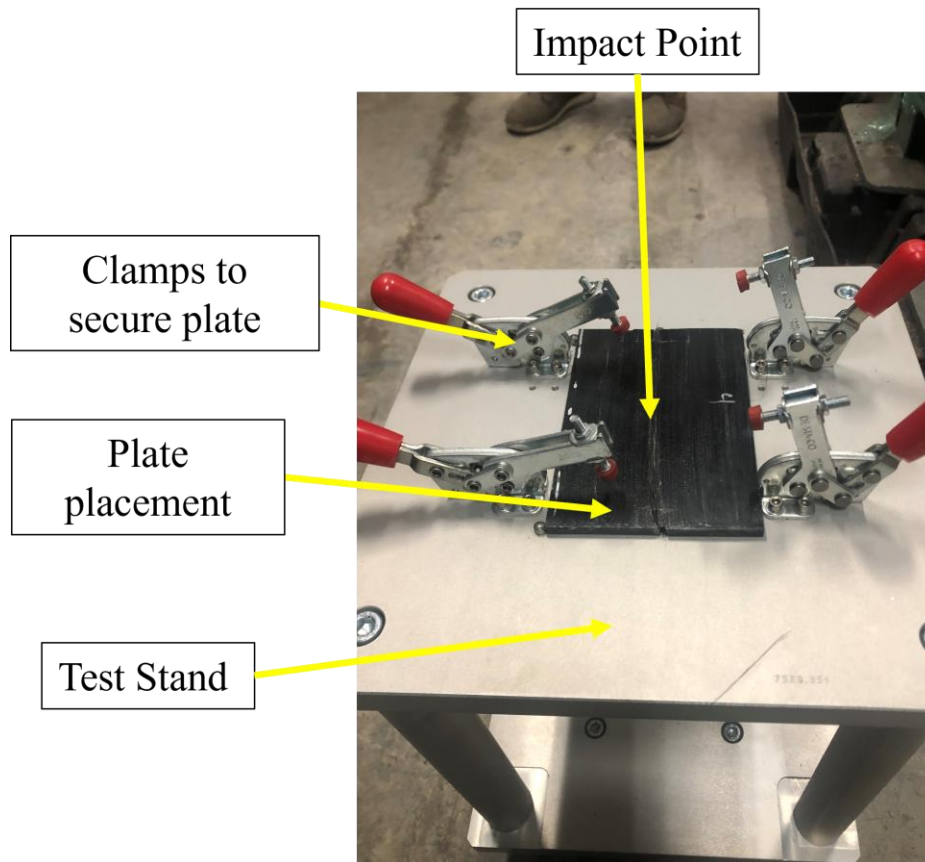


Figure 16: Low Velocity Impact (LVI) Test setup. Sample is placed and clamped down to insure no movement of the plate. This set up is then placed into a climate-controlled chamber where a steel weighted head strikes the center of the plate.

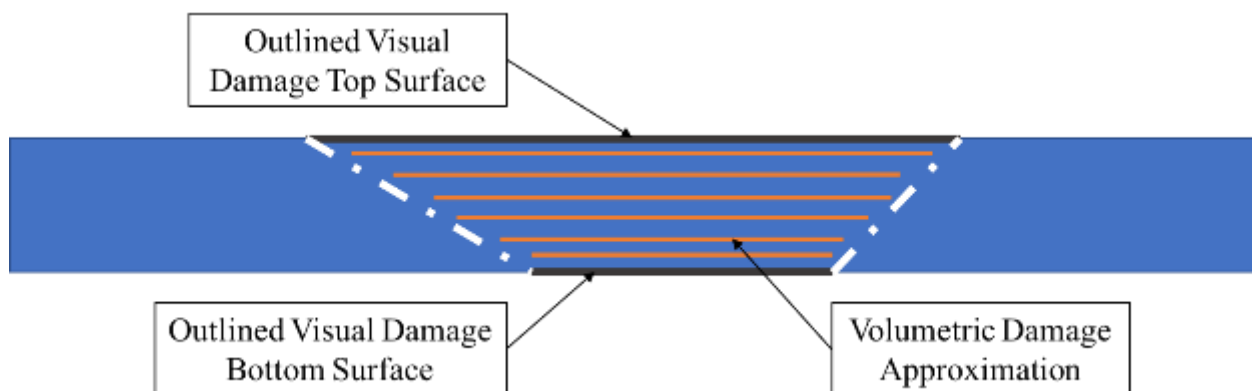


Figure 17: 2D visualization of volumetric damage approximation used for LVI samples.

to the observed failure region (Equation 14). Volumetric damage was calculated in samples laid up in a 0/90 orientation using a truncated cone equation (Equation 15).

$$\text{Equation 14} \quad \text{Volumetric Damage Trapezoidal Prism} = (b_1 b_2) * \left(\frac{h}{2} (b_1 + b_2) \right)$$

$$\text{Equation 15} \quad \text{Volumetric Damage Truncated Cone} = \frac{1}{3} \pi (r_1^2 + r_1 r_2 + r_2^2) h$$

3.11 Thermal analysis

TGA was performed on a TGA Q50 V20. Samples were tested from all plates that were used in this study to determine the consistency of fiber weight by percentage. TGA samples were tested in the temperature range of 24°C to 600°C.

Chapter 4: Results and Discussion

4.1 Thermal Analysis

Based on the preliminary studies of extruder flow rate and puller speed impregnation line parameters were set to achieve a fiber weight of 35%. TGA was performed on each CM and ATP plate to confirm consistent fiber weight fraction (FWF) and fiber volume fraction (FVF). Multiple TGA samples were tested from each plate that was produced. Table 6 show the average FWF and FVF of all materials that were produced. The average FWF and FVF was found to be 35.86% and 24.48% respectively with a standard deviation of 1.13. With the standard deviation well below 10% of the average this thermal analysis shows that the material produced was consistent across all manufacturing cycles and within 1% of expected values. Confirmation of FWF was critical in determining the consistency of the processing line and to support the validity of experimental results.

4.2 ATP Processing Parameters Study

4.2.1 Examination of Void Content in Process Parameters Study

To determine the optimal processing parameters for the use of TCF-PP and ZT-PP tape on an ATP system a study was performed to determine the processing parameters with the lowest void content and dimensional stability. This study was performed by laying two layers of tape on a flat mandrel. Samples were analyzed by taking images under a scanning electron microscope. Images were stitched together and void content was measured by image analysis of the stitched images. Void content was determined to be very low within all samples with a maximum void content of 0.91% and a minimum of 0.0168% void content. Along with void content, notes were taken of each sample and rated 1-5 on how well the material laid down on the mandrel and each sample was inspected for fiber waviness.

4.2.2 Effect of Process Parameters on In Plane Waviness

In plane waviness in ATP processed samples can be defined as a deformation of fiber at the edges of the ply. Fiber waviness is generated under the compaction roller due to the high

Table 6: Average fiber weight and fiber volume percentages for all material plates produced. Overall average fiber weight (FWF) was 35.86% and average fiber volume (FVF) was 24.48%.

	ZT-PP 0/90 Flex	ZT-PP Uni Flex	ZT-PP Tensile	ZT-PP ATP	TCF-PP 0/90 Flex	TCF- PP Uni Flex	TCF- PP Tensile	TCF- PP ATP
Average FWF	35.73%	35.49%	36.85%	36.77%	35.09%	37.93%	34.77%	35.47%
Average FVF	23.86%	23.71%	24.61%	24.56%	24.49%	27.53%	24.26%	24.75%
Footnote: Unidirectional Flexural Samples (Uni Flex), 0/90 Flexural samples (0/90 Flex), Tensile Samples (Tensile), Automated Tape Placement (ATP)								

temperatures and cooling rates which induce compressive thermal residual stresses at the nip point^{76,83}. In plane waviness has been shown to occur where the coefficients of thermal expansion of the laminate and mandrel differ⁸⁴. In addition to waviness, fiber wash was observed due the polymer flow out from under the compaction roller due to uncontrolled matrix flow. This was observed by the reduced thickness and increased width of the processed material. After inspecting all samples, a significant trend could be observed. Low processing speeds produced a high degree of fiber waviness and fiber wash during the lay down process. This was likely due to higher compressive residual stresses where the placed tape has a longer time under pressure and increased time in contact with the hot convective gasses as compared to faster processing rates. Figure 18 shows an image two ZT-PP process parameter samples showing the effect of laydown speed on fiber waviness. Both samples were processed with 140 lb.'s of force and with a HGT nozzle temperature of 450 C. The top sample was processed at 4in/s and the bottom sample was processed at 2 in/s. Higher processing speeds trended toward more consistent samples throughout the entire manufacturing cycle. When investigating CF-PA6 ATP processing Stokes et al⁸⁵ found that matrix squeeze out occurred at high processing temperatures. This can be directly correlated to the matrix squeeze and fiber wash observed in this study. The convective heat transfer during the HGT ATP process is highly time dependent where a decrease in processing rate will increase the energy absorbed during the placement phase. This study shows evidence that the laydown speed has a larger effect on fiber waviness and matrix squeeze then HGT temperature and compaction pressure. This increase in temperature decreases the viscosity of the polymer allowing polymer flow that can be observed as fiber wash. A more in-depth study involving the effect of processing rate on polymer temperature and viscosity could help to better understand the phenomenon.

4.2.3 Relationship of ATP Processed Width and Thickness

This is further backed by Figure 19 which (A) shows the relationship between fiber width and thickness and (B) which shows the correlation between fiber width and thickness in relation to the laydown speed. A direct relationship between fiber width and thickness can be drawn as an increase in processed width corresponds to matrix squeeze. An average processed width and thickness was calculated for laydown speeds of 2, 3 and 4 in/s. A decrease in width and increase in thickness of the processed tape was found with higher processing speed (Figure 19 – B).

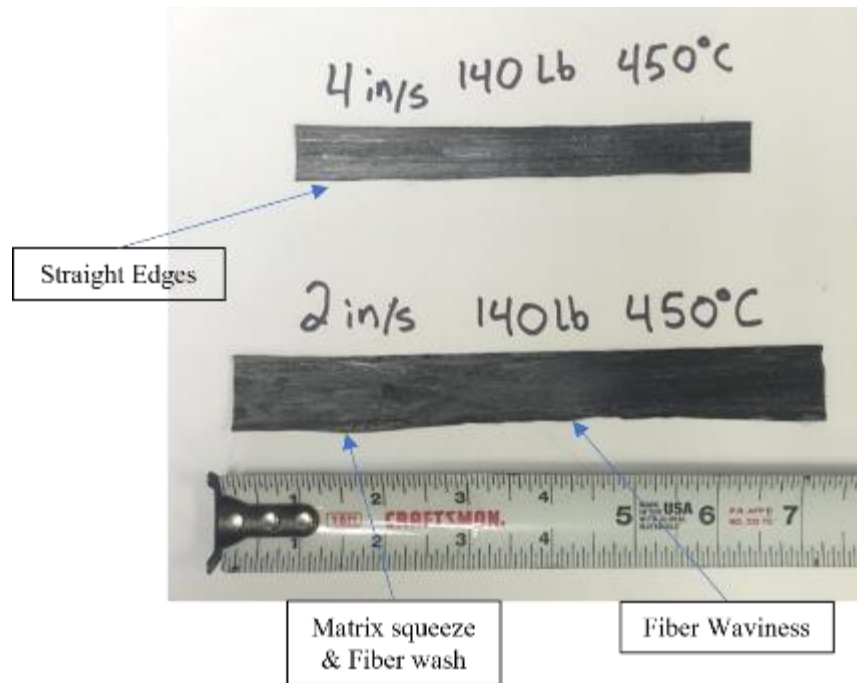


Figure 18: Fiber waviness and increased width between fast and slow speed processing. Straight and consistent edges can be observed with faster processing speeds (4 in/s – 140lb. – 450° C). Inconsistent laydown width can be observed due to matrix squeeze can be observed in low processing speeds (2 in/s – 140lb. – 450 °C)

4.2.4 Process Parameters Conclusion

The chosen process parameters for plate ATP production used 140 lb force, 4 inches per second and 450°C. These processing parameters were chosen based off the results of the previous study. Hoang⁸⁶ studied the void content within an ATP processed laminate and the effect of compaction cycles or repasses on the laminate structure. There was found to be a strong correlation between reduction in void content and repass cycles within an ATP processed laminate especially nearing the top surface of the laminate. However, resin rich and fiber rich regions were not found to be effected by increased compaction cycles. This was likely due to the surface roughness of processed tape trapping resin pockets that could not be removed during the repass cycle. Compaction cycles have been well documented to help with the consolidation of ATP processed laminates^{64,86,87}.

For this study ATP in-situ consolidated plates were produced by winding ZT-PP and TCF-PP tape around a flat mandrel where 10 ply's of tape was laid down. After every three ply's a compaction cycle was run by allowing the HGT head to roll over the previously laid material applying heat and pressure as described in Hoang⁸⁶.

4.3 ILSS Results

4.3.1 Effect of Fiber Shape on ILSS Properties CM

Interlaminar shear (ILSS) results have been compared between the two manufacturing systems: compression molding (CM) and ATP. Across both manufacturing methods ZT-PP samples performed approximately 20% higher than TCF-PP (21.2% for CM and 19.7% for ATP) (Figure 20). Through microscopy analysis it can be observed that the fiber cross section of Zoltek_PX35 fiber is drastically different than TCF. The cross-sectional shape of CF has been shown to have a profound effect on the fiber matrix interface and the composite mechanical properties⁶⁸.

Observationally, (Figure 21). ZT fibers exhibit a kidney bean shape where TCF fibers are circular in nature. This kidney bean shape provides a higher surface area to volume increasing the contact surface of the fiber matrix interface allowing increased load to be transferred from the matrix to the fiber particularly within shear planes of the composite^{71,72}. This kidney bean shape could be attributed to the observed higher mechanical performance of ILSS between the

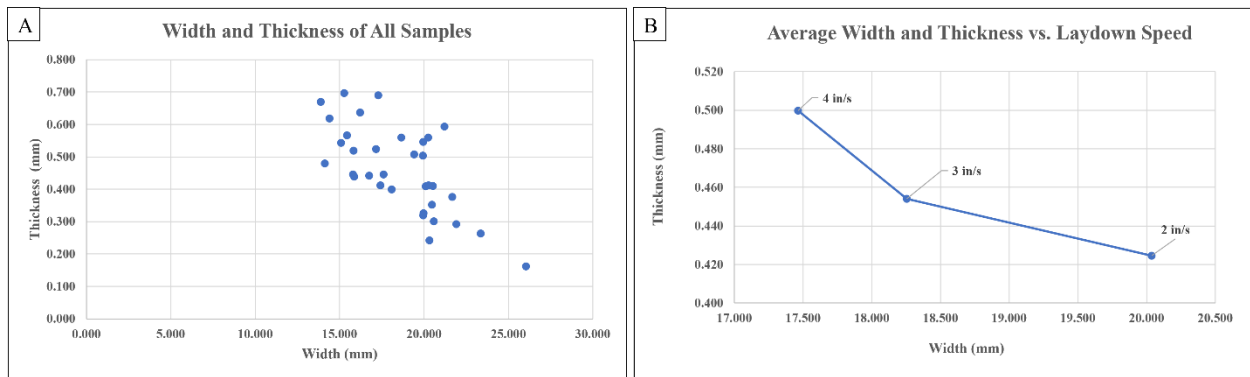


Figure 19: (A) shows the trend of two layers of ATP processed tape and how an increase in thickness was quantifiable correlated to a decrease in width. (B) shows the average thickness and width of ATP processed materials with respect to laydown speed.

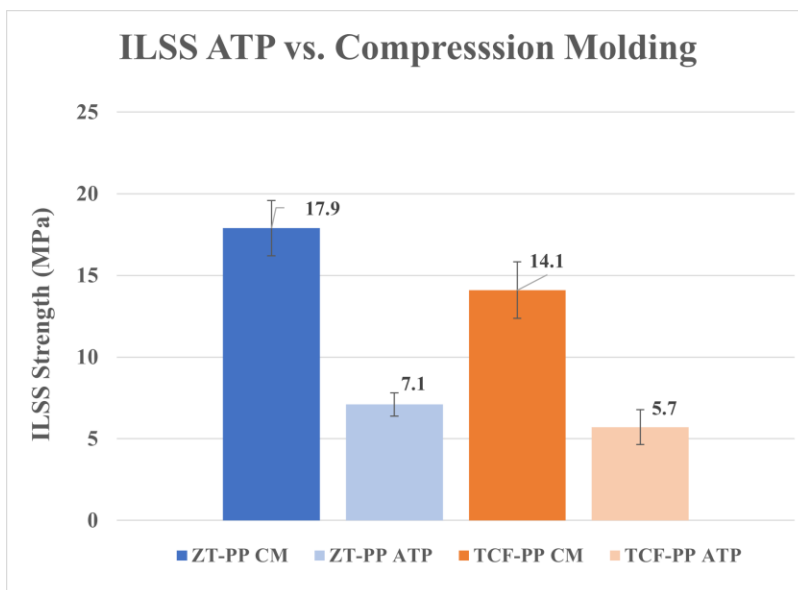


Figure 20: ILSS Properties of ZT-PP and TCF-PP plates produced with compression molding (CM) and an Automated Tape Placement (ATP) process. An average ILSS strength of ZT-PP and TCF-PP CM samples was found to be 17.9 MPa and 14.1 MPa respectively. ZT-PP and TCF-PP ATP samples were found to have an ILSS strength of 7.1 MPa & 5.7 MPa respectively.

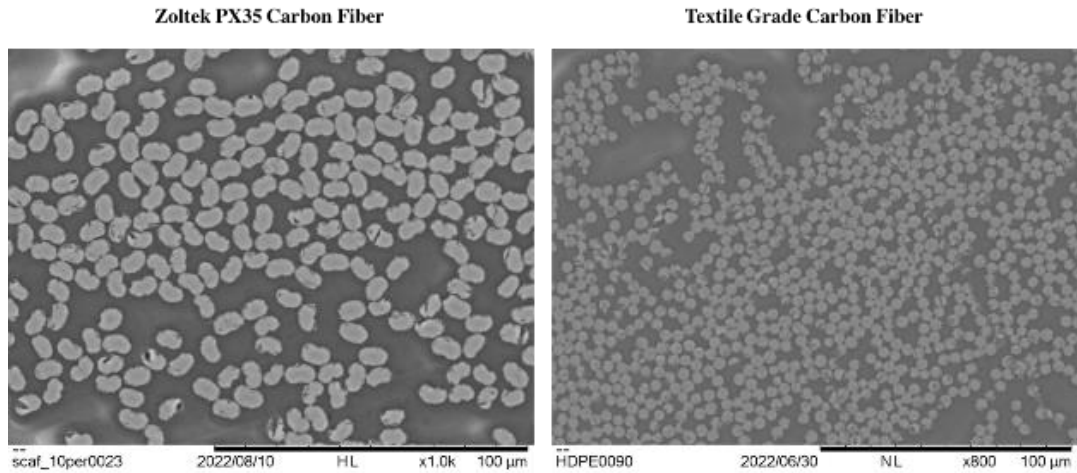


Figure 21: SEM Images of Zoltek PX35 fiber vs Textile Grade Carbon Fiber. Zoltek fiber exhibits a kidney bean shape while TCF fibers are circular in nature. This Shape could be attributed to the higher tensile strength of ZT-PP over TCF-PP. This kidney bean shape may allow for better interfacial bond between the fiber and matrix allowing the fibers to carry a higher tensile load.

two fiber types. A more in-depth study would be needed into the effect of this phenomenon when comparing ZT-PP and TCF-PP composites.

Hiremath⁸⁸ compared mechanical and morphological properties of a TCF 400K-600K tow size and Zoltek PX_35 fiber infused with an A-based epoxy resin (Araldite® LY 1568, Huntsman Corporation). Hiremath found TCF exhibited a kidney bean shape contradicting this presented work. Fiber shape is highly dependent on the processing conditions and precursor used during the CF manufacturing process⁸⁹. The fiber used in this study was a 363K tow of TCF (section 0) where processing conditions may have varied for different tow sizes during TCF development effecting resultant fiber shape.

4.3.2 ATP vs CM Processed Materials

When studying the ILSS performance between CM and ATP process methods a severe drop in mechanical performance can be observed. ATP processed ILSS samples were found to be approximately 40% that of compression molded samples (39.7% for ZT-PP & 40.4% for TCF-PP). Much of the research in processing of CF materials have been done on high performance polymers like PEEK and PEAK with the use of a laser heating system (LAPT). Comer et al.⁷⁴ and Ray et al.⁹⁰ investigated mechanical performance of LAPT processed PEEK. When evaluating ILSS and flexural strength of LAPT processed laminates they performed approximately 70% and 68% that of autoclave manufactured samples respectively. It was found that this reduction in mechanical performance was likely due to an 18% reduction in crystallinity. Qureshi et al.⁶¹ performed in-situ consolidation of using both HGT and LAPT processing methods and compared mechanical properties to a reference composite produced using traditional autoclave manufacturing. ILSS values for HGT and LAPT methods of manufacturing were found to be 55% and 85% that of autoclave manufactured samples respectively. This was also confirmed by Nanami et al.⁹¹ where HGT ATP provided ILSS values of 55% that of autoclave consolidation. In this study ILSS values were found to perform lower than that of other literature values.

During the compression molding process, the material heat soaks fully melting the matrix allowing maximum diffusion of the laminates. Also, the cooling rate during thermoplastic

processing has the largest effect on crystallinity of the composite structure⁷⁶. An increase in cooling rate has a negative effect on the crystallization of the polymer⁹². During the compression molding cycle the composite plate is cooled under pressure over an approximate 35 minute period. When compared to an ATP process the compaction cycle of newly applied laminates takes place within microseconds. This fast compaction cycle means the majority of cooling takes place under ambient conditions within short time cycles. Consequently, the fast cooling rates reduces crystallinity and allows for increased void formation within the composite microstructure⁶⁵.

4.3.3 Effect of microstructure on ILSS strength of ATP laminates

When examining the laminate structure of ATP vs. CM processed material with optical microscopy some observation can be made. Figure 22 shows optical microscopy images of ZT-PP samples processed using both methods of manufacturing. Within both samples resin rich and fiber rich regions can be observed likely due to the non-uniformity of the original tape. When observing void content within CM and ATP samples void location highly differed. Figure 23 show an image of CM and ATP processed TCF-PP samples. Voids located within CM samples were located within polymer rich regions where air pocket were likely trapped during the CM process. ATP process material was observed to have voids along the ply interfaces and within fiber rich regions. This was likely due to incomplete bonding between laminates during the in-situ consolidation process.

Figure 24 compares microscopy images of ZT-PP tape processed with CM and ATP methods. ATP processed materials show clear ply boundaries (interfaces) with minimal intermingling of plies. In CM processed laminates, it is difficult to discern ply boundaries. This implies intermingling between layers of uni-directional tape likely due to the continuously applied pressure during the manufacturing process, ultimately increasing the ILSS strength (Figure 24).

The lab scale melt impregnation system used to produce these LCCF tapes should be considered when evaluating the mechanical properties of ATP processed material. Despite full impregnation of the continuous tapes work is still needed to improve the surface finish during tape production.

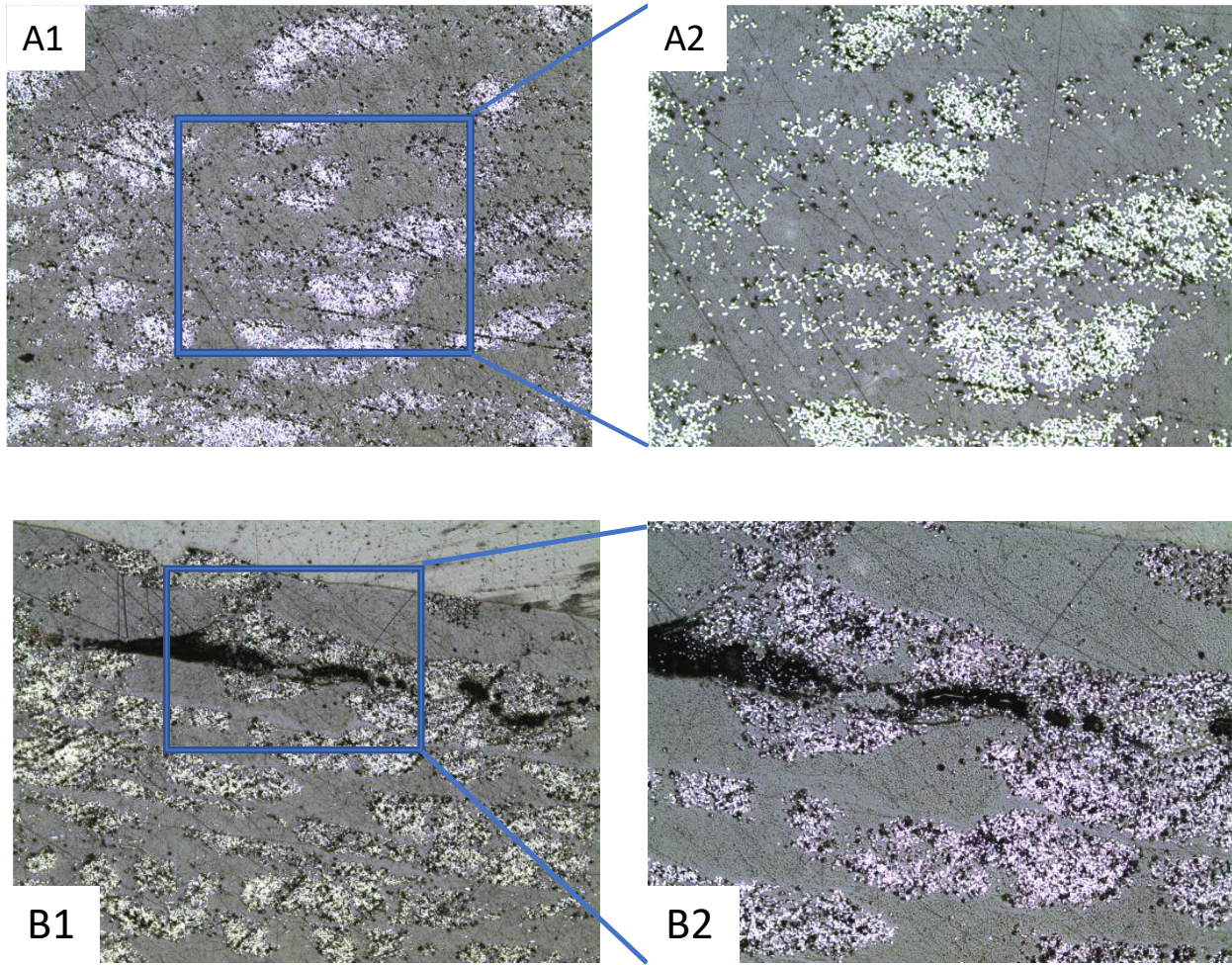


Figure 22: A1 & A2 Show laminate structure of ZT-PP compression molded (CM) sample. B1 & B2 show ZT-PP processed using ATP methods of manufacturing. A large crack can be observed along the top laminate due to incomplete autohesion of the laminates during in-situ consolidation.

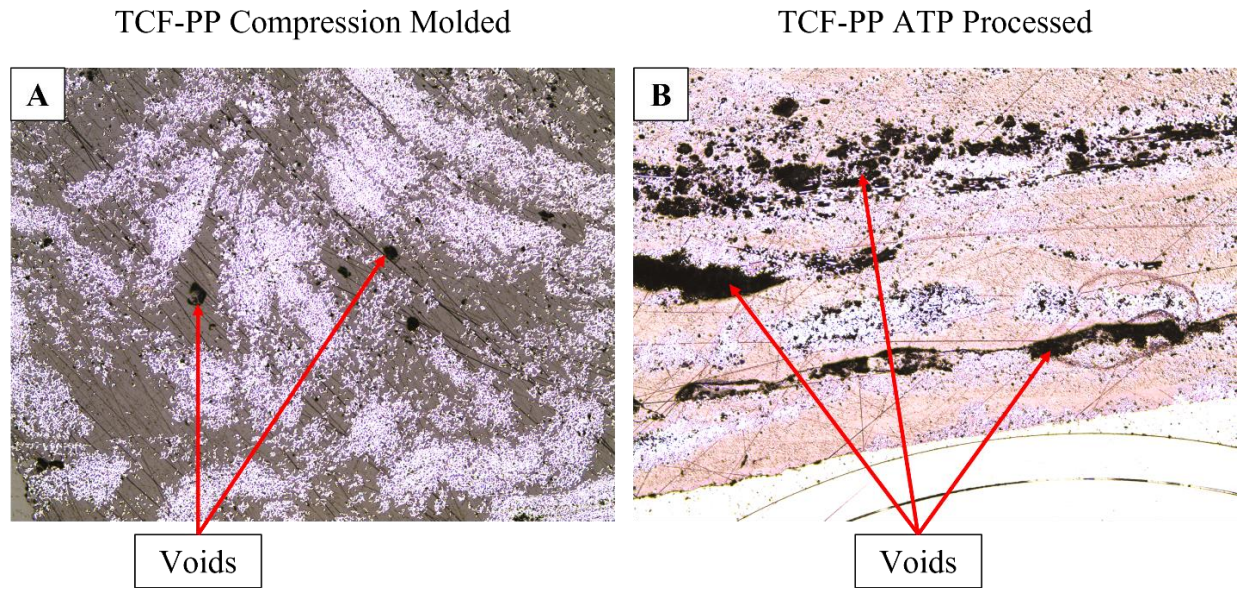


Figure 23: CM vs ATP processed laminates where voids are present. (A) shows TCF-PP CM samples with voids mostly present within polymer rich regions likely due to trapped air bubbles within the sample. (B) Shows TCF-PP ATP processed material where voids were mostly present in fiber rich regions or at ply boundaries.

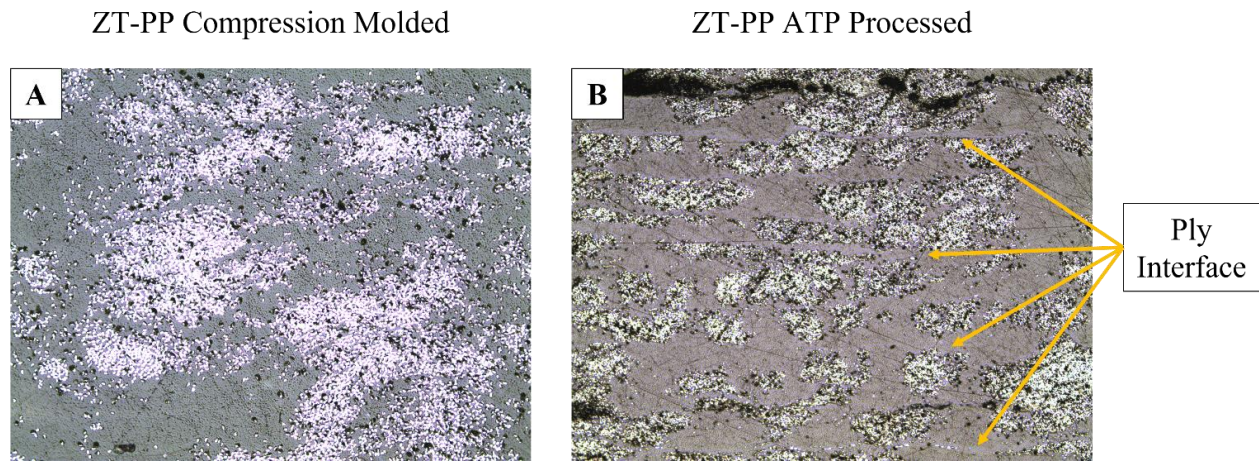


Figure 24: (A) ZT-PP Compression Molded. Laminates structures are not visible due to complete diffusion of the laminate's plies. (B) ZT-PP ATP processed materials show signs of little fiber dispersion between laminate plies.

Currently this lab scale tape production line does not have a way of controlling the thickness of the material which may influence the tape laying process. Industrial grade PEAK is produced with a thickness of 0.3 mm while the tape produced on the production line used in this study can vary from 0.3 mm to .8 mm. The thickness of the material may not allow for complete melting of the tape during in-situ consolidation affecting the autohesion of the laminates.

During the tape manufacturing process, occasionally sections of the tape would have dry fibers on the bottom part of the tape due to the introduction of polymer to the top of the fiber bed. This can be observed in the SEM image shown in Figure 25. These imperfections could amplify the problems with bonding during the tape laying process. As discussed in work by Qureshi et al.⁶¹ showed that a resin rich region on the surface of the tapes equal to one filament diameter is recommended for providing adequate resin flow and autohesion of the ply laminates during an ATP process. A low content of PP on the surface of the tape would affect the diffusion of polymer and fiber along the ply interface. This was particularly evident with the TCF-PP tape as the large tow count (363K) represents a challenge during all stages of processing. A study on thermoplastic tape surface finish and its effect on the ATP process could help to provide more insight into this phenomenon.

4.4 Tensile Results

4.4.1 LCCF CM Samples and Theoretical Values

Tensile strength of Zoltek PX35 fiber impregnated with Polypropylene (PP) (ZT-PP) was tested and compared with TCF fiber impregnated with PP (TCF-PP). ZT-PP and TCF-PP tape produced with a fiber weight fraction (FWF) of 35%. It was observed that the average ZT-PP tensile strength (459.09 MPa) was approximately 38.7% higher than the average TCF-PP tensile strength (281.55) (**Error! Reference source not found.** & Figure 27). The tensile strength for Zoltek PX35 fiber was reported to be 4137 MPa showing approximately 27.4% higher strength over the reported tensile strength of TCF (3000 MPa). Rule of mixtures can be used to determine the theoretical modulus for TCF-PP and ZT-PP (Equation 16)⁷³.

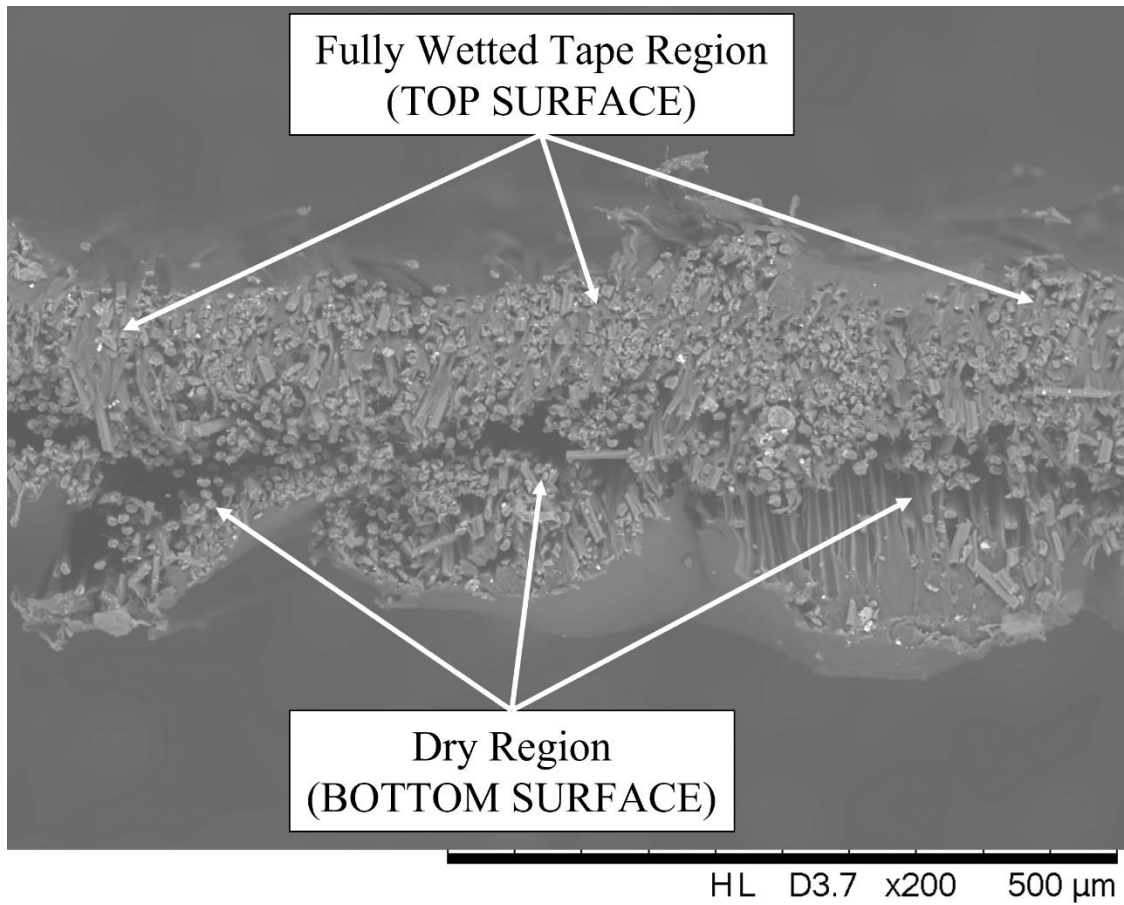


Figure 25: SEM image unpolished tape with fully impregnated top surface and dry region on the bottom surface. This was due to the polymer injection sight on the top surface of the fiber bed.

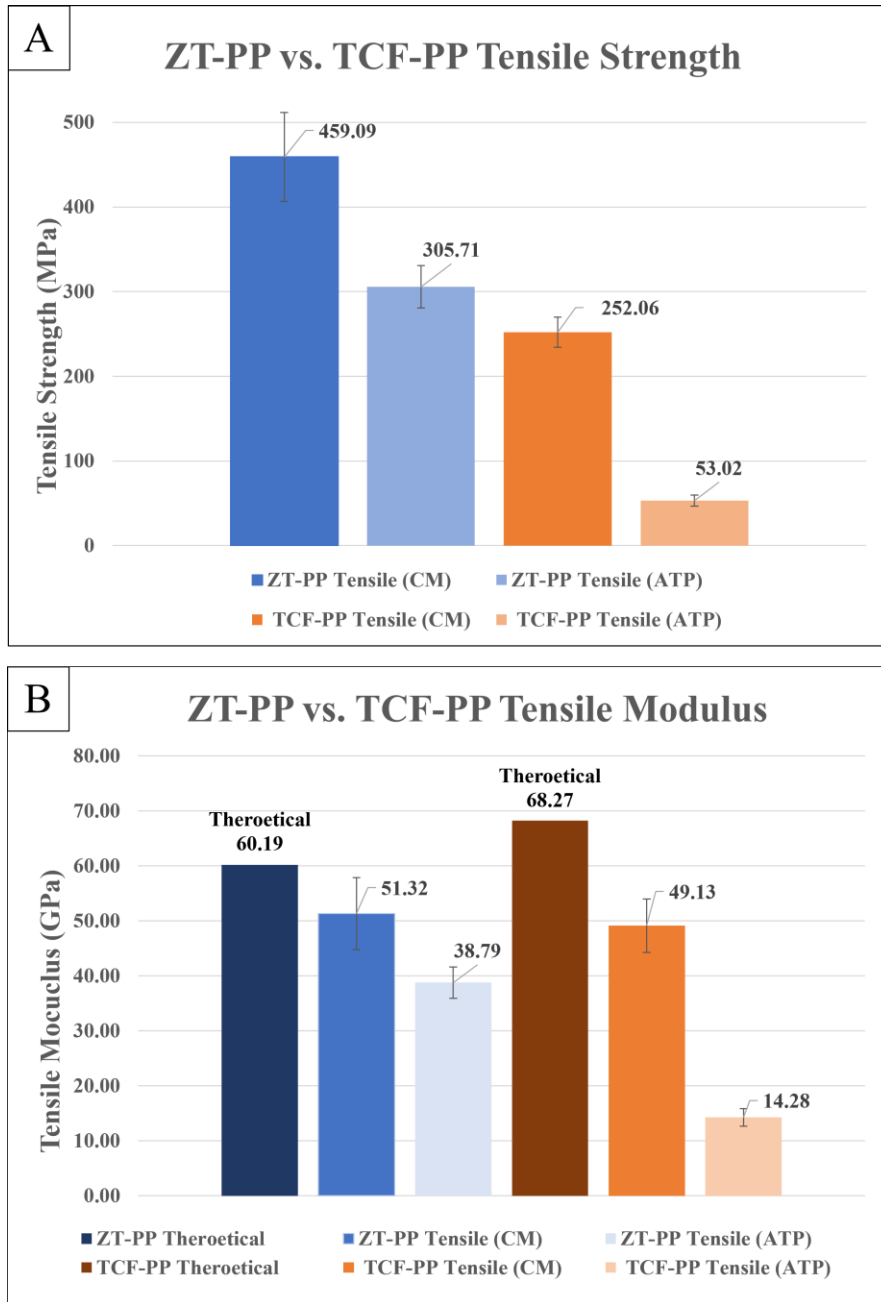


Figure 26: Tensile strength and modulus of unidirectional ZT-PP composite tape shown with unidirectional TCF-PP composite tape.

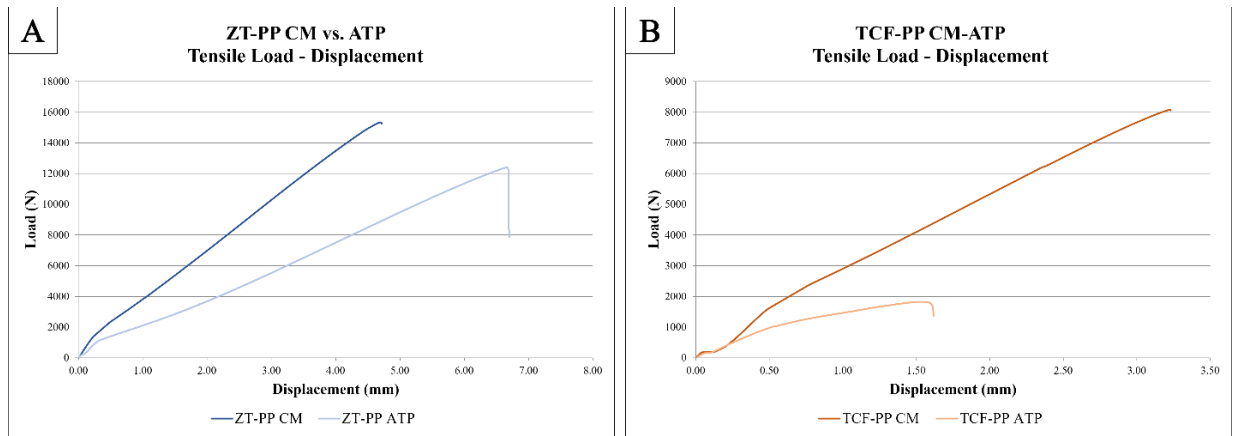


Figure 27: Representative Force vs displacement curves for tested tensile samples. (A) Representative curves for ZT-PP CM and ATP processed tensile samples. (B) Representative curves for TCF-PP CM and ATP processed tensile samples.

Rule of mixtures equation

Equation 16

$$E = E_f * v_f + E_p(1 - v_f)$$

E = Theoretical modulus

E_f = Modulus of Fiber

E_p = Modulus of Polymer

v_f = Fiber volume percentage

Theoretical modulus was calculated to be 60.19 GPa and 68.27 GPa for 35.86% FWF ZT-PP and TCF-PP respectively based on the industry reported modulus values. Based on these calculated values, ZT-PP CM samples achieved approximately 84.4% that of theoretical values while TCF-PP CM samples reported 71.2% of theoretical modulus values. Pethe⁵² performed tensile mechanical analysis on CM TCF-PP tapes where the reported average tensile strength and modulus was found to be 150.58 MPa and 45.05 GPa respectively with an approximate FWF of 30%. The presented research was compared to theoretical values using the rule of mixtures where the reported tensile modulus and strength was 11% and 70% less than theoretical values respectively. The lower actual mechanical properties were attributed to the non-homogenous distribution of reinforcement fibers within the matrix causing stress concentration and crack propagation within the matrix.

4.4.2 CM vs ATP Tensile Strength and modulus

Tensile strength for ATP processed ZT-PP and TCF-PP laminates were found to be 305.71 MPa and 53.02 MPa respectively. Average tensile modulus was observed to be 38.79 GPa and 14.28 GPa for ATP processed ZT-PP and TCF-PP samples respectively. ATP processed ZT-PP samples were found to perform approximately 66.59% that of CM samples while TCF-PP ATP samples performed much lower with tensile results performing 21.03% that of CM samples. Modulus values were decreased as well with ZT-PP performing 75.58% and TCF-PP performing 29.06% of CM processed tensile samples. The reduction in mechanical performance within ATP processed materials was likely due to fiber waviness that was observed on the surface of the samples. Fiber waviness has been shown to have a significant effect on tensile properties⁹³. Fiber waviness occurs due to thermal stress during the manufacturing process where the difference in

CTE of the matrix and reinforcement fiber cause internal residual stresses leading to fiber waviness⁹⁴. Zaidi B et al.⁹⁵ reports that due to fiber waviness some fibers take on more load than others resulting in premature failure of the composite.

ASTM standard D3039⁸⁰ gives a description of how typical failure occurs during tensile loading. As described in the standard TCF-PP ATP failure was observed to be LGM where failure corresponds to lateral failure within the middle section of the gage length. The difference in failure modes is likely evidence to TCF-PP ATP samples poor tensile performances due to the presence of fiber waviness. Also, dry fibers could be observed at the points of failure on the tensile samples. This is attributed to poor matrix packing and fiber pull out within TCF-PP. All other samples (ZT-PP CM, ZT-PP ATP and TCF-PP CM) had similar failure where edge delamination and long spitting could be observed throughout the middle of the gage length (Figure 28, Figure 29).

4.5 Flexural Results

4.5.1 CM and ATP Processed Flexural Results

Average flexural strength of ZT-PP and TCF-PP CM samples were found to be 220.6 MPa and 198.0 MPa respectively. The modulus of these two fiber types within CM samples were observed to be 28.0 GPa and 26.8 GPa for ZT-PP and TCF-PP respectively. ZT-PP was recorded to have a 10.2% and 4.07% higher flexural strength and modulus over TCF-PP within CM samples respectively (Figure 30). ATP processed materials exhibited significant reduction of mechanical properties with ZT-PP and TCF-PP flexural strength found to be 71.66 MPa and 58.47 MPa respectively. Flexural strength of ZT-PP and TCF-PP HGT in-situ consolidated laminates were shown to be 32.5% and 29.5% that of CM processed composites. ATP ZT-PP and TCF-PP processed flexural modulus values were 6.49 GPa and 4.05 GPa respectively. The modulus values were found to perform 23.2% and 15.11% that of CM processed materials. This represents a significant reduction in mechanical properties of HGT ATP in-situ consolidation processing methods.

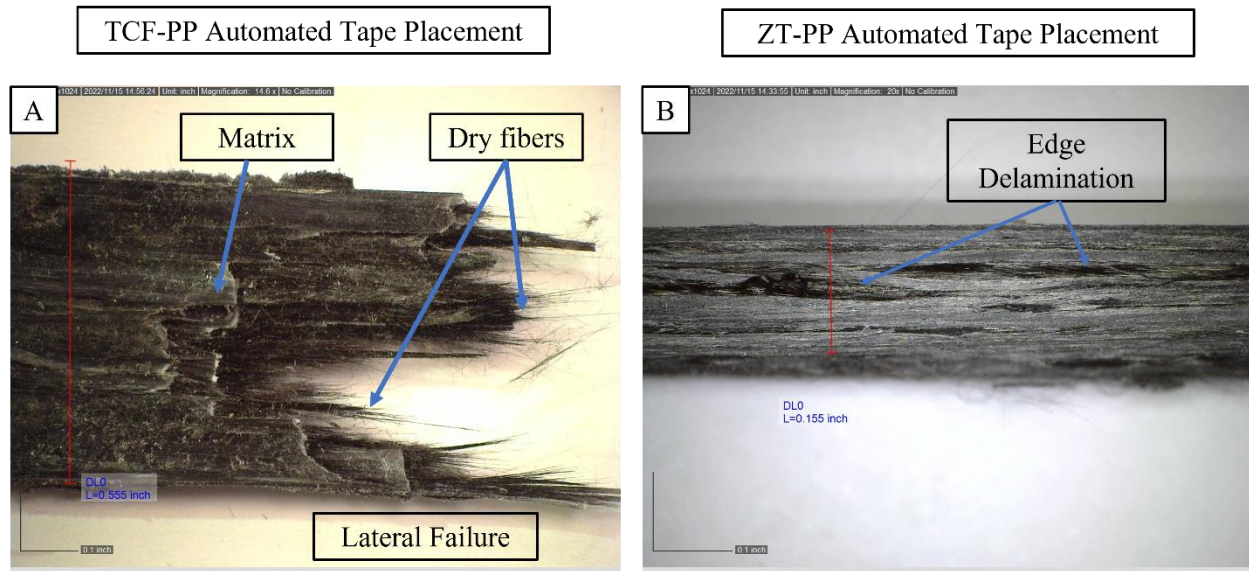


Figure 28: Failure points and failure modes of ATP processed TCF-PP and ZT-PP tensile samples. (A) shows lateral failure (B) Shows edge delamination the primary failure mode of ZT-PP ATP samples.

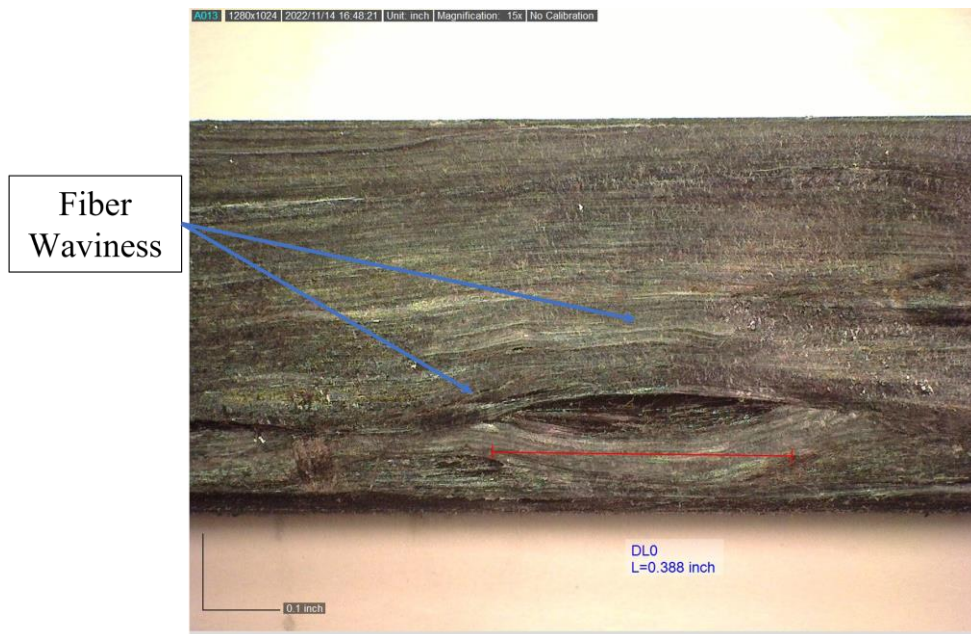


Figure 29: Fiber waviness found within TCF-PP ATP samples. Surface of samples were found to have unconsolidated regions.

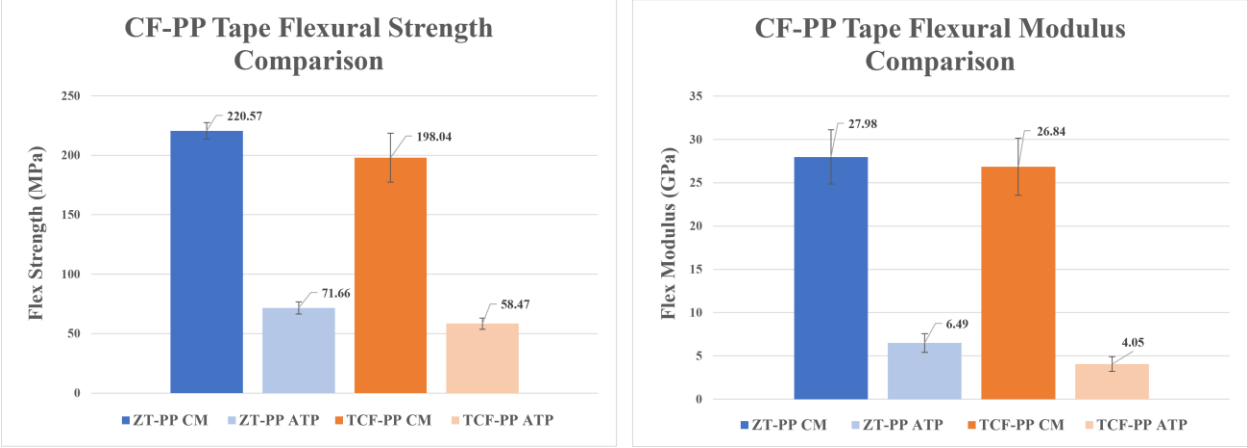


Figure 30: Flexural strength and modulus comparison chart of unidirectional ZT-PP and TCF-PP composite tape processed using compression molding and automated tape placement.

Literature values presented by Nanami et al.⁹¹ have shown HGT processed CFRP's to exhibit flexural strengths in the range of 38% - 49% that of hot compression molding. These reported flexural strengths back the significant reduction in mechanical results found in this study. A closer look at the at the force response and failure modes may provide some insight into the approximate 30% mechanical strength of ATP processed materials when compared to CM manufacturing.

4.5.2 Force response curves CM vs. ATP

Figure 31 shows the representative force response curves for tested flexural samples where (A) shows ZT-PP CM and ATP samples and (B) shows TCF-PP CM and ATP processed samples. A clear difference can be seen where both TCF-PP and ZT-PP ATP samples show a ductile response with a consistent but non-linear modulus where the force response gradually increased before failure. CM ZT-PP and TCF-PP showed similar responses with a linear response until failure. ZT-PP CM samples showed signs of delamination failure where a sudden drop in force preceded by a linear increase before total failure. Figure 31: Representative force vs displacement curves for tested flexural samples. (A) Representative curves for ZT-PP CM and ATP processed flexural samples. (B) Representative curves for TCF-PP CM and ATP processed flexural samples.

4.5.3 Failure modes of Flexural Samples

Figure 32 shows the failure modes for ZT-PP and TCF-PP produced using CM and ATP processing methods. It can be observed that one of the major failure modes for CM processed samples was compression buckling where the top surface of the sample while under compression experiences compression failure. Delamination was also observed within CM samples but were present at or near the bottom surface of the flexural sample (Figure 32 – B).

Conversely, the major failure mode for ATP processed samples was delamination at the interface between laminates (Figure 32 – C & D). Combined with the ductile force response curves and

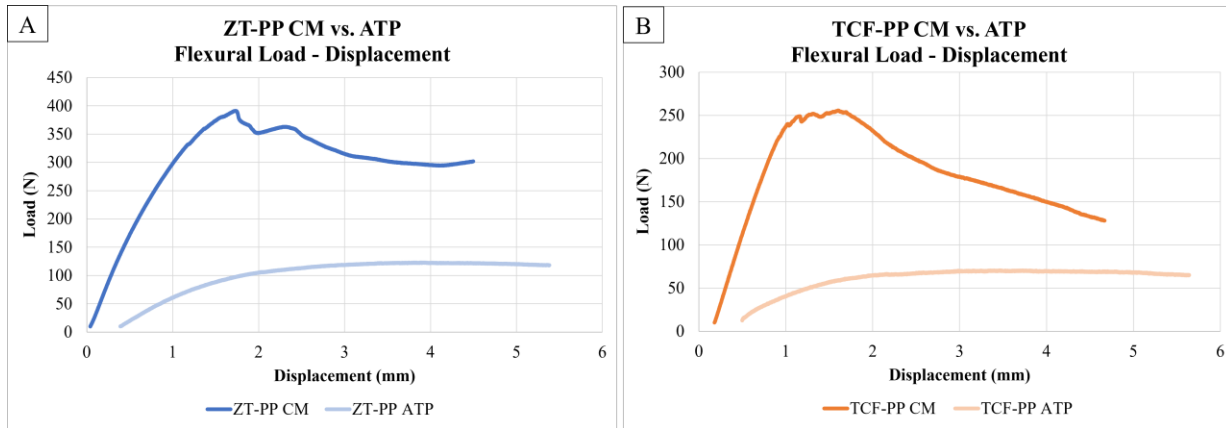


Figure 31: Representative force vs displacement curves for tested flexural samples. (A) Representative curves for ZT-PP CM and ATP processed flexural samples. (B) Representative curves for TCF-PP CM and ATP processed flexural samples.

microscopy images of laminate cross-sections (Figure 32), this approximately 70% reduction in mechanical performance was likely due to incomplete ply laminate adhesion during the in-situ manufacturing process.

4.6 LVI Drop Tower Results

4.6.1 LVI Failure Modes

It should be noted that impacts can be broadly classified with accordance to the energy level applied during impact. These broad classifications are referred to as high and low energy impacts pertaining to the extent of damage after impact. High energy impacts refer to impact energies where total failure of the material is displayed, noted by complete tote penetration. Low energy impacts are correlated to specimens where damage is present, but without complete fracture. The main fracture modes for low energy impacts are in plane delamination and transvers shear cracking. The other failure mode that can be observed is of plane deformation observed as a protrusion on the back side of a panel. This bending deformation often produces tensile and compressive stresses in the bottom of the specimen directly below the impact point ⁸².

A more precise breakdown of failure modes in LVI samples are described by the increase in failure as impact energy increases. Failure modes include: (A) Matrix Mode, described as cracking of the matrix parallel to the fiber orientation, (B) Delamination Mode where laminates dis-adhere to each other due to internal stresses, (C) Fiber Mode which is described as tensile failure within the fiber bed observed as fiber breakage and compression buckling and (D) Penetration Mode where the impactor completely penetrates the laminate structure⁹⁶. These four failure modes well describe the observed damage after an LVI impact.

4.6.2 ZT-PP vs TCF-PP Results

Low velocity impact (LVI) testing was preformed to show impact properties of continuous LCCF composites with fiber orientations of unidirectional and 0/90° Cross ply. Table 7 shows LVI drop tower results for the two materials and fiber orientations. Figure 33 shows force vs time response of the tote corresponding to increasing LVI Drop energies. A more complete interpretation of these curves can be found in section 4.6.3.

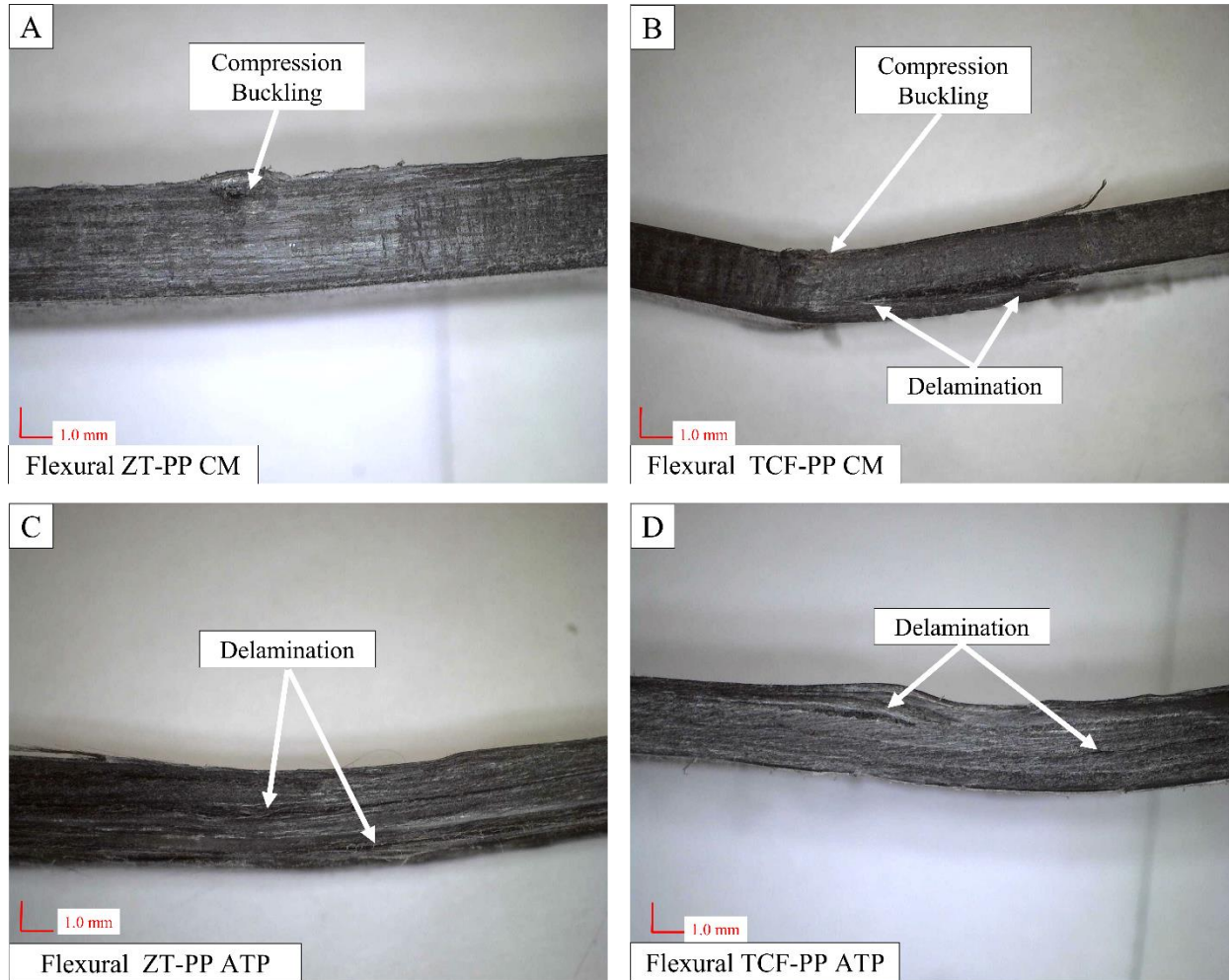


Figure 32: Flexural samples and failure modes: (A) ZT-PP CM sample showed signs of compression buckling, (B) TCF-PP CM showed signs of compression buckling and delamination on the bottom of the laminate, (C) ZT-PP ATP sample showed signs of delamination inside the laminate due to interlaminar delamination and (D) TCF-PP ATP sample showed signs of interlaminar delamination.

ZT-PP unidirectional samples were observed to absorb 16.7% higher impact energy and experienced a 22.4% higher peak force than TCF-PP. ZT-PP 0/90 samples were observed to absorb 37.5% higher impact energy and 46.8% higher peak force than TCF-PP 0/90 samples. This directly correlates to the approximately 38.7% higher tensile strength of ZT-PP over TCF-PP (**Error! Reference source not found.**) due to the majority of failure accruing during fiber mode failure (Discussed in more detail in section 4.6.4).

4.6.3 Peak Force vs Impact Energy

When comparing peak force and impact energy it can be observed that the peak force during impact often drops when nearing high energy impacts. This is likely due to the transition from elastic deformation to plastic deformation at higher energy levels. ZT-PP 0/90 samples display this phenomenon perfectly which can be observed in Figure 34. Impact energies of 30J and 40J display elastic deformation with rounded force vs time curves (Figure 33 - C). This represents little to no failure of the sample which can be observed by visibly inspecting the LVI sample where a small impression created by the tote impact and slight surface delamination can be seen. Moving on to the higher impact energies of 50J, 60J, 70J and 80J plastic deformation can be observed. Plastic deformation is displayed in the force vs time graphs by the immediate force spike followed by intense force oscillation. Immediately after the spike the force drops and plateaus during the unloading phase⁶⁶.

4.6.4 Laminate Structures Effect on Failure Modes

0/90 cross-ply LVI samples were expected to withstand higher impact energies than unidirectional samples due to the load transfer between transvers laminates. Although, while investigating failure modes, several interesting observations were observed. Uni-directional failure was observed to be along the fiber direction with the majority of failure occurring within the matrix. The majority of failure in these samples was within the matrix until full tote penetration of the sample occurred. TCF-PP uni-directional samples showed some signs of fiber mode failure directly beneath the impact point on the back side of the plate although the majority

Table 7: Impact results from TCF-PP and ZT-PP compression molded tape.

TCF – PP 0/90 LVI Tests						
	Drop Energy	Total Mass	Impact Hight	Impact Velocity	Peak Force	Damage Assessment
Plate 1	20 J	5.715 kg	357 mm	2.65 m/s	1778 N	Delamination Mode
Plate 2	25J	5.715 kg	446 mm	2.96 m/s	2218 N	Delamination Mode
Plate 3	30J	5.715 kg	535 mm	3.24 m/s	2436 N	Fiber Mode
Plate 4	40J	5.715 kg	714 mm	3.74 m/s	3146 N	Fiber Mode
Plate 5	50J	5.715 kg	892 mm	4.18 m/s	2305 N	Fiber Mode

TCF – PP Unidirectional LVI Tests						
	Drop Energy	Total Mass	Impact Hight	Impact Velocity	Peak Force	Damage Assessment
Plate 1	10 J	5.715 kg	178 mm	1.87 m/s	1789 N	Matrix Mode
Plate 2	15J	5.715 kg	286 mm	2.89 m/s	2158 N	Matrix & Fiber Mode
Plate 3	20J	5.715 kg	357 mm	2.65 m/s	2004 N	Matrix & Fiber Mode
Plate 4	22.5J	5.715 kg	401 mm	2.81 m/s	1979 N	Matrix & Fiber Mode
Plate 5	25J	5.715 kg	446 mm	2.96 m/s	1583 N	Penetration Mode

ZT – PP 0-90 LVI Tests						
	Drop Energy	Total Mass	Impact Hight	Impact Velocity	Peak Force	Damage Assessment
Plate 1	30 J	5.715 kg	535 mm	3.24 m/s	5630 N	Delamination Mode
Plate 2	40 J	5.715 kg	714 mm	3.71 m/s	5864 N	Delamination Mode
Plate 3	50 J	5.715 kg	892 mm	4.18 m/s	6181 N	Fiber Mode
Plate 4	60 J	5.715 kg	1070 mm	4.58 m/s	6126 N	Fiber Mode
Plate 5	70 J	7.215 kg	989 mm	4.41 m/s	5919 N	Fiber Mode
Plate 6	80 J	7.715 kg	1057 mm	4.55 m/s	5761 N	Fiber Mode

ZT – PP Unidirectional LVI Tests						
	Drop Energy	Total Mass	Impact Hight	Impact Velocity	Peak Force	Damage Assessment
Plate 1	10 J	5.715 kg	178 mm	1.87 m/s	2150 N	Matrix Mode
Plate 2	15 J	5.715 kg	268 mm	2.29 m/s	2555 N	Matrix Mode
Plate 3	20 J	5.715 kg	357 mm	2.65 m/s	2515 N	Matrix Mode
Plate 4	25 J	5.715 kg	446 mm	2.96 m/s	2737 N	Matrix Mode
Plate 5	30 J	5.715 kg	535 mm	3.24 m/s	2781 N	Penetration Mode

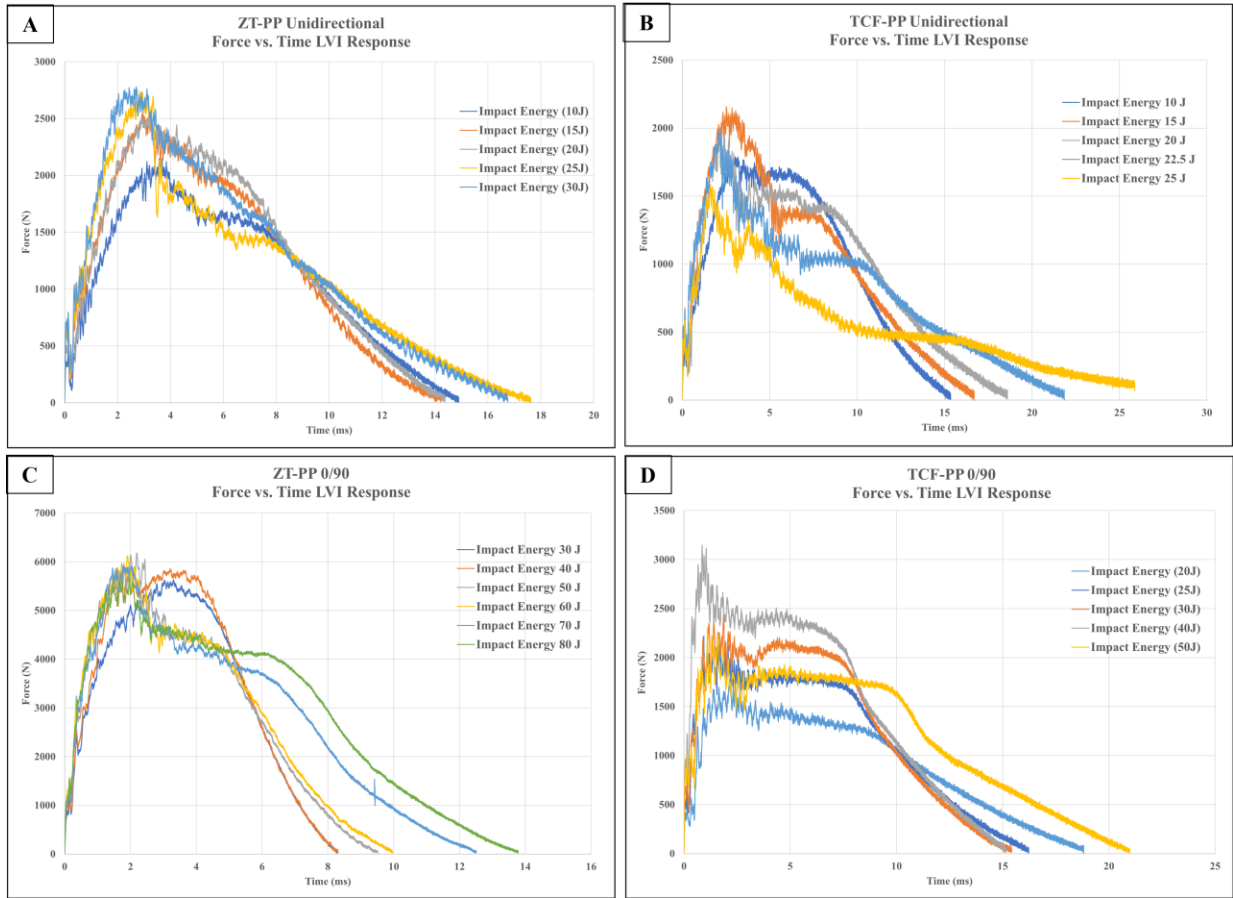


Figure 33: Force vs time graphs of LVI samples. (A) ZT-PP force vs time. All strikes represent plastic deformation. (B) TCF-PP Unidirectional Force vs. Time Plastic deformation. (C) ZT-PP 0/90 cross ply samples where 30J and 40J are elastic and 50-80 are plastic deformation. (D) TCF-PP 0/90 cross ply plastic deformation.

of failure can be attributed to matrix mode failure until the laminate structure was fully penetrated at the highest energy level. Cross ply samples on the other hand were observed to have failure modes correlated to delamination mode and fiber mode at higher energy levels. Figure 34 displays this parametric trend of peak force vs drop energy where the peak energy can be correlated to the transition of failure modes between low and high energy impacts. This was particularly evident within the cross ply laminates. Within cross-ply laminates load transfer occurs within the matrix region at the surface of the structure. The resulting load is transferred through the matrix to the proceeding ply where some of the energy is transferred to the fiber while the remaining energy is carried through the matrix. This pattern progresses until all energy is absorbed or delamination failure occurs. Figure 35 shows a visual representation of failure propagation through a cross-ply laminate during the onset of an LVI impact ⁹⁷.

4.6.5 Volumetric Damage Trends

Figure 36 displays the trends between volumetric damage during an LVI corresponded to energy during impact. TCF-PP samples displayed a more noticeable trend than ZT-PP with a linear increase in volumetric damage corresponding to the increase in drop energy. ZT-PP samples did not present a clear linear response of volumetric damage with an increase in drop energy after. Under visual inspection of the ZT-PP unidirectional samples impacted with 20J, 25J and 30J a large crack was found along the fiber direction where the matrix was split at the point of impact. This could help to explain the ZT-PP unidirectional volumetric damage response after 20J where volumetric damage seemingly stopped increasing. ZT-PP 0/90 samples volumetric damage response was shown to be unpredictable from 50J to 80J of impact energy. This could be related to the transition from delamination mode to fiber mode failure as shown in Table 7. X-Ray CT or ultrasonic scanning would be needed to corroborate the volumetric damage response after the LVI testing^{98,99}.

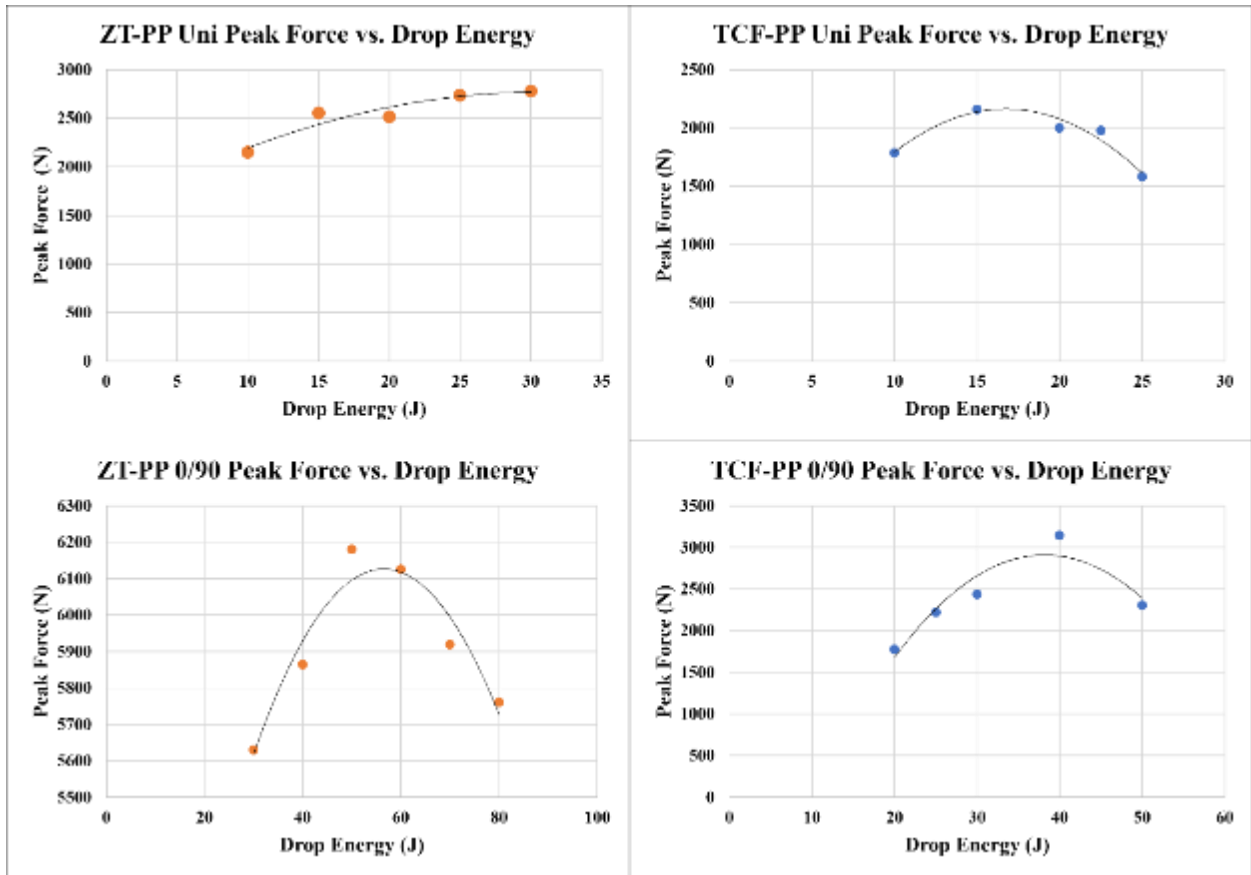


Figure 34: LVI Peak force vs drop energy. A parametric relationship between peak force and drop energy can be observed which was correlated the transition from delamination mode failure to fiber mode failure.

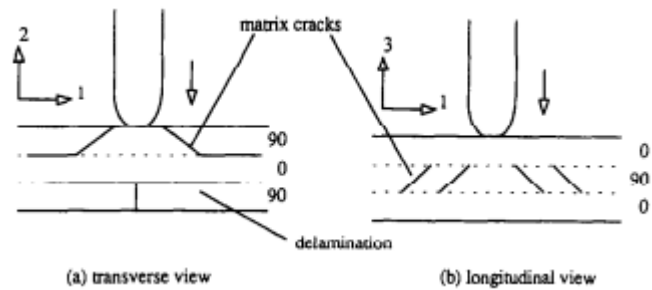


Figure 35: Initiation of LVI damage within a 0/90/0 composite structure. Failure occurs within the matrix region and load is take up by the preceding ply⁹⁷.

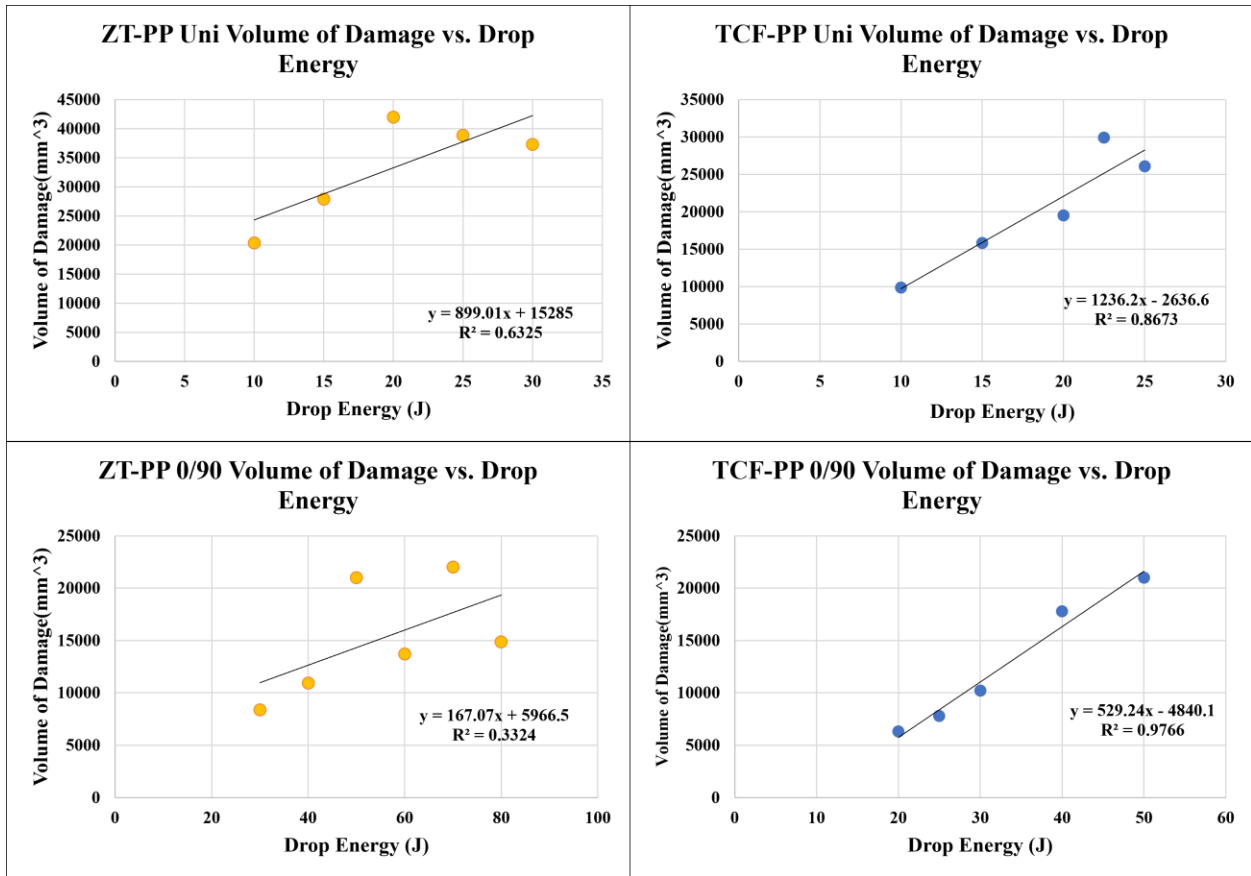


Figure 36: Volumetric damage vs. impact energy trends. TCF -PP Samples show a linear trend between calculated volumetric damage and impact energy while ZT-PP samples did not.

Chapter 5: Conclusions

This research focuses on the processing and manufacturing of low-cost carbon fiber (LCCF) for the use in non-aerospace applications. This LCCF, specifically textile grade CF (TCF) and Zoltek PX_35 CF was processed on a hot melt impregnation line to create an intermediate composite tape material. The two main objectives of this thesis were to firstly, study mechanical and morphological properties of two types of LCCF and secondly to compare mechanical properties of manufactured plates using compression molding and automated tape placement (ATP).

Thermogravimetric analysis (TGA) was conducted across all samples to provide confirmation of consistent fiber weight fraction (FWF) and fiber volume fraction (FVF) after the manufacturing cycles. During tape production extruder and line speeds were set to produce composite tape of 35% FWF which was confirmed through TGA with a standard deviation of 1.13.

A detailed process parameters study was conducted to determine the best processing temperature, pressure and laydown speed for CF-PP tape on a hot gas torch (HGT). An array of 36 samples was produced across all processing methods to provide conclusive trends for ATP manufacturing. Temperature and laydown speed was found to have the highest effect on processability while no discernable trend could be determined between the pressure and morphological tape structure. More research would be needed into the effect of pressure on crystallinity within the matrix.

Based on the determined processing parameters mechanical performance was evaluated on HGT ATP processed samples to mechanically characterize the performance of the materials. This ATP processed material was then compared to hot compression molded (CM) samples which provided a baseline of ZT-PP and TCF-PP results. Tensile, ILSS and flexural properties were mechanically characterized using the two processing methods. Few research has been conducted on the mechanical properties of ATP processed CF-PP composites, so this research was compared to the mechanical performance of other thermoplastic ATP results. It was determined ATP processed materials performed within acceptable bounds for ILSS and flexural strength.

TCF-PP tensile strength was significantly reduced preforming approximately 20% that of CM samples. The ATP process was found to have significant effect on modulus values for both TCF-PP and ZT-PP across all mechanical characterization. This was likely due to the reduction of fiber matrix diffusion between laminates and crystallinity during in-situ consolidation.

Low velocity impact testing was performed on ZT-PP and TCF-PP unidirectional and 0/90 cross ply laminates. Cross ply samples were expected and found to perform significantly better than unidirectional samples due to load transfer between transvers laminates. Within cross ply samples, ZT-PP was found to absorb a 48% higher peak force than TCF-PP which was attributed to a higher tensile strength and lower modulus of the reported ZT fibers.

This thesis was intended to assess mechanical characterization of two types of previously mentioned LCCF composites manufactured from PP tape produced on a hot melt impregnation line and consolidated using CM and ATP processing methods. Higher process control of tape thickness could improve the morphology and mechanical performance of composites produced through in-situ consolidation.

The ever-growing demand for cost effective, high strength and lightweight materials in the automotive industry has pushed the researchers and CF manufacturers to investigate alternative LCCF without compromising on performance. TCF and Zoltek_PX35 fibers have been the response to these demands where the estimated cost per lb has been foreshadowed to be approximately \$5 per lb. In combination with this hot melt impregnation technique, an intermediate low-cost composite tape can be produced that has been shown to have good mechanical performance when consolidated through CM. Automation is critical to the required rapid part production and process control within the automotive industry. Although in-situ consolidation has been shown as a promising automated method of tape placement more research is needed into the improvement of properties of in-situ consolidation low-cost PP composites.

BIBLIOGRAPHY

1. Corporate Average Fuel Economy. <https://www.nhtsa.gov/laws-regulations/corporate-average-fuel-economy#:~:text=The%20final%20rule%20establishes%20standards,annually%20for%20model%20year%202026.> (2022).
2. Kore, S., Theodore, M., Pillai, R., Thomas, V. & Vaidya, U. Improvement of interfacial adhesion of unidirectional textile grade carbon fiber (TCF) with unsized, epoxy and urethane sizing reinforced in thermoset urethane composites. *Mater Today Commun* **28**, 102669 (2021).
3. Yeole, P. *et al.* Characterization of textile-grade carbon fiber polypropylene composites. *Polymers and Polymer Composites* **29**, 652–659 (2021).
4. Khan, H., Kaur, J., Naebe, M., Hutchinson, S. & Varley, R. J. Continuous, pilot-scale production of carbon fiber from a textile grade PAN polymer. *Mater Today Commun* **31**, 103231 (2022).
5. Hiremath, N. *et al.* Low cost textile-grade carbon-fiber epoxy composites for automotive and wind energy applications. *Compos B Eng* **198**, 108156 (2020).
6. Rezaei, F., Yunus, R., Ibrahim, N. A. & Mahdi, E. S. Development of Short-Carbon-Fiber-Reinforced Polypropylene Composite for Car Bonnet. *Polym Plast Technol Eng* **47**, 351–357 (2008).
7. Baker, D. A. & Rials, T. G. Recent advances in low-cost carbon fiber manufacture from lignin. *J Appl Polym Sci* **130**, 713–728 (2013).
8. Sudo, K. & Shimizu, K. A new carbon fiber from lignin. *J Appl Polym Sci* **44**, 127–134 (1992).
9. Otani, S. and F. Y. and I. B. and S. K. Method for producing carbonized lignin fiber. (1969).
10. Sarah Black. Alternative precursor R&D: What are the alternatives to PAN? <https://www.compositesworld.com/articles/alternative-precursor-rd-what-are-the-alternatives-to-pan> (2016).
11. Kadla, J. F. *et al.* Lignin-based carbon fibers for composite fiber applications. *Carbon N Y* **40**, 2913–2920 (2002).

12. Liu, J., Chen, X., Liang, D. & Xie, Q. Development of pitch-based carbon fibers: a review. *Energy Sources, Part A: Recovery, Utilization, and Environmental Effects* **0**, 1–21 (2020).
13. Frank, E., Hermanutz, F. & Buchmeiser, M. R. Carbon Fibers: Precursors, Manufacturing, and Properties. *Macromol Mater Eng* **297**, 493–501 (2012).
14. Yao, S. S., Jin, F. L., Rhee, K. Y., Hui, D. & Park, S. J. Recent advances in carbon-fiber-reinforced thermoplastic composites: A review. *Compos B Eng* **142**, 241–250 (2018).
15. Jam, J. E. & Ahangari, M. Study of the Mechanical, Thermal Properties and Morphology of Polypropylene Nanocomposites in the Presence of Compatibilizer. *Polym Plast Technol Eng* **51**, 1186–1192 (2012).
16. Shaikh, H. *et al.* Progress in Carbon Fiber and Its Polypropylene- and Polyethylene-Based Composites. *Polym Plast Technol Eng* **53**, 1845–1860 (2014).
17. Markarian, J. Long fibre reinforced thermoplastics continue growth in automotive. *Plastics, Additives and Compounding* **9**, 20–24 (2007).
18. Minchenkov, K., Vedernikov, A., Safonov, A. & Akhatov, I. Thermoplastic Pultrusion: A Review. *Polymers (Basel)* **13**, (2021).
19. Kropka, M., Muehlbacher, M., Neumeyer, T. & Altstaedt, V. From UD-tape to Final Part – A Comprehensive Approach Towards Thermoplastic Composites. *Procedia CIRP* **66**, 96–100 (2017).
20. Dhinakaran, V., Surendar, K. v, Hasunfur Riyaz, M. S. & Ravichandran, M. Review on study of thermosetting and thermoplastic materials in the automated fiber placement process. *Mater Today Proc* **27**, 812–815 (2020).
21. Choi, D., Kil, H. S. & Lee, S. Fabrication of low-cost carbon fibers using economical precursors and advanced processing technologies. *Carbon N Y* **142**, 610–649 (2019).
22. McGetrick, L. IV. 3. Carbon Fiber Technology Facility—Oak Ridge National Laboratory. *Lightweight Materials R\&D Program* 123–139 (2014).
23. Bill Regan. *IV.1 Development and Commercialization of a Novel Low-Cost Carbon Fiber²Zoltek Companies, Inc.*
<https://www.energy.gov/sites/prod/files/2015/07/f24/DOE%20VTO%202014%20Material%20Annual%20report.pdf#page=212> (2014).

24. Metal Miner. Metal Miner Sourcing & Trading Intelligence for Global Metal Markets. <https://agmetalmminer.com/mmwp/metal-prices/carbon-steel/>.
25. AZO Materials. AISI 1010 Carbon Steel (UNS G10100). <https://www.azom.com/article.aspx?ArticleID=6539>.
26. Vagas Fastener Manufacturing. Aluminum 2024 Vegas Fastener Manufacturing. <https://www.vegasfastener.com/materials/2024-aluminum/>.
27. Brian Wang. Glass Fiber and Basalt Fiber Industries. *Next Big Future* <https://www.nextbigfuture.com/2010/08/glass-fiber-and-basalt-fiber-industries.html> (2010).
28. JPS Composite Material. E-glass and S-glass by JPS Composite Material. [https://jpscm.com/products/e-glass-s-glass/#:~:text=E%2Dglass%E2%80%94also%20known%20as,%3A%203%2C400%20MPa%20\(490%20ksi\)](https://jpscm.com/products/e-glass-s-glass/#:~:text=E%2Dglass%E2%80%94also%20known%20as,%3A%203%2C400%20MPa%20(490%20ksi)).
29. Toray. *TORAY Data Sheet*. https://www.cf-composites.toray/resources/data_sheets/#anc1.
30. ZOLTEK PX35 Commercial Carbon Fiber. <https://zoltek.com/products/px35/>.
31. Kore, S. *et al.* Textile-Grade Carbon Fiber-Reinforced Polycarbonate Composites: Effect of Epoxy Sizing. *Ind Eng Chem Res* **60**, 3981–3991 (2021).
32. Bhatt, A. T., Gohil, P. P. & Chaudhary, V. Primary Manufacturing Processes for Fiber Reinforced Composites: History, Development & Future Research Trends. *IOP Conf Ser Mater Sci Eng* **330**, 012107 (2018).
33. Yassin, K. & Hojjati, M. Processing of thermoplastic matrix composites through automated fiber placement and tape laying methods: A review. *Journal of Thermoplastic Composite Materials* **31**, 1676–1725 (2018).
34. Zou, X., Lin, H., Feng, P., Bao, Y. & Wang, J. A review on FRP-concrete hybrid sections for bridge applications. *Compos Struct* **262**, 113336 (2021).
35. Song, Y. S., Youn, J. R. & Gutowski, T. G. Life cycle energy analysis of fiber-reinforced composites. *Compos Part A Appl Sci Manuf* **40**, 1257–1265 (2009).
36. Stokes-Griffin, C. M. & Compston, P. An inverse model for optimisation of laser heat flux distributions in an automated laser tape placement process for carbon-fibre/PEEK. *Compos Part A Appl Sci Manuf* **88**, 190–197 (2016).

37. Torey Advanced Composites. Technology and Applications of Advanced Thermoplastic Composites. <https://www.azom.com/article.aspx?ArticleID=7983> (2012).
38. History and Future of Plastics. *Science History Institute* <https://www.sciencehistory.org/the-history-and-future-of-plastics>.
39. Jogur, G., Khan, A. N., Das, A., Mahajan, P. & Alagirusamy, R. Impact properties of thermoplastic composites. *Textile Progress* **50**, 109–183 (2018).
40. Vedernikov, A. *et al.* Investigation on the Shape Distortions of Pultruded Profiles at Different Pulling Speed. *Procedia Manuf* **47**, 1–5 (2020).
41. Raper, K. S., Roux, J. A., McCarty, T. A. & Vaughan, J. G. Investigation of the pressure behavior in a pultrusion die for graphite/epoxy composites. *Compos Part A Appl Sci Manuf* **30**, 1123–1132 (1999).
42. Yn, M. S., Ma, C. C. M., Lin, S. H. & Wu, Y. D. Pultrusion of poly(ϵ -caprolactam)/poly(butadiene-co-acrylonitrile) composites: I. Simulation and a mathematical model. *Compos Sci Technol* **54**, 123–131 (1995).
43. Svensson, N., Shishoo, R. & Gilchrist, M. Manufacturing of Thermoplastic Composites from Commingled Yarns-A Review. *Journal of Thermoplastic Composite Materials* **11**, 22–56 (1998).
44. Luisier, A., Bourban, P. E. & Månson, J. A. E. Reaction injection pultrusion of PA12 composites: process and modelling. *Compos Part A Appl Sci Manuf* **34**, 583–595 (2003).
45. Larock, J. A., Hahn, H. T. & Evans, D. J. Pultrusion Processes for Thermoplastic Composites. *Journal of Thermoplastic Composite Materials* **2**, 216–229 (1989).
46. Hartness, T., Husman, G., Koenig, J. & Dyksterhouse, J. The characterization of low cost fiber reinforced thermoplastic composites produced by the DRIFT™ process. *Compos Part A Appl Sci Manuf* **32**, 1155–1160 (2001).
47. Esfandiari, P., Silva, J. F., Novo, P. J., Nunes, J. P. & Marques, A. T. Production and processing of pre-impregnated thermoplastic tapes by pultrusion and compression moulding. *J Compos Mater* **56**, 1667–1676 (2022).
48. di Blasi, C. Transition between regimes in the degradation of thermoplastic polymers. *Polym Degrad Stab* **64**, 359–367 (1999).
49. Teun Weustink. Development of Rapid Thermoplastic Impregnation Device. (de Technische Universiteit Delft, 2007).

50. Xu, H. H. K., Ostertag, C. P., Braun, L. M. & Lloyd, I. K. Effects of Fiber Volume Fraction on Mechanical Properties of SiC-Fiber/Si₃N₄-Matrix Composites. *Journal of the American Ceramic Society* **77**, 1897–1900 (1994).
51. Pan, N. Theoretical determination of the optimal fiber volume fraction and fiber-matrix property compatibility of short fiber composites. *Polym Compos* **14**, 85–93 (1993).
52. Saurabh Pethe. Thermoplastic Impregnation of Textile Grade Carbon fiber to produce tapes. . (University of Tennessee, Knoxville, 2022).
53. Gebart, B. R. Permeability of Unidirectional Reinforcements for RTM. *J Compos Mater* **26**, 1100–1133 (1992).
54. Bates, P. J. & Charrier, J. M. Effect of Process Parameters on Melt Impregnation of Glass Roving. *Journal of Thermoplastic Composite Materials* **12**, 276–296 (1999).
55. Han, K., Jiang, S., Zhang, C. & Wang, B. Flow modeling and simulation of SCRIMP for composites manufacturing. *Compos Part A Appl Sci Manuf* **31**, 79–86 (2000).
56. Comer, A. J. *et al.* Mechanical characterisation of carbon fibre–PEEK manufactured by laser-assisted automated-tape-placement and autoclave. *Compos Part A Appl Sci Manuf* **69**, 10–20 (2015).
57. Qureshi, Z., Swait, T., Scaife, R. & El-Dessouky, H. M. In situ consolidation of thermoplastic prepreg tape using automated tape placement technology: Potential and possibilities. *Compos B Eng* **66**, 255–267 (2014).
58. Stokes-Griffin, C. M. & Compston, P. An inverse model for optimisation of laser heat flux distributions in an automated laser tape placement process for carbon-fibre/PEEK. *Compos Part A Appl Sci Manuf* **88**, 190–197 (2016).
59. Rizzolo, R. H. & Walczyk, D. F. Ultrasonic consolidation of thermoplastic composite prepreg for automated fiber placement. *Journal of Thermoplastic Composite Materials* **29**, 1480–1497 (2015).
60. Kagan, V. A., Bray, R. G. & Kuhn, W. P. Laser Transmission Welding of Semi-Crystalline Thermoplastics—Part I: Optical Characterization of Nylon Based Plastics. *Journal of Reinforced Plastics and Composites* **21**, 1101–1122 (2002).
61. Qureshi, Z., Swait, T., Scaife, R. & El-Dessouky, H. M. In situ consolidation of thermoplastic prepreg tape using automated tape placement technology: Potential and possibilities. *Compos B Eng* **66**, 255–267 (2014).

62. Mazumdar, S. K. & Hoa, S. v. Determination of Manufacturing Conditions for Hot-Gas-Aided Thermoplastic Tape Winding. *Journal of Thermoplastic Composite Materials* **9**, 35–53 (1996).
63. Zachary August, G. O. J. M. D. H. RECENT DEVELOPMENTS IN AUTOMATED FIBER PLACEMENT OF THERMOPLASTIC COMPOSITES. *SAMPE* (2014).
64. Tafreshi, O. A., Hoa, S. van, Shadmehri, F., Hoang, D. M. & Rosca, D. Heat transfer analysis of automated fiber placement of thermoplastic composites using a hot gas torch. *Advanced Manufacturing: Polymer & Composites Science* **5**, 206–223 (2019).
65. Boon, Y. di, Joshi, S. C. & Bhudolia, S. K. Review: Filament Winding and Automated Fiber Placement with In Situ Consolidation for Fiber Reinforced Thermoplastic Polymer Composites. *Polymers (Basel)* **13**, (2021).
66. Xu, Z., Yang, F., Guan, Z. W. & Cantwell, W. J. An experimental and numerical study on scaling effects in the low velocity impact response of CFRP laminates. *Compos Struct* **154**, 69–78 (2016).
67. Nogueira, C. L. P. J. M. F. de and R. M. C. Effect of the interfacial adhesion on the tensile and impact properties of carbon fiber reinforced polypropylene matrices. *Materials Research* (2005).
68. Yang, L., Liu, X., Wu, Z. & Wang, R. Effects of triangle-shape fiber on the transverse mechanical properties of unidirectional carbon fiber reinforced plastics. *Compos Struct* **152**, 617–625 (2016).
69. Ma, Y., Yang, Y., Sugahara, T. & Hamada, H. A study on the failure behavior and mechanical properties of unidirectional fiber reinforced thermosetting and thermoplastic composites. *Compos B Eng* **99**, 162–172 (2016).
70. DiBenedetto, A. T. Tailoring of interfaces in glass fiber reinforced polymer composites: a review. *Materials Science and Engineering: A* **302**, 74–82 (2001).
71. Xu, Z. *et al.* Effect of kidney-type and circular cross sections on carbon fiber surface and composite interface. *Compos Part A Appl Sci Manuf* **39**, 301–307 (2008).
72. Xu, Z. *et al.* Surface characteristics of kidney and circular section carbon fibers and mechanical behavior of composites. *Mater Chem Phys* **106**, 16–21 (2007).
73. Novo, P. J., Silva, J. F., Nunes, J. P. & Marques, A. T. Pultrusion of fibre reinforced thermoplastic pre-impregnated materials. *Compos B Eng* **89**, 328–339 (2016).

74. Comer, A. J. *et al.* Mechanical characterisation of carbon fibre–PEEK manufactured by laser-assisted automated-tape-placement and autoclave. *Compos Part A Appl Sci Manuf* **69**, 10–20 (2015).
75. Tierney, J. & Gillespie, J. W. Modeling of In Situ Strength Development for the Thermoplastic Composite Tow Placement Process. *J Compos Mater* **40**, 1487–1506 (2006).
76. Liu, X. *et al.* Isothermal crystallisation ATP process for thermoplastic composites with semi-crystalline matrices using automated tape placement machine. *Compos B Eng* **227**, 109381 (2021).
77. Chanteli, A., Bandaru, A. K., Peeters, D., O’Higgins, R. M. & Weaver, P. M. Influence of repress treatment on carbon fibre-reinforced PEEK composites manufactured using laser-assisted automatic tape placement. *Compos Struct* **248**, 112539 (2020).
78. *ExxonMobil™ PP3155*.
79. ASTM Standards. ASTM D7136/D7136M-20 Standard Test Method for Measuring the Damage Resistance of a Fiber-Reinforced Polymer Matrix Composite to a Drop-Weight Impact Event. *ASTM* (2020).
80. ASTM Standards. ASTM D3039 Standard Test Method for Tensile Properties of Polymer Matrix Composite Materials. *ASTM* (2017).
81. ASTM Standards. ASTM D790 Standard Test Methods for Flexural Properties of Unreinforced and Reinforced Plastics and Electrical Insulating Materials. *ASTM D790* (2017).
82. Thanomsilp, C. & Hogg, P. J. Penetration impact resistance of hybrid composites based on commingled yarn fabrics. *Compos Sci Technol* **63**, 467–482 (2003).
83. Mizukami, K. *et al.* Detection of in-plane fiber waviness in cross-ply CFRP laminates using layer selectable eddy current method. *Compos Part A Appl Sci Manuf* **82**, 108–118 (2016).
84. Galos, J. Novel method of producing in-plane fibre waviness defects in composite test coupons. *Composites Communications* **17**, 1–4 (2020).
85. Stokes-Griffin, C. M., Kollmannsberger, A., Compston, P. & Drechsler, K. The effect of processing temperature on wedge peel strength of CF/PA6 laminates manufactured in a laser tape placement process. *Compos Part A Appl Sci Manuf* **121**, 84–91 (2019).

86. Hoang, M. D. Procedure for making flat thermoplastic composite plates by Automated Fiber Placement and their mechanical properties. (Concordia University, 2015).
87. Rajasekaran, A. & Shadmehri, F. Steering of carbon fiber/PEEK tapes using Hot Gas Torch-assisted automated fiber placement. *Journal of Thermoplastic Composite Materials* 08927057211067962 (2022) doi:10.1177/08927057211067962.
88. Hiremath, N. *et al.* Low cost textile-grade carbon-fiber epoxy composites for automotive and wind energy applications. *Compos B Eng* **198**, 108156 (2020).
89. Hunt, M. A., Saito, T., Brown, R. H., Kumbhar, A. S. & Naskar, A. K. Patterned Functional Carbon Fibers from Polyethylene. *Advanced Materials* **24**, 2386–2389 (2012).
90. Ray, D. *et al.* Fracture toughness of carbon fiber/polyether ether ketone composites manufactured by autoclave and laser-assisted automated tape placement. *J Appl Polym Sci* **132**, (2015).
91. Norimichi Nanami, Takashi Sato, Tadashige Ikeda & Takashi Ishikawa. Flexural Performance and Process Conditions of Thermoplastic Composite Laminates Processed by Automated Tape Placment. in *20th International Conference on Composite Materials* (2015).
92. Lee, W. I., Talbott, M. F., Springer, G. S. & Berglund, L. A. Effects of Cooling Rate on the Crystallinity and Mechanical Properties of Thermoplastic Composites. *Journal of Reinforced Plastics and Composites* **6**, 2–12 (1987).
93. Lee, B., Leong, K. H. & Herszberg, I. Effect of Weaving on the Tensile Properties of Carbon Fibre Tows and Woven Composites. *Journal of Reinforced Plastics and Composites* **20**, 652–670 (2001).
94. Mohamed, M., Selim, M. M., Ning, H. & Pillay, S. Effect of fiber prestressing on mechanical properties of glass fiber epoxy composites manufactured by vacuum-assisted resin transfer molding. *Journal of Reinforced Plastics and Composites* **39**, 21–30 (2019).
95. Zaidi, B. M., Magniez, K. & Miao, M. Prestressed natural fibre spun yarn reinforced polymer-matrix composites. *Compos Part A Appl Sci Manuf* **75**, 68–76 (2015).
96. Richardson, M. O. W. & Wisheart, M. J. Review of low-velocity impact properties of composite materials. *Compos Part A Appl Sci Manuf* **27**, 1123–1131 (1996).
97. Richardson, M. O. W. & Wisheart, M. J. Review of low-velocity impact properties of composite materials. *Compos Part A Appl Sci Manuf* **27**, 1123–1131 (1996).

98. Tan, W., Falzon, B. G., Chiu, L. N. S. & Price, M. Predicting low velocity impact damage and Compression-After-Impact (CAI) behaviour of composite laminates. *Compos Part A Appl Sci Manuf* **71**, 212–226 (2015).
99. Kumar, V. *et al.* Internal arcing and lightning strike damage in short carbon fiber reinforced thermoplastic composites. *Compos Sci Technol* **201**, 108525 (2021).

APPENDIX

- Electrical Control System Development

A new and improved electrical system was developed to improve user interface and process control of the thermoplastic impregnation system. This electrical system was designed in collaboration with Stephen Sherriff (Staff Engineer), Saurabh Pete (MS Student), Nicholas Crowder (UG), Joel Rodeghiero (UG) and Mason Rucinski (UG). The electrical system was designed for 3 phase, 240 Volt, 100-amp power supply. Phase 1 powered the pin die system which required 120 volt input. Phase 2 and Phase 3 were used as the 240 Volt power supply to the coat hanger, extruder, and preheaters. Each phase was limited to 33.3-amps and the system was designed to have a factor of safety above 1.5 with no phase exceeding 20-amps. All heater control systems were controlled by individual PID's connected to SSR's. Two emergency stop systems were integrated onto the impregnation line with one on each end of the system that was connected to an arc suppressing contactor for immediate shut off of the system. DC power was supplied by phase 2 and was converted by a switching mode power supply. DC power controlled the motor control display and drivers were run and programed by an Arduino Mega.

The main power supply box was split into two sections. The bottom section housed all AC power connections while the top section housed DC powered instruments. The SSR's were used as the dividing line due to their use of both AC and DC signals. The main power supply box controls the temperature feed back system where all wires are fed into a secondary junction or distribution box. This junction box was used as a stable platform to disperse the heater/motor power to their respective systems. This box also was used to house the clutch and loadcell control for the take-up system. This entire electrical system was designed to be able to be moved with ease due to detachable connection points at both Electrical Boxes.

Figure 37 displays pictures of the main electrical control system, Secondary electrical junction box and removable connections between the two boxes.

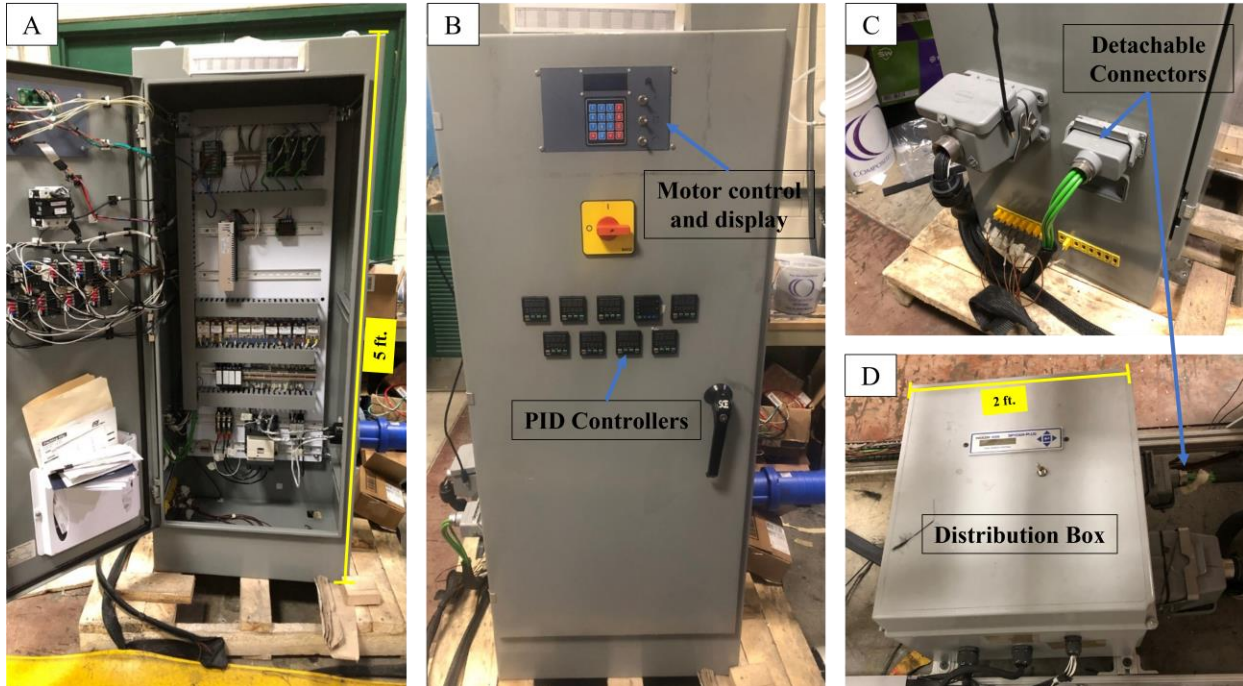


Figure 37: Images of Thermoplastic impregnation line electrical system. (A) Front view of electrical box. (B) View of the open electrical box. (DC – Top Section) (AC – Bottom Section) (PID wires on open door). (C) Distribution box on the base of the tape line. (D) Quick connects on the side of the main electrical box where wires can be easily removed.

- New Pin Die Development

After the original development of the tape line open pin die system, it was observed that there was freezing and boiling of the polymer during the impregnation process. It was observed that due to the placement of the thermocouple the temperature feedback system was inaccurately measuring the temperature of the die system. These large thermal spikes oscillating within an approximate one hour period was correlated to the placement of the thermocouple (Figure 38). Figure 39 shows the approximate location of the thermocouples where their location was pressed up against the end of the heater. Heaters have a no heat zone located at each end where an insulated cap is placed. Furthermore, heaters have a large temperature gradient across the length of the heater where the highest temperature is located at the center gradually decreasing towards the end. This problem further amplifies the difference between the observed temperature and the actual temperature of the heaters at the center where the feedback system cannot keep up with the actual temperature. For these reasons, a new pin die system was developed to correct the issue. This was solved by increasing the overall length and diameter of the pin system helping to reduce the temperature difference from the center to the edges of the pins by allowing the pins to act as a heat sink. Also, custom cartridge heaters with thermocouples located at the center of the heaters allowed for accurate temperature feedback for the PID system. To further insure accurate temperatures each heater was fitted with its own thermocouple compared to the old system where there was one thermocouple controlling two heaters. The thermocouples for each of the dual pins was averaged by connecting the thermocouples together in parallel. This ensures all heaters are connected to the temperature control system providing feed back to the PID system.

A study was conducted to confirm the engineering design. Data collection was taken every 15 minutes over multiple hours. Figure 38 (b) shows new pin die temperature over time and that the temperature moves at most 5 degrees over a 3-hour period. This confirms that the design process which was implemented provides precise temperature control of the individual pins over long time intervals.

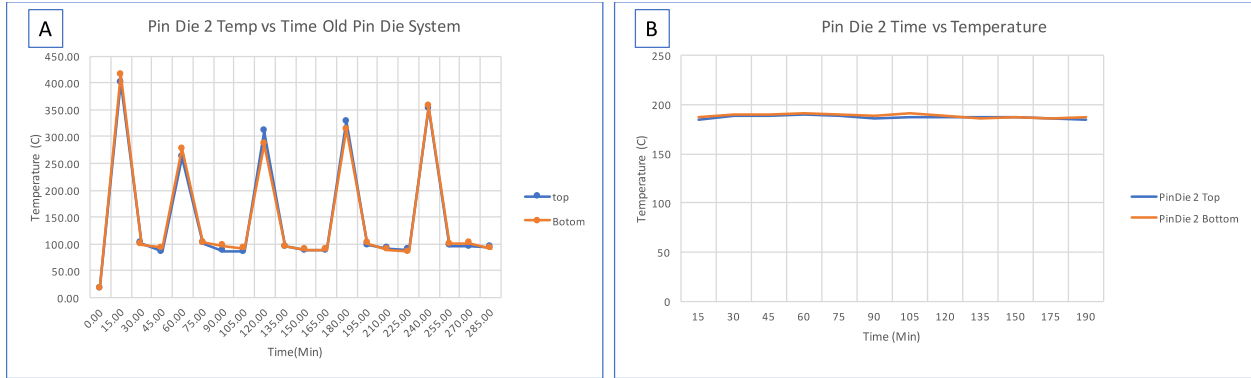


Figure 38: Temperatures vs. Time graphs of the old and new pin die system. Temperature grades for the old pin dies system (A) varied between as much as 200°C during a 15-minute period while the new pin die system (B) remains constant with in around 5° degrees.

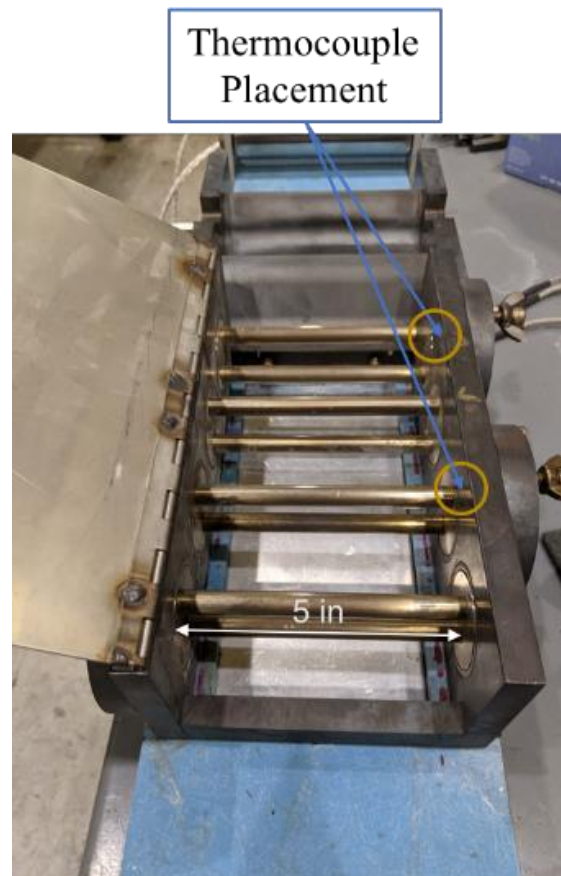


Figure 39: Old 5 in Pin Die system with thermocouples located at the end of the heaters. Due to the placement of the heaters large thermal spikes and a high thermal gradient could be observed within the system

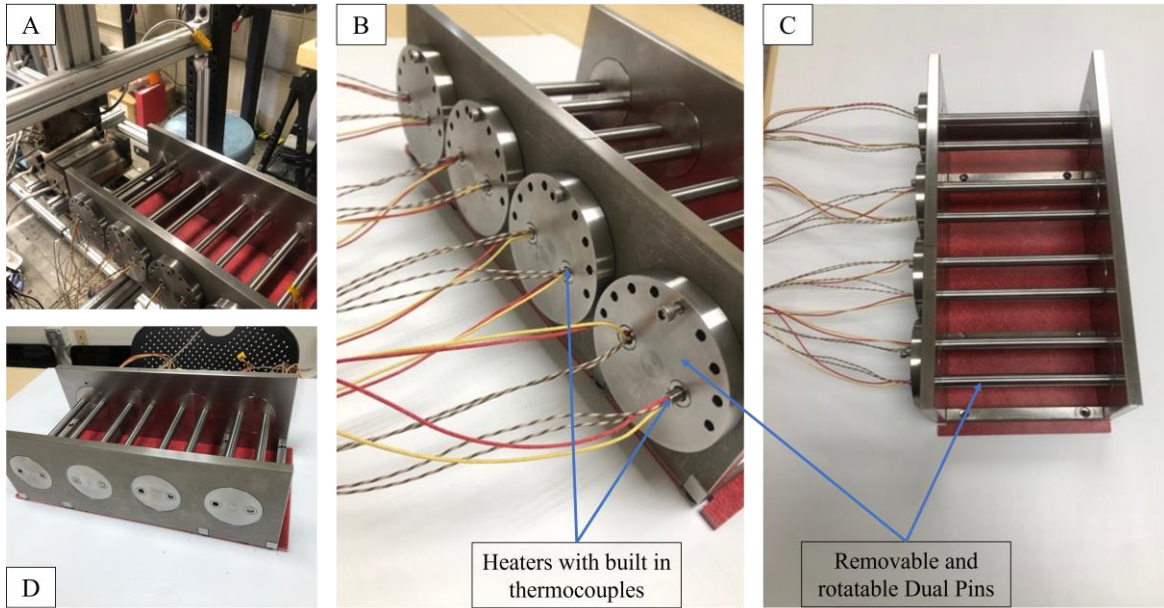


Figure 40: New Pin Die System. (a) View of Pin die system mounted onto the tape impregnation (b) Front side view showing heater and thermocouple wires inserted into rotating pins. Pins can be turned and locked into places at intervals of 22.5° covering a 180° operational window. (c). Top view (d) Back side view

- Tape Slitting System

Development of the tape slitting system was initiated to cut thermoplastic tapes produced on the thermoplastic impregnation system for the processing on an ATP System. The design philosophy for this tape slitting system was to have multiple rotating blades spaced at precise intervals where the tape could be pulled along under tension and be cut into long strips. This simplistic design incorporated three parts: Rotary blades, Spacers, and a pinch roller as seen in Figure 41. The custom rotary blades were made from titanium to insure the cutting system could withstand the abrasiveness of continuous slitting of CF. The spacers and pinch roller was produced through additive manufacturing (AM) of Thermoplastic Polyurethanes (TPU) with a 40% infill. TPU was chosen due to its natural flexibility allowing the pinch system to deform as the slitting system rotates. The pinch roller was designed with ½ inch spaced slots to allow for the blades to pass through while firmly pressing the tape into the spacers allowing the tape to be cut. An axial rotates on a mounted barring which was fitted to the top and bottom sitting/pinch system. Shaft collars were fitted on the axials to insure the pinch system would stay centered and aligned with the tensioning system.

To slit the tape, the tape line was set up to run backwards where the load cell and clutch system worked in tandem to apply tension to the line. The tape was placed on the on the winding system and was fed over the load cell. Finally, the tape was fed through the pinch slitting system and puller system to maintain a constant line speed. To ensure consistent slitting of the material, 15 kg of tension was applied to the line with the clutch.

- Open LFT and Rod Die Design

An open die concept was developed to produce long fiber thermoplastic (LFT) pellets and rods in-line with the hot melt impregnation system. Traditional manufacturing systems for LFT pellets and rods use a closed die design as a part of a pultrusion system. These closed die pultrusion systems were initially developed for thermoset resin systems and were modified when thermoplastic pultrusion systems started to be developed. Often fiber breakage within a die system can mean a shutdown of a production line costing extensive time, money, and resources.

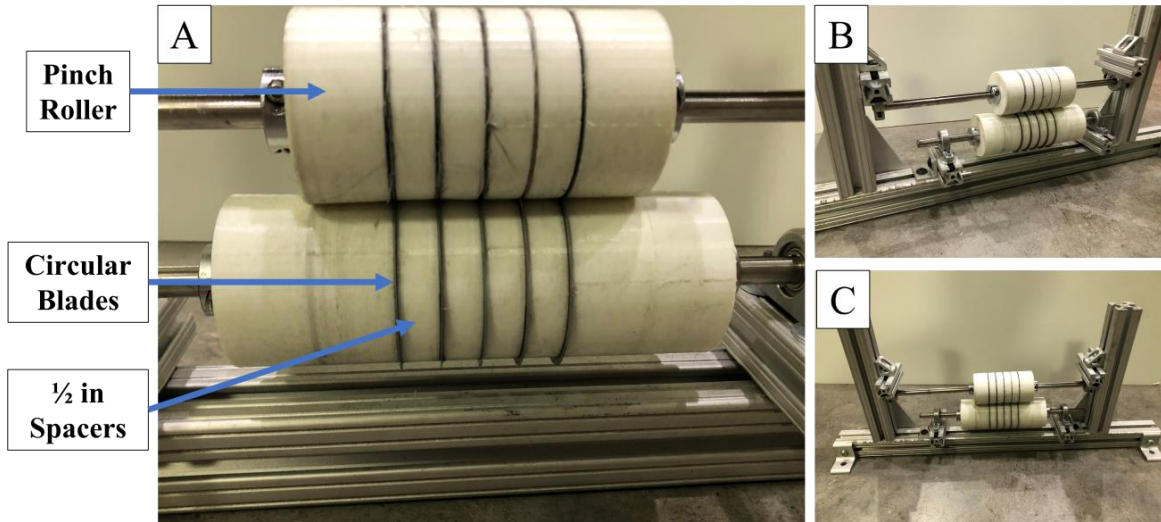


Figure 41: Tape Slitting system. (A) large view of tape slitting. (B & C) close up of AM manufactured spacers and pinch rollers. This system was designed to allow for the ease of taking on and off the line by the removal of two bolts. Five blades are attached to continuously slit 4 one half inch tapes to be placed on an automated tape placement system.

A complete rethink of how pultrusion systems form shapes is needed for thermoplastic manufacturing especially for the production of ultra-wide tow CF. Processing of ultra-wide tow TCF is difficult due to handling issues and its tendency to fray. For this an open die design was designed to produce continuous rods. Two die systems have been designed which include (a) rod system and (b) LFT die system. The rod system was designed to consolidate a 350K tow of CF Tape into a single rod. This rod could be used as composite rebar in construction applications. The LFT die system was designed to consolidate a 350K tow into five rods approximately 3 mm in diameter. These fully impregnated rods could then be chopped and used in an injection molding or extrusion compression process. This type of system does have some limitation as it would only be able to produce non-tolerance rods but as an intermediate material (LFT) tolerancing is a non-issue. For the rod die system partial consolidation would occur within the open die. A secondary rotating gear with a coolant system could finish the consolidation process and provide indentations for construction applications of CF rebar.

A thermal model was created to observe the heat distribution across the die systems. This thermal loading was used to determine the best placement for the thermocouple for controlled temperature feedback. As expected the thermal model showed the highest temperature to be in the thinnest region of both die systems. Figure 42 & Figure 43 displays the cad models of the LFT and rod die systems along with the thermal model.

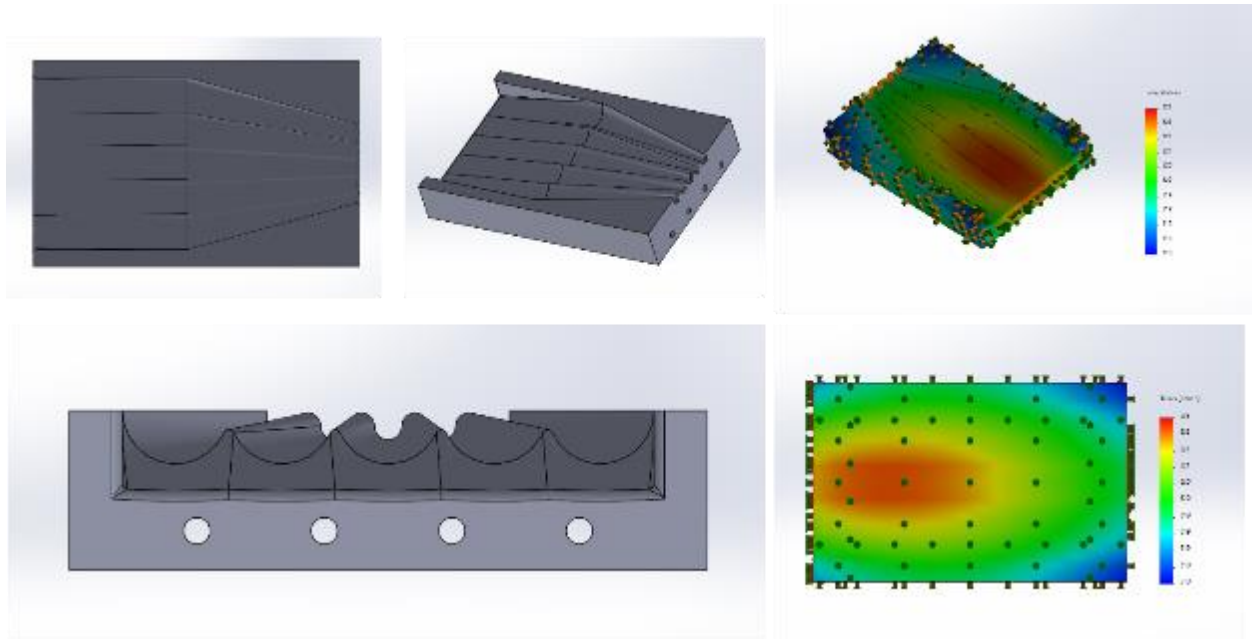


Figure 42: LFT Die CAD model and Thermal model

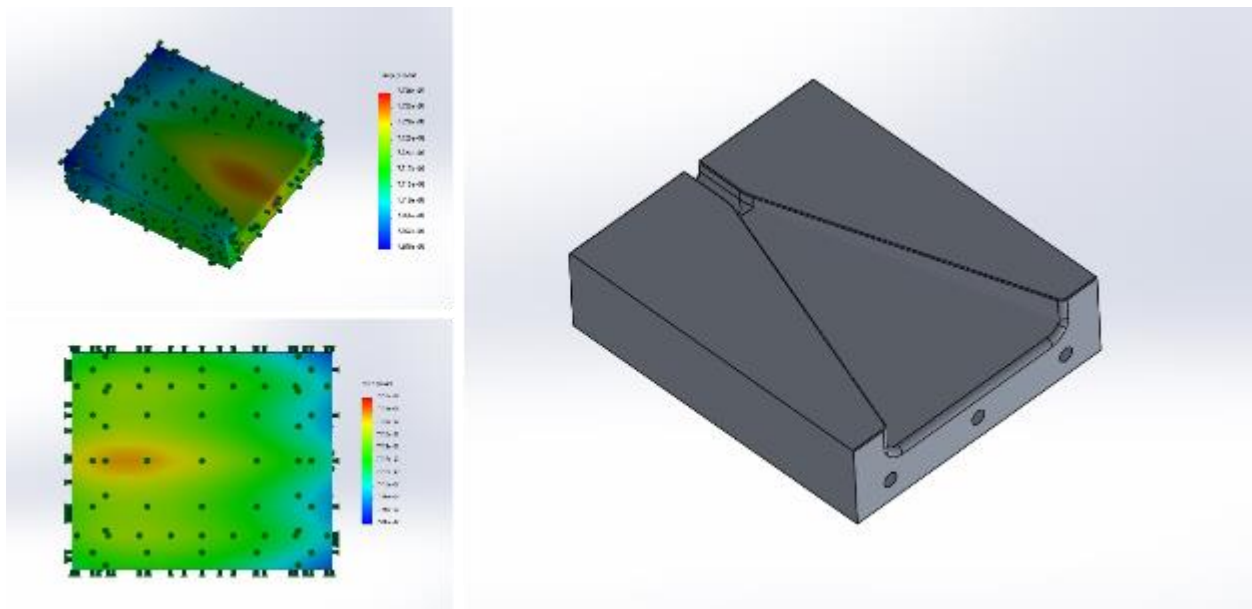


Figure 43: Rod die cad and thermal model

- Extra Graphs and Tables

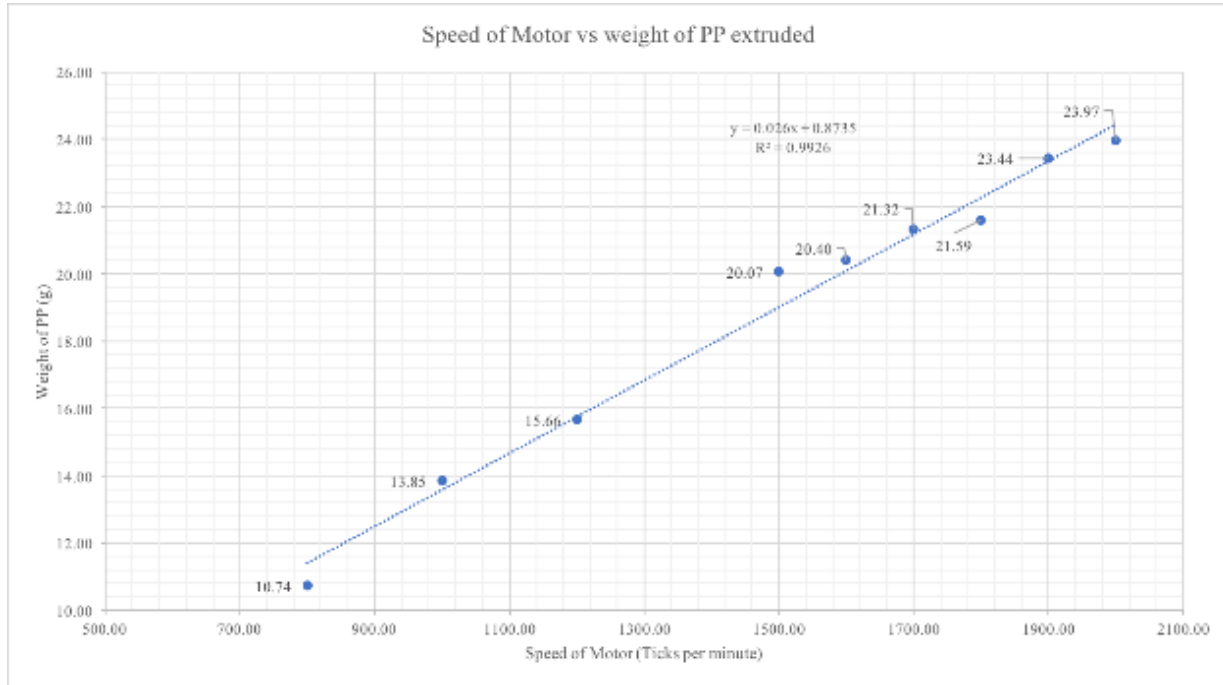


Figure 44: Extruder speed vs Weight of PP (Grams/min)

Table 8: Mechanical Characterization Data for all Mechanical Tests

Test Method and Material			ZT-PP CM	ZT-PP ATP	TCF-PP CM	TCF-PP ATP
Tensile	Strength	Mean	459.09	183.80	252.06	53.02
	(Mpa)	STD	52.42	25.07	17.95	6.52
	Modulus	Mean	51.32	39.78	49.13	14.28
	(Mpa)	STD	6.54	2.85	4.85	1.60
		Theoretic al Modulus	60.52	--	68.64	--
Flexura l Uni	Strength	Mean	220.57	71.66	198.04	58.47
	(Mpa)	STD	6.92	5.08	20.62	4.72
	Modulus	Mean	27.98	6.49	26.84	4.05
	(Mpa)	STD	3.13	1.09	3.30	0.85
Flexura l 0/90	Strength	Mean	119.48	--	115.65	--
	(Mpa)	STD	19.85	--	9.83	--
	Modulus	Mean	15.92	--	20.70	--
	(Mpa)	STD	2.92	--	2.15	--
ILSS	Strength	Mean	17.90	7.10	14.10	5.70
	(Mpa)	STD	1.69	0.71	1.74	1.07
	Modulus	Mean	17.90	7.10	14.10	5.70
	(Mpa)	STD	1.69	0.71	1.74	1.07

Table 9: Low Velocity Impact Data

	Plate #	Total Drop Mass (kg)	Impact Hight (mm)	Peak Force (N)	Drop Energy (J)	Impact Velocity (m/s)
ZT-PP 0/90	1	5.715	535	5630	30	3.24
	2	5.715	714	5864	40	3.71
	3	5.715	892	6181	50	4.18
	4	5.715	1070	6126	60	4.58
	5	7.215	989	5919	70	4.41
	6	7.215	1057	5761	80	4.55
ZT-pp Uni	1	5.715	178	2150	10	1.87
	2	5.715	268	2555	15	2.29
	3	5.715	357	2515	20	2.65
	5	5.715	446	2737	25	2.96
	6	5.715	535	2781	30	3.24
TCF-PP 0/90	1	5.715	357	1778	20	2.65
	2	5.715	446	2218	25	2.96
	3	5.715	535	2436	30	3.25
	4	5.715	714	3146	40	3.74
	5	5.715	892	2305	50	4.18
TCF-PP Uni	1	5.715	178	1789	10	1.87
	2	5.715	286	2158	15	2.89
	3	5.715	357	2004	20	2.65
	4	5.715	401	1979	22.5	2.81
	5	5.715	446	1583	25	2.96

Table 10: Volumetric Damage Data

	Plate #	Top Surface Area (mm ²)	Bottom Surface Area (mm ²)	Thickness (mm)	Approximate Radius 1 (mm)	Approximate Radius 2 (mm)	Volume Damage (mm ³)	Depth of Damage (mm)
ZT-PP 0/90	1	2076.65	1114.94	5.33	25.71	18.84	8373.82	-1
	2	3235.83	1064.65	5.33	32.09	18.41	10938.16	-1.5
	3	4605.29	3309.34	5.33	38.29	32.46	20997.59	-1.5
	4	3304.07	1912.46	5.33	32.43	24.67	13734.12	-2.5
	5	4772.66	3517.55	5.33	38.98	33.46	22008.53	-3.7
	6	3366.27	2253.91	5.33	32.73	26.79	14879.01	-4.8
ZT-pp Uni	1	3680.56	3410.71	5.33	--	--	20336.50	-0.6
	2	4645.55	3480.58	5.33	--	--	27865.39	-1.1
	3	7520.89	6814.58	5.33	--	--	41968.66	-1
	5	6825.22	5909.41	5.33	--	--	38819.10	-1.2
	6	6399.79	7609.51	5.33	--	--	37334.79	-2.2
TCF-PP 0/90	1	760.95	2478.48	4.10	15.56	28.09	6304.08	-2.2
	2	756.16	3134.45	4.30	15.51	31.59	7783.20	-2.4
	3	1230.81	3128.34	4.85	19.79	31.56	10219.58	-2.2
	4	2380.17	4587.53	5.20	27.53	38.21	17804.97	-3.2
	5	3139.14	5950.62	4.70	31.61	43.52	21011.78	-6.6
TCF-PP Uni	1	1951.39	2141.58	4.81	--	--	9843.60	-1.4
	2	3246.64	3337.37	4.81	--	--	15834.54	-2.8
	3	2751.25	4569.09	5.33	--	--	19508.73	-3.2
	4	5922.87	5684.17	4.95	--	--	29909.00	-3.7
	5	5206.08	5886.40	4.70	--	--	26067.33	-10.4

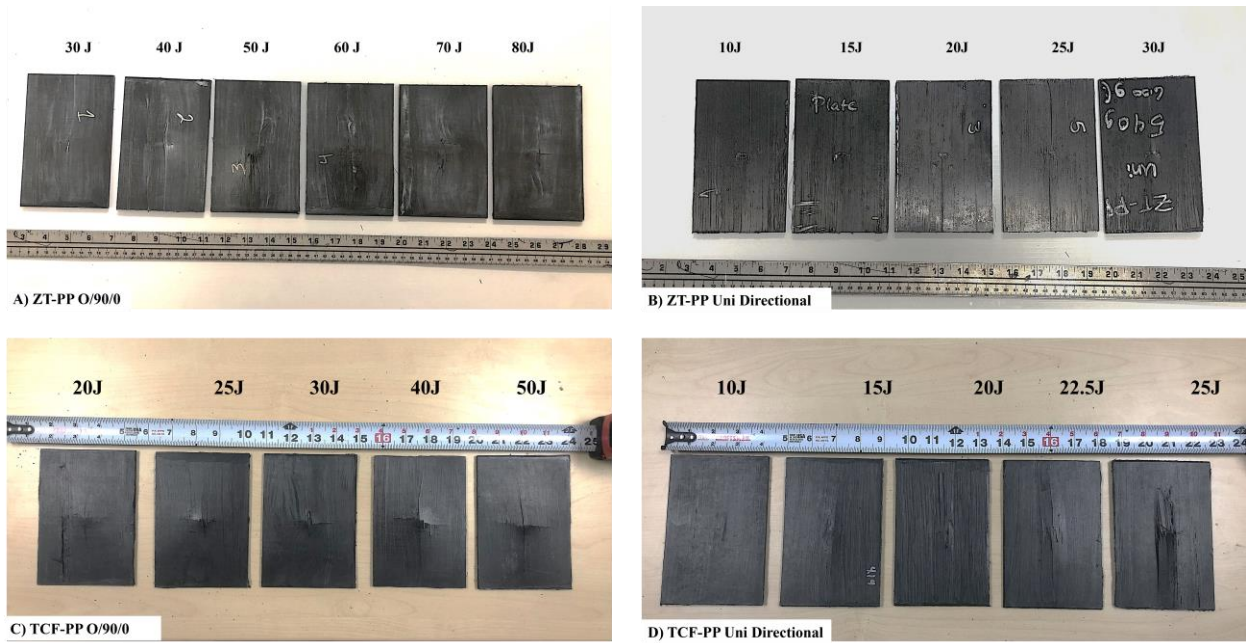


Figure 45: Low velocity impact samples after testing. (A) ZT-PP 0/90 samples from 30J - 80J, (B) ZT-PP Unidirectional Samples from 10J - 30J, (C) TCF-PP 0/90 samples from 20J - 50J and (D) TCF-PP Unidirectional samples from 10J - 25J

VITA

Benjamin Ursitti Schwartz

2015-2020 B.A. Mechanical Engineering, University of Tennessee, Knoxville
2020-2023 M.A. Mechanical Engineering, University of Tennessee, Knoxville

FIELD OF STUDY

Mechanical Engineering focused on composites manufacturing.